

NEW PHYSICAL EFFECTS IN METAL DEUTERIDES

Contract No. HR0011-05-C-0089 SRI Project No. P16816

Prepared by:

Michael C.H. McKubre and Francis L. Tanzella Materials Research Laboratory Physical Sciences Division SRI International 333 Ravenswood Avenue Menlo Park, CA 94025

Collaborators:

I. Dardik, A. El Boher, H. Branover, S. Lesin and T. Zilov, Energetics Technologies

E. Greenspan, Energetics Technologies and U.C. Berkeley

V. Violante, ENEA, Frascati

P. Hagelstein, MIT

G. Hubler and K. Grabowski, NRL

Prepared for: DARPA/DSO ATTN: Dr. Valerie M. Browning 3701 N. Fairfax Drive Arlington, VA 22203-1714

Naval Research Laboratory Materials & Sensors Branch ATTN: Dr. Graham K. Hubler Code 6360 4355 Overlook Avenue, S.W. Washington, DC 20375-5320

Approved by: Angel Sanjurjo, Director Materials Research Laboratory

Physical Sciences Division

CONTENTS

EXPERIMENTAL PLAN	l
Introduction	
Background	
The SRI – Energetics Replication Plan	4
ENERGETICS DATA ACQUISITION	6
Experimental	
Superwave Signal and Measurement	10
Results	
SRI DATA ACQUISITION	17
Introduction	17
Current Perturbation	20
Non-Steady-State Analysis	22
POST TEST ANALYSES	59
NRL Summary	59
NRL Conclusions	59
HELIUM	60
Tritium	60
SUMMARY AND CONCLUSIONS	69
Introduction	69
Heat Effects	69
Nuclear Effects	
Improved Cell Design	
Post-Process Analysis Summary	
Conclusions	
ACKNOWLEDGMENTS	81
REFERENCES	82

EXPERIMENTAL PLAN

INTRODUCTION

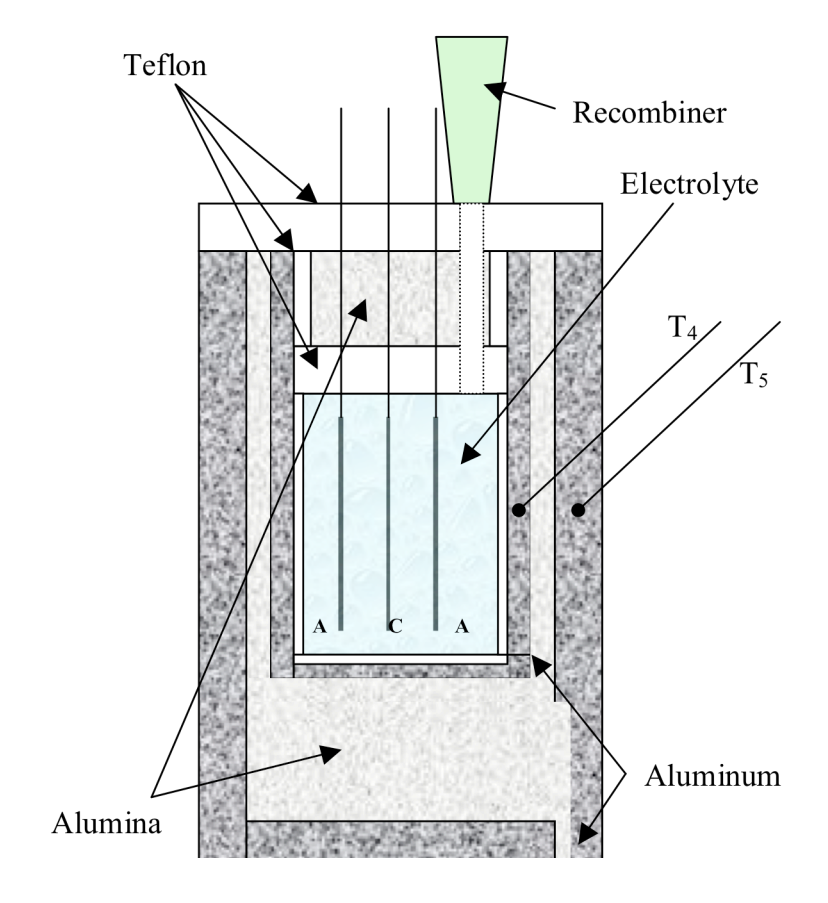
A series of experiments was undertaken to replicate isoperibolic calorimetry results obtained from heavy water electrolysis at specially prepared palladium foil cathodes. The original experiments were performed and reported by a private corporation, Energetics LLC in Omer, Israel, based on concepts developed in New Jersey. Three features distinguish the Energetics experiments and results from numerous others in the so-called "cold fusion" or condensed matter nuclear science (CMNS) field:

- 1. The use of a complex, fractally nested, non-sinusoidal input current rather than simple dc or pulse electrolysis.²
- 2. Achievement of very high loading of D into the Pd cathodes at atom fractions approaching and exceeding D/Pd = 1. Such atom fractions have rarely been reported, and never with such high reproducibility.³
- 3. The appearance of excess heat at unprecedented levels in glow discharge and Fleischmann-Pons electrolytic cells.

The reproducibility of high D/Pd loading obtained by Energetics, as well as the high proportional levels of excess heat and high absolute levels of excess energy, prompted the replication activity described below.

BACKGROUND

Experiments were performed in cell and calorimeter basically as shown in Figure 1. Two platinum anodes of dimension (20 mm x 80 mm x 100 µm thick) sandwich a palladium cathode (typically 7 mm x 80 mm x 50 µm thick) with anode-cathode separation 6 mm. This three-electrode structure is positioned at the center of a 49 mm dia. by 185 mm tall cylindrical PTFE cup that comprises the electrochemical cell outer boundary.



¹ References 1-3.

² Throughout the report this stimulus will be referred to as superwave.

³ Reference 4

A fitting cell top machined from PTFE and alumina insulation completes the cell boundary and acts to reduce vertical conductive heat transfer. The fitting top is penetrated by:

- i) two current wires to the anode and cathode (the cell voltage is measured just external to the cell),
- ii) four small wires used to make four terminal measurements of the cathode axial resistance, and
- iii) three stainless steel and PTFE sheathed 100Ω platinum resistance temperature device (RTD) sensors used to measure the cell electrolyte temperature at various positions relative to the anode/cathode/anode "sandwich." These electrolyte temperature sensors are designated as T_1 - T_3 .

Also penetrating the top is a 120-mm inside diameter (i.d.) PTFE tube connecting the vapor space of the cell to a tightly sealed chamber containing an Agua Gen® recombiner catalyst. Electrolytically generated O_2 and D_2 bubble from the electrolyte and rise to the recombiner to form D_2O and flow back down to the cell. The heat of recombination is thus largely communicated to the environment. The small fraction that is returned to the cell with the downcoming D_2O as well as influences of ambient temperature on the calorimetry are taken into account with the calibration.

The calorimeter is considered isoperibolic in the sense that the two aluminum cups in Figure 1 are taken to be the calorimetric boundary perimeters at constant temperature: the inner wall at temperature T_4 , and the outer at temperature T_5 . Separating the two boundaries is a well-defined thickness of alumina powder having a well-characterized (and constant) thermal conductivity. For the limiting case where the temperature of the inner and outer boundaries both can be represented by a single temperature measured as T_4 and T_5 , respectively, then the steady state heat flow in or out of the calorimeter in the absence of ambient or recombinant effects is given by

$$H = k * [T_4 - T_5]$$
 [1]

In practice the outer boundary T_5 is held constant by immersing the calorimeter in a water bath at a well–controlled, constant temperature. At both Energetics and SRI, a bath temperature of ~ 5 °C was normally chosen to increase the extent of deuterium absorption into the palladium cathodes.

The working electrolyte volume of the cell shown in Figure 1 is $\sim\!230~\text{cm}^3$. Electrolytes were prepared by adding 5.25 ml of 9 wt. % LiOD/D₂O (Sigma – Aldrich CN 347450) to 225 ml of low tritium content D₂O (Sigma – Aldrich CN 151890) to yield an electrolyte concentration of 0.1 M LiOD.

The electrodes typically used by Energetics and SRI were of the form shown in Figure 2. Foils 80 mm long, 7 mm wide and \leq 50

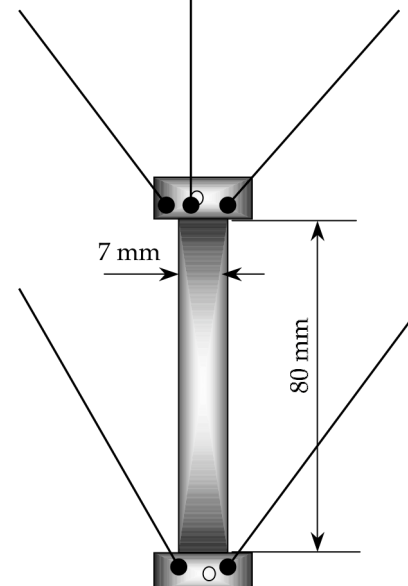


Figure 2. Cathode geometry.

⁴ Manufactured by Hoppecke, designed for use in lead-acid batteries and of proprietary formulation.

µm thick were prepared by successive rolling and annealing procedures, as described by Violante.⁵ Electrolysis current was supplied to the cathode by a 0.3-mm-dia. Pt wire sheathed in PTFE. Four additional 0.3-mm-dia. PTFE sheathed Pt wires were used to measure the axial resistance of the Pd cathode to determine the D/Pd (or H/Pd) loading. Anode current was supplied using 500 μm Pt wires attached to the Pt anodes.

The most pronounced excess heat results obtained by Energetics are reproduced as Figure 3 (excess power) and Figure 4 (excess energy). A maximum thermal output power of ~34 W was obtained twice at an input power of less than 1 W. The duration of this episode was approximately 14 h, terminating apparently spontaneously with an integrated energy of electrical input of 40 kJ, and integrated output heat energy of 1.14 MJ.

Despite the relatively low operating temperature (~60°C), the power and energy multiples seen in the data of Figure 3 and 4, if real, reproducible, and obtainable on demand, clearly suggest the possibility of practical energy production. For this reason, and because of the obvious non-chemical origin of the excess heat, SRI offered to host a sponsored confirmation attempt as described below.

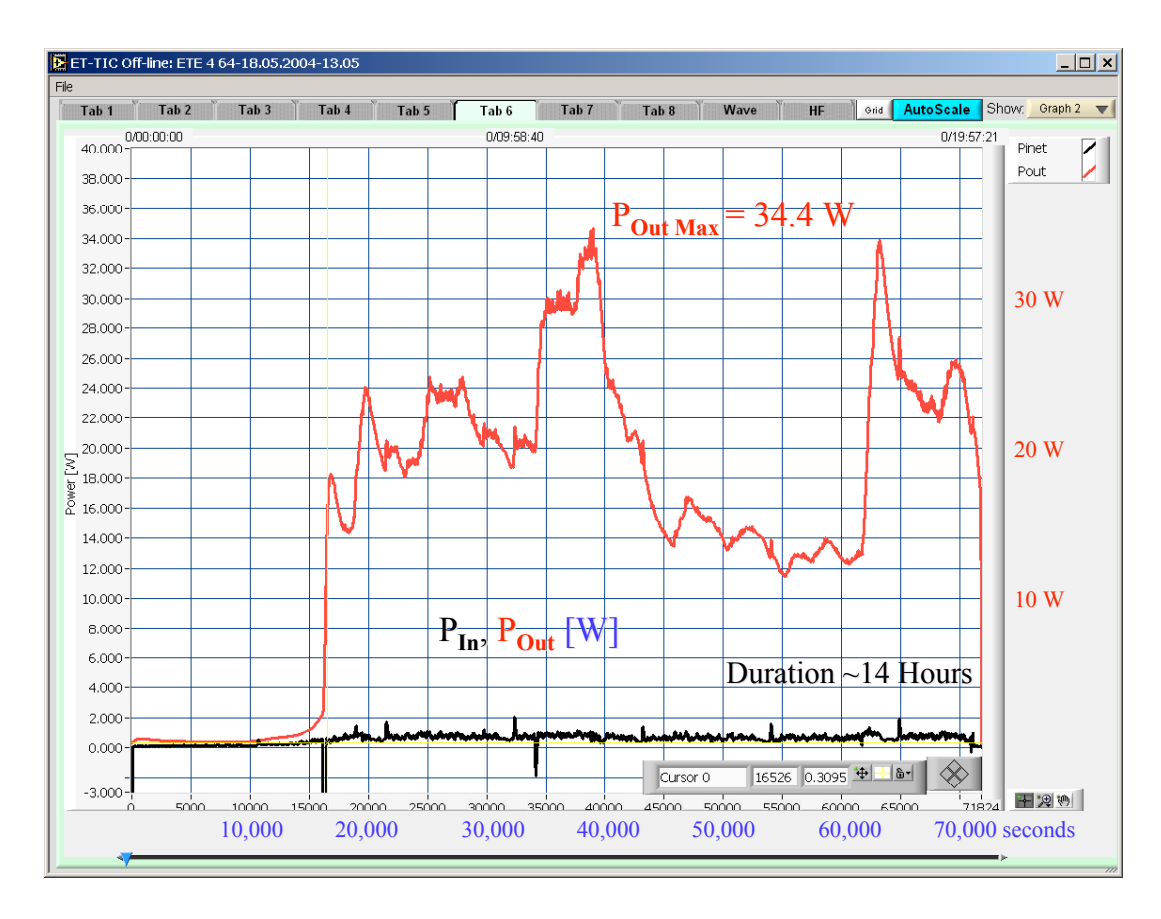


Figure 3. Energetics excess power results for cell ETE #64.

_

⁵ Reference 5

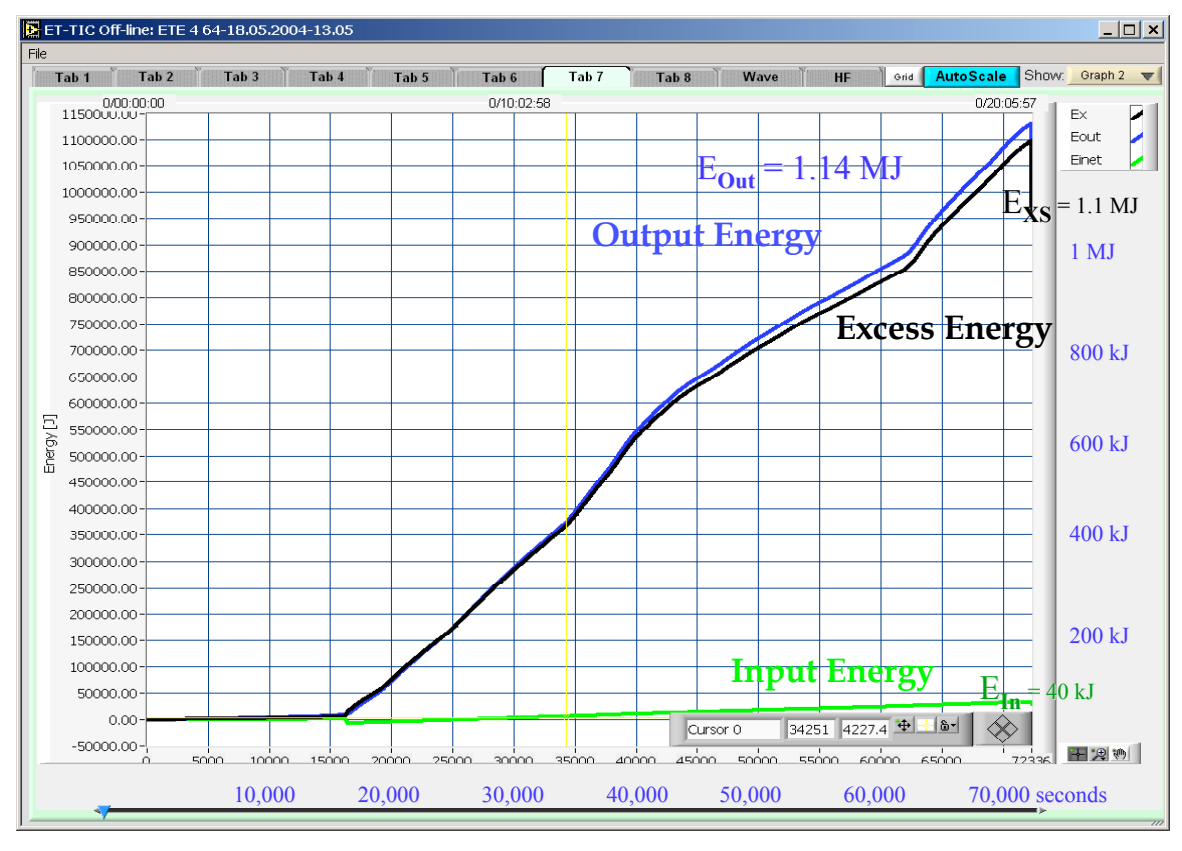


Figure 4. Energetics excess energy results for cell ETE #64.

THE SRI – ENERGETICS REPLICATION PLAN

Since 1989, SRI has attempted to replicate roughly ten experimental results reported in the field of cold fusion or condensed matter nuclear science (CMNS). A reproduction protocol has been developed to maximize the chances of success and useful learning in this process. The SRI reproduction protocol employed for the replication of Energetics' results described below involves three steps.

- 1. A "host hands off" rebuild by the original experimenter at SRI allowing simple technical support, but with conscientious effort <u>not</u> to improve the experiment at this point. In this step, SRI scientists provide simple technical, computing, and plumbing support. This first phase is complete when the results of testing are deemed satisfactory by the guest experimenter; that is, when the experiment is operating at SRI in the same manner as it was on the original site.
- 2. The second step, largely taken within the first, but often overlapping with the third, is a complete transfer of procedures and performance characteristics from the guest to the host. When the experiment is running to the satisfaction of the originator, and the host scientists believe they understand what is being done, the originator is invited to leave operation to the SRI scientists.
- 3. The third step involves host (SRI) operation of the experiment with added diagnostics as suggested or required from the results of Step 1. Only when the experiment is running at SRI in the same way and with the same results as for the originator do we succumb to the

temptation to "improve." In the present program, such "improvement" was restricted to data analysis, as the underlying Energetics protocol was demonstrated to be sound.

This strict and formalized engineering replication protocol was found to be necessary because of the large number of variables that need to be controlled in successful CMNS experiments, and the likely presence of at least one uncontrolled variable, often unknown. Step 1 began with the construction and assembly of three electrolytic cells and calorimeters in Omer, Israel, in July and August 2005. These were shipped to SRI and operated initially by Energetics scientists between September and December 2005 using Energetics data acquisition software and hardware.

The phased transition from Step 1 through Step 2 to Step 3 occurred between January and March of 2006. The most significant change involved the transition from the original Energetics data collection software and computers to a functionally equivalent but independent version developed at SRI. A major purpose of this transition was to gain better insight at the raw data level, and to ensure that a systematic error was not present in the (necessarily opaque) LabView data collection algorithms used by Energetics. We distinguish these two phases of operation corresponding to Step 1 and Step 3 above, and roughly to 2005 and 2006, respectively, as "Energetics Data Acquisition" and "SRI Data Acquisition." This separation is for convenience of reporting and should not be regarded as indicating a systematic difference. The results in these two phases are consistent, although overall data quality and reproducibility level were higher in the second phase as a result of experience gained and the number of experiments already performed.

ENERGETICS DATA ACQUISITION

EXPERIMENTAL

In the initial series, nine experiments were performed using the data acquisition procedure and hardware employed originally by Energetics in Israel. This setup consisted of a recent Pentium 4 computer with the Windows XP operating system. Three National Instruments model PCI-6052E data acquisition cards and three Agilent 4338B milli-ohmeters were used – one for each cell – to collect Pd resistance data. An Agilent model 34970A/34901A digital multimeter/20 channel scanner was used to record temperatures. Three Kepco model 50-8 bipolar power supplies were used to supply superwave current to the three cells. National Instruments LabView software (v 6.2 for the Windows) was used to perform all data measurement and instrument control tasks.

The electrochemical cell and calorimeter were as shown in Figure 1, with calorimetric heat flow being measured using the temperature difference between the presumed isothermal boundaries T₄ and T₅. Energetics' practice is to calibrate each calorimeter/heat combination using a dummy joule heating element substituting in position for the anode/cathode electrode "sandwich." Calibrations were performed with the cell containing 230 ml of H₂O, the thermal conduction properties of D₂O and H₂O being considered to not differ significantly.

The results of initial calibration are shown in Figure 5. Energetics record individual temperatures but display excess power using the equation:

$$P_{Out} = K \Delta T$$
 [2]

where
$$\Delta T = T_4 - T_5$$
 [3]

The constant K can be seen in Figure 5 to be not quite unity, and not quite constant for the three different cell bodies. Energetics data acquisition accommodates this temperature dependence of the heat flow coefficient by using a lookup table for K. An equivalent procedure was adopted at SRI by defining a parabolic function for K⁶

$$P_{Out} = \Delta T^{\circ} + a \Delta T + b \Delta T^{2}$$
 [4]

The coefficients ΔT° , a, and b are evaluated by linear regression fit of the calibration heater power versus ΔT as shown in Figure 5.

_

⁶ This function is so close to linear that orders higher than 2 were not needed.

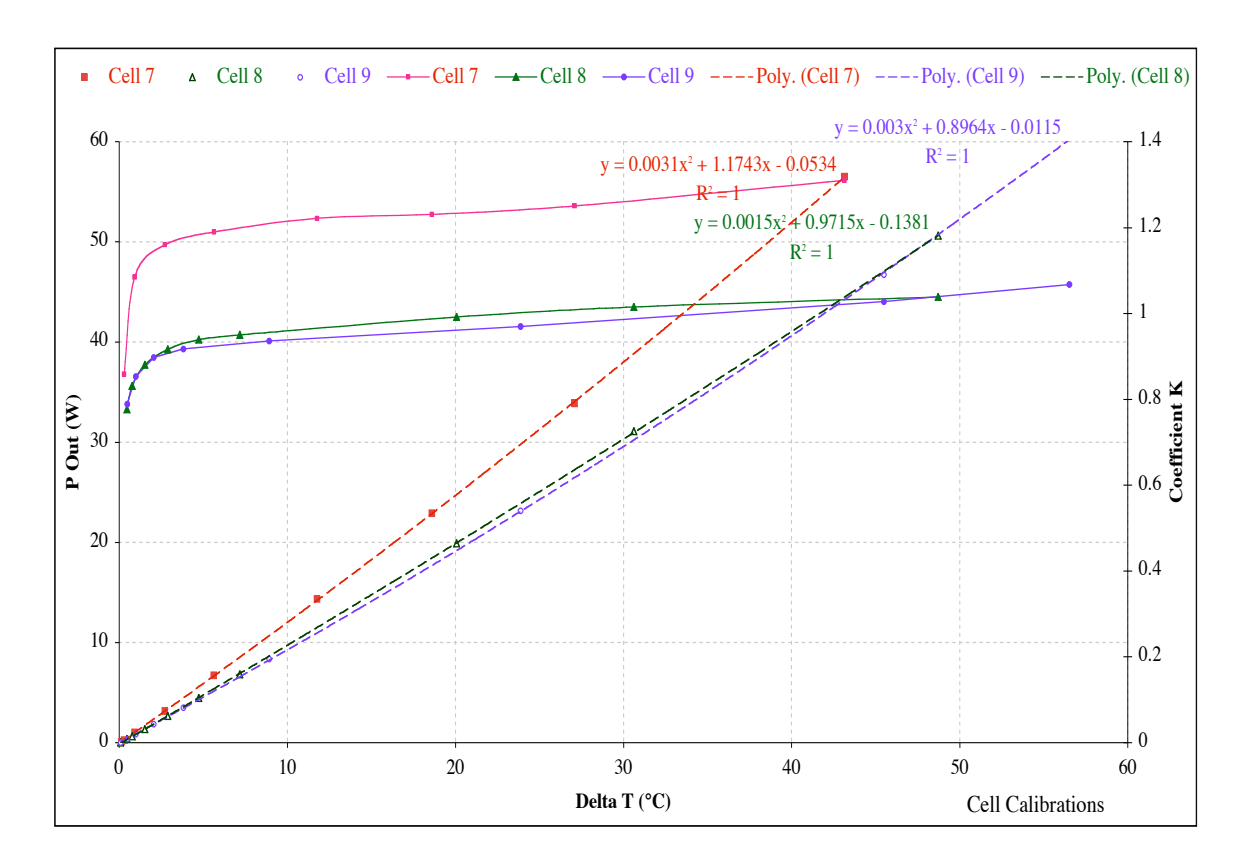


Figure 5. Calibration of calorimeters 7-9.

Although isoperibolic calorimetry is a well-established and much discussed discipline⁷, several factors need further elaboration before results are discussed:

- 1) Offset. The coefficient ΔT° might be expected to be zero. For no input power there should be no ΔT . Two factors contribute to ΔT° , one real and one a measurement artifact.
 - a) <u>Calibration</u>. The platinum resistance temperature devices (RTDs) used in this study⁸ have a nominal 100Ω resistance (R°, with tolerance $\pm 0.012\%$) at T° = 0 °C. To first order the measured resistance,

$$R = R^{\circ} [T^{\circ} + \alpha (T - T^{\circ})]$$
 [5]

so that for $T^{\circ} = 0^{\circ}C$,

$$T / {}^{\circ}C = R / \alpha R^{\circ}$$

References 6-13

⁷ References 6-13.

⁸ PT-100 manufactured by Sensotherm Temperatursensorik GmbH sensor type PTFC

where α is temperature linear coefficient of resistance of Pt (presumed to be known and identical for each RTD). In practice, the RTDs have R values different from 100Ω so that

$$\Delta T^{\circ}_{1} = \left(\frac{R_{4}}{R_{4}^{\circ}} - \frac{R_{5}}{R_{5}^{\circ}}\right)/\alpha$$
 [6]

where subscripts 4 and 5 refer to the calorimetric temperature sensors. This term is accommodated in the Energetic calibration procedure and contributes significantly to the curvature of K as ΔT tends to zero (Figure 5).

b) Ambient heat leakage. Even with well-calibrated temperature sensors, T_4 is observed to be slightly higher than T_5 at zero input power. This real heat leak term is due to coupling of the ambient heat (at typically $22 \pm 2^{\circ}$ C) into the cell through the imperfect insulation of the cell top. For this contribution,

$$\Delta T^{\circ}_{2} = K_{\text{Top}} \left(T_{\text{Ambient}} - \overline{T}_{\text{Cell}} \right)$$
 [7]

where K_{Top} is the effective thermal conductivity of the cell top, penetrating wires and vents, and \overline{T}_{Cell} is some average temperature of the contents of the cell up to and including the T_4 isothermal boundary. This effect also is accommodated with the Energetic calibration procedure, but this term is handled differently using the SRI data acquisition method discussed in the next section.

- 2) <u>Nonlinearity</u>. Deviations from linear heat flow are expected whenever heat leaves or enters the cell by means other than simple conduction. Such means include the convection of water vapor and electrolysis gases out of the cell, and heat transport by radiative exchange between the cell and its environment. These terms are small, so the nonlinearities seen in the Figure 5 calibrations are slight.
- 3) <u>Chemical energy</u>. Exothermic chemical reactions taking place within the cell will produce an offset ΔT. Because of the small chemical inventory these reactions are few (if any), small, and transient. We need to consider two endothermic processes, the first of small thermally but large experimental significance, and the second important in both regards:
 - a) <u>Loading.</u> Absorption of H or D into Pd from the respective molecular gases is an exothermic process up to D/Pd ≈ 0.7 (a little lower for H) at 1 Atm of gas pressure. At higher loading the partial molar enthalpy of absorption becomes positive (endothermic), and the total integrated enthalpy up to the operating point of our cells, D/Pd $\approx 0.925 \pm 0.025$ is endothermic. This is a conservative effect that we have neglected in the following analysis.
 - b) <u>Recombination</u>. In thermodynamically open (although physically partially closed) cells such as those operated by Energetics, the chemical energy of the electrolyzed

⁹ This coefficient is not linear but is closely approximated by a single constant over the limited temperature range of cell operation.

gases, D₂ or H₂ and O₂, are conveyed out of the cell. These may be vented or, as in the case of the Energetics cell design, externally recombined and the recombinant liquid returned to the cell. The rate of the return liquid flow is low at the currents experimentally employed, and the return path is well coupled to the ambient. Thus the returning fluid contributes to the ambient heat leakage (1b above), but the exothermic heat of recombination is deposited largely outside the calorimetric boundary. To account for this endothermic term, the electrolytic input power is modified as

$$P_{In} = I (V - V_{TN})$$
 [8]

Where V_{TN} , the thermo-neutral voltage, is 1.54V for the electrolysis of D_2O and is 1.48V for H_2O , and P_{In} , I and V are all functions of time.

- 4) <u>Calibration errors</u>. The Energetics calibration procedure uses an electrical Joule heater in H₂O whereas active cells use D₂O with the input power being that of electrolysis as given by equation 8. Two systematic differences might be considered to give rise to potential sources of error:
 - a) Properties of water. The thermal conductivity, viscosity and density of H₂O and D₂O are measurably different at the same temperature. These properties affect the conductive and convective transport of heat in the cell from its source near the center to the T₄ thermal integrating boundary. We have not attempted to model the effect of these differences. The strategy in the Energetics (and all similar) calorimeters is to rely on the well characterized thermal barrier between the T₄ and T₅ boundaries to be stable and large, and for the insulation at the top of the cell to be stable and much larger, compared to internal heat paths. Also, if performed after the calorimeter reaches steady state then the different thermo-physical properties of H₂O and D₂O will not significantly affect the calibration or calorimeter accuracy.
 - b) Stirring. A similar issue is raised in comparison of electrical and electrolytic heating. Although electrical heating will cause upwelling to generate convection cells and vortices, ¹⁰ the buoyancy effect of O₂ and D₂ (or H₂) released within the electrode "sandwich" structure is expected to be more effective in promoting cell electrolyte convection. To the extent that this causes a systematic error in the measurement of excess heat from electrolytic cells, this effect may not be calorimetrically conservative. The less well stirred situation of the electrical Joule heater will have higher temperatures near the heat source. If this enhances heat leakage from the top of the cell, the measured T₄-T₅ difference will be lower for the same input power. Again, no attempt has been made to model this potential error source in this study, ¹¹ although it has been discussed previously ¹² and is discussed further in the analysis of results. The best guarantee that the problem is small and the calibration sound is the observation of no excess heat for a dead or dummy cathode.
- 5) Non-steady-state effects. The calorimetry defined by Equations 2, 4 and 8 represents the condition of a steady state. Because of variations in rates and surface conditions affecting

¹⁰ Reference 14.

¹¹ Energetics have compared the calibrations obtained using ohmic and electrolytic heating and have found no difference.

¹² See discussion in Reference 13.

the anode and cathode interfacial impedances, this condition is seldom achieved even with simple dc electrolysis. Use of the complex superwave electrical input guarantees that this condition is never met. Departures from the steady state produce transient excursions caused by delay between the moment of input or excess power change and the time of response of the different temperature sensors. Such effects are easily recognized and do not result in any error in the integral energy. We provide an introduction to the two most important non-steady-state effects here. The corrections are fully described and implemented in the following section, which documents the second phase of research.

- a) $\underline{\delta P/\delta t}$. The power that enters the calorimeter via Equation 8 is presented and measured essentially immediately. In contrast, the output that results and is measured as a rise in T₄, that is converted to power using Equation 2 or 4, is substantially delayed by two factors:
 - i) the rate of heat transport from the electrodes to the cell walls and
 - ii) the time taken to establish a new dynamic balance between the heat flow in, and the heat flow out across the controlled heat leak path between the T₄ and T₅ boundaries.

We therefore expect the output power response of the calorimeter to a step function change in input power, ΔP_{In} at t^o , to exhibit a double exponential delay, something of the form,

$$P_{\text{Out,New}} = P_{\text{Out,Old}} + \Delta P_{\text{In}} \left(1 - e^{-\Delta t/\tau} \right) \left(1 - e^{-\Delta t/\tau} \right)$$
 [9]

where $\Delta t = t - t^{\circ}$ and τ_1 and τ_2 are time constants for heat transfer processes (i) and (ii) above. The three Energetics isoperibolic calorimeters delivered to SRI were observed to follow closely the form of Equation 9, with $\tau_1 \le 5$ minutes (0.083 h) and $\tau_2 \approx 53$ minutes (0.880 h).

b) $\underline{\delta T/\delta t}$. Heat is stored and released from the calorimeter due to the heat capacities of the contents (mostly 230 ml of heavy water), the thermal integrating T_4 cylinder (aluminum), and the thermal insulator (alumina). A correction can be made to the measured output power using the known heat capacities of D_2O and AI,

$$\Delta P_{\text{Out}} = M_{\text{D,O}} C_{\text{p,D,O}} \Delta \overline{T} / \Delta t + M_{\text{Al}} C_{\text{p,Al}} \Delta T_4 / \Delta t$$
 [10]

where M and C_p are the effective masses and heat capacities of D_2O and Al, \overline{T} is the average electrolyte temperature taken as the average of T_1 , T_2 T_3 and T_4 , and Δt is the measurement interval.

SUPERWAVE SIGNAL AND MEASUREMENT

The input perturbation function used in this phase of experimentation was supplied by Energetics and replicates wave patterns used successfully to produce excess heat in their Israel laboratories. The working signal is shown in Figure 6.

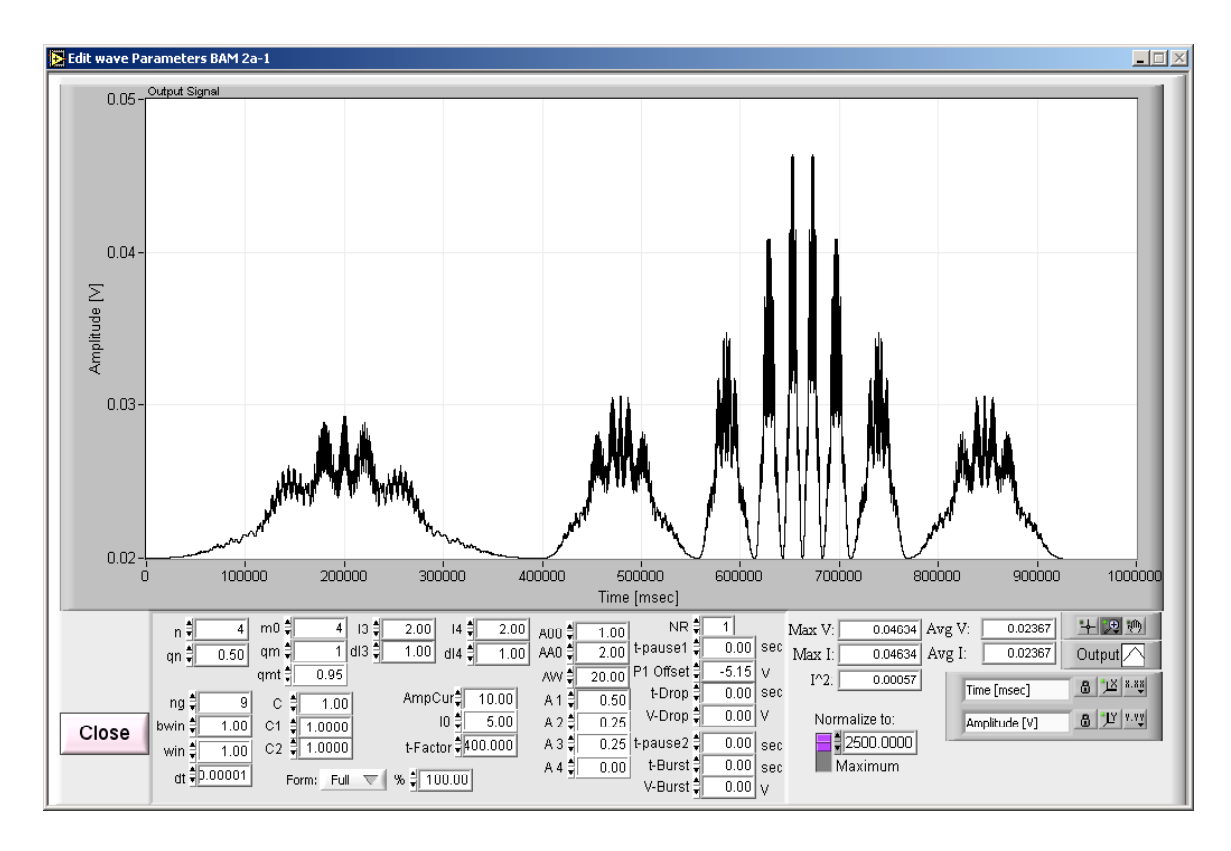


Figure 6. Energetics superwave.

Because of the relatively high-frequency component of the input current function (up to 100 Hz), considerable caution is needed to make accurate measurements of the power as the product of current and voltage using Equation 8. The Energetics data acquisition strategy was to measure the current and voltage independently 50,000 times a second. The Pd resistance and cell temperatures were recorded every 2 seconds.

Each PCI-6052E card was used to both generate the superwave and measure the voltage and current from the cell. The wave was supplied from a file of 1,000,000 current points output to the power supply at the rate of 1,000 points/second and immediately repeated. The voltage proportional to the superwave current was supplied from each cell's respective D/A card to the analog programming input of each cell's respective Kepco power supply. The output of the power supply was connected directly to the cathode and anode of its respective cell. The voltage and current data were collected using the cell's particular power supply's analog output terminals at the rate of 50,000 Hz. Every 2 seconds 100,000 V-I pairs were multiplied, with the average power over that 2-second time interval recorded to hard disk.

The five cell temperatures and the ambient and bath temperatures were recorded using an Agilent model 34970A/34901A digital multimeter/scanner. All seven temperatures were also recorded every 2 seconds. The linear cathode resistances was measured using three Agilent 4338B milli-ohmeters. These meters were coupled to the cathodes using transformers to prevent ground-loops in the system. The four Agilent meters communicated to the computer using the GPIB protocol, via the National Instruments PCI-GPIB card also installed in the computer. At least 20 other calculated parameters were recorded for each cell every 2 seconds.

Because the same complex current inputs are used in calibration, any systematic error introduced by phase effects causing mismeasurement of IV will tend to be suppressed. Comparison also can and has been made between dc and superwave inputs, with no significant input measurement errors revealed.

RESULTS

Nine experiments were performed in this first step using the Energetics procedures and data collection system. The variables studied and results obtained are summarized in Table 1.

Table 1. Step 1 Results; Energetics Data Acquisition.

Number	Started	Electrode	Rolled	Annealed	Min. R/R°	Max. Excess
ETI 009 ¹³	9/9/05 14:00	Lot A	Frascati	Frascati	1.77	< 5%
ETI 011	9/14/05 13:00	L5(2)	Frascati	Omer	1.67	25-60%
ETI 012	9/17/05 12:56	Lot A	Frascati	Frascati	1.84	< 5%
ETI 015	11/8/05 12:34	L5(1)	Frascati	Omer	1.77	< 5%
ETI 016	11/10/05 10:40	L5(4)	Frascati	Omer	1.86	< 5%
ETI 017	11/11/05 10:19	L1(1)	Frascati	Omer	1.55	20%
ETI 021	1/9/06 12:28	# 830	Frascati	Frascati	1.92	< 5%
ETI 022	1/9/06 17:20	L5(3)	Frascati	Omer	1.80	30%

Figure 7 shows the calorimetric results of the first 360 h of electrolysis of cell ETI 016-8. This cell employed a cathode prepared at ENEA Frascati but annealed by Energetics in Omer. The cathode loaded to a minimum resistance of 1.86 on the right side of the resistance maximum, corresponding to a maximum loading of D/Pd \approx 0.87. This is a low loading value, and no excess power was observed outside the measurement uncertainty. This result is reported to demonstrate the quality of the calibration and the performance of the calorimeter in response to the superwave input.

_

¹³ The experiment designation used throughout the report is ETI (Energetics Technology Inc.) plus laboratory notebook page number (*e.g.*, 006) with a suffix -7, -8 or -8 to specify the calorimeter body in which the experiment was performed.

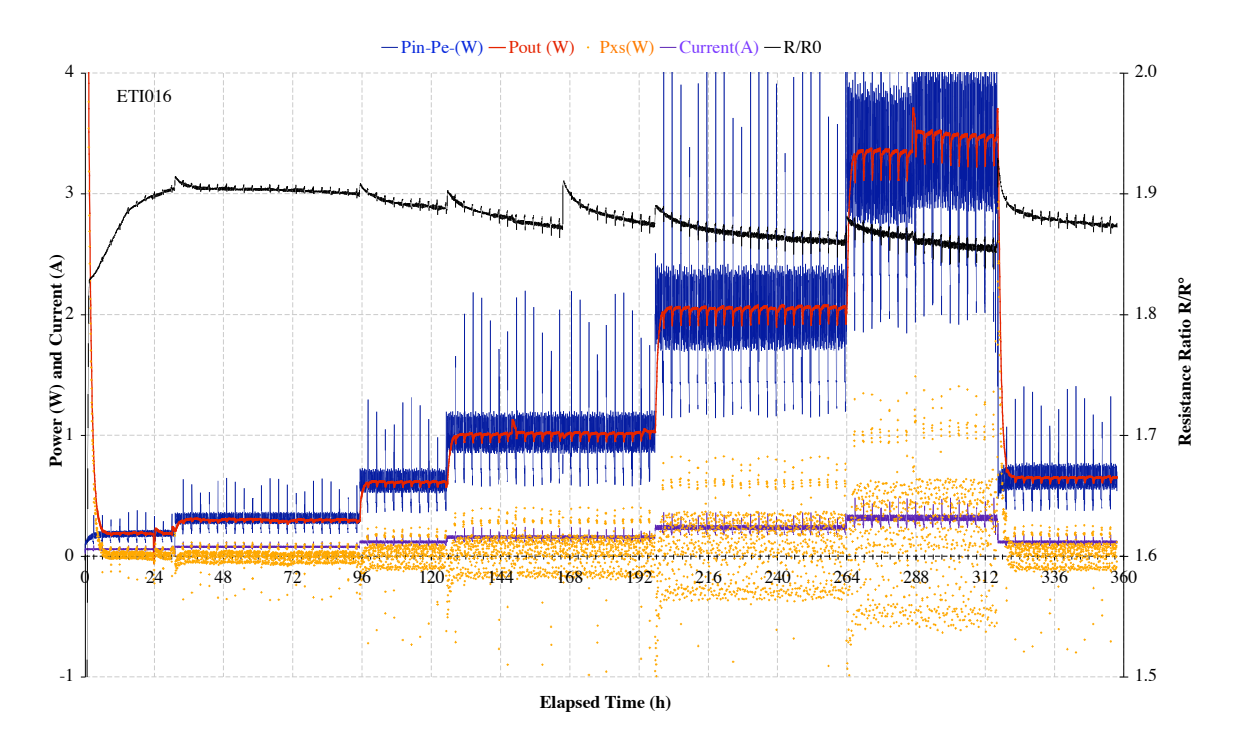


Figure 7. Results of ETI 016-8.

The solid black line at the top of Figure 7 is the temperature-corrected resistance ratio referred to the right axis. Plotted on the left axis are the input, output, and excess power in watts, as these respond to the changing in cell current in amps. The sharp spikes in the input power correspond to the superwave current maxima shown in Figure 6. Because of the thermal integrating character of the calorimeter (Equations 9 and 10), the power output response is damped but nevertheless has the same average value as the input power. The excess power, calculated as the difference between the measured output and input powers without attempt to correct for non-steady-state departure, shows considerable scatter (\sim 10% of P_{In}). The average value of P_{XS} is, however, very close to zero, indicating that this means of calorimetry is perfectly adequate to obtain an average null thermal balance. The total excess energy calculated as the integral of P_{XS} in the interval shown in Figure 7 was -0.1 ± 5 kJ.

Figure 8 plots the calorimetric results for a slightly longer period of cell ETI 017-9. The two cells, ETI 016 and 017, were operated simultaneously with aliquots of the same electrolyte, identical data acquisition systems, and intentionally similar cathodes. Nevertheless, the loading obtained in ETI 017 and the excess power response were significantly greater, as can be seen by comparing Figure 8 to Figure 7.

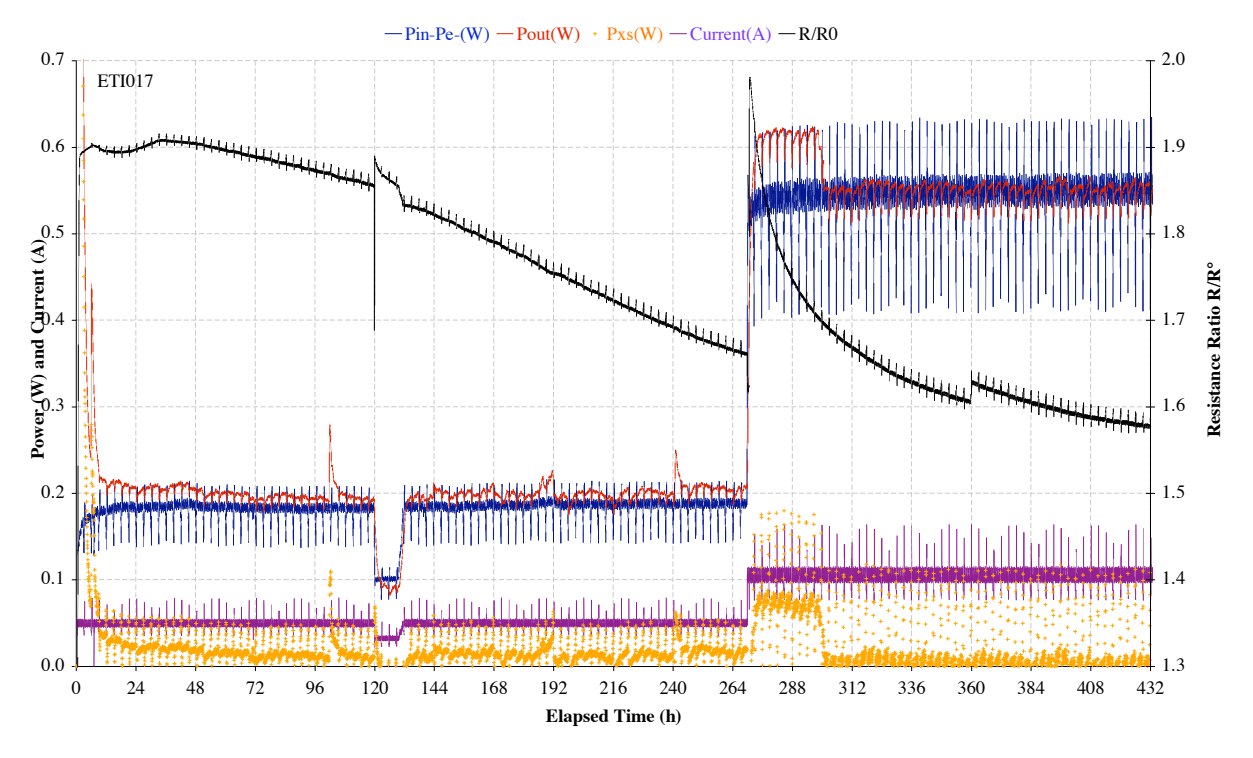


Figure 8. Results of ETI 017-9.

The scales in Figures 7 and 8 are different to reflect the greater loading (lower R/R°) at lower input power for ETI 017. Several other features of Figure 8 are significant. When rational calorimetry was first achieved at ~12 h after initiation, the output power appeared to be slightly, but systematically and significantly, above the input. An attempt was made to verify the calorimeter calibration and ensure that the small apparent power excess was not due to an offset error ΔT° as discussed above in relationship to Equation 5. At ~120 h the input current was reduced from an average value of ~50 to ~30 mA. As a result of this change, the loading decreased and the output power dropped to a value close to or possibly below the input. When the cathodic current was restored, the output and excess powers returned approximately to their prior values. At a later stage of the experiment, some days after the current had been increased to an average value of ~100 mA, the input and output power measured the same average values and the excess power average fell to zero. The results of these tests tend to indicate that there is not a temperature offset error in the calorimeter and that meaningful excess power was present in this experiment essentially from the beginning. This point will be further examined in the Discussion and Conclusions section.

Probably the most interesting feature of Figure 8 is the response of the loading and excess power at \sim 270 h. Following a brief current strip, the average cathodic current was stepped from \sim 50 to 100 mA. The electrode responded in an extremely dynamic manner with rapid absorption of deuterium evidenced by the decreasing R/R $^{\circ}$, and an apparent burst of excess power of average amplitude roughly 80 mW for \sim 24 h. At the end of this time the excess power fell to zero, possibly correlated with the decreased rate of deuterium absorption, but not obviously associated with any other or intentional manipulation of the cell. This 15-20% effect, while small

in absolute value ($P_{XS} \sim 80$ mW), appears to have been stimulated by a rational trigger (current and loading increase) and to have disappeared spontaneously. These two features of the data increase our confidence in the reality of this observation. At ~ 300 h the average excess power fell to zero and remained zero for the duration of the experiment.

An earlier result also obtained with foils produced at ENEA and annealed in Omer (see Table 1) conformed more closely to the behavior of excess power observed previously at SRI (and predicted by Equation 11 as discussed in the next section). Figure 9 plots current and input, output and excess power on the left axis and resistance ratio on the right axis for a 360 h (15 day) period commencing 18 h after experiment initiation. This lapse in early time is due to an experimental problem that resulted in failed data storage. By the time this problem had been remedied, the cathode was already well loaded ($R/R^{\circ} = 1.7$ implies a D/Pd loading of \sim 0.91) and the cell was apparently producing \sim 110 mW of excess heat at an average input power of 150mW and current of \sim 60mA. In an attempt to produce higher levels of power excess, the average current density was stepped progressively to 90, 120, 210 and 270 mA. The current step at \sim 258 h was accompanied by an inadvertent doubling of the superwave generation rate. This was corrected at \sim 300 h.

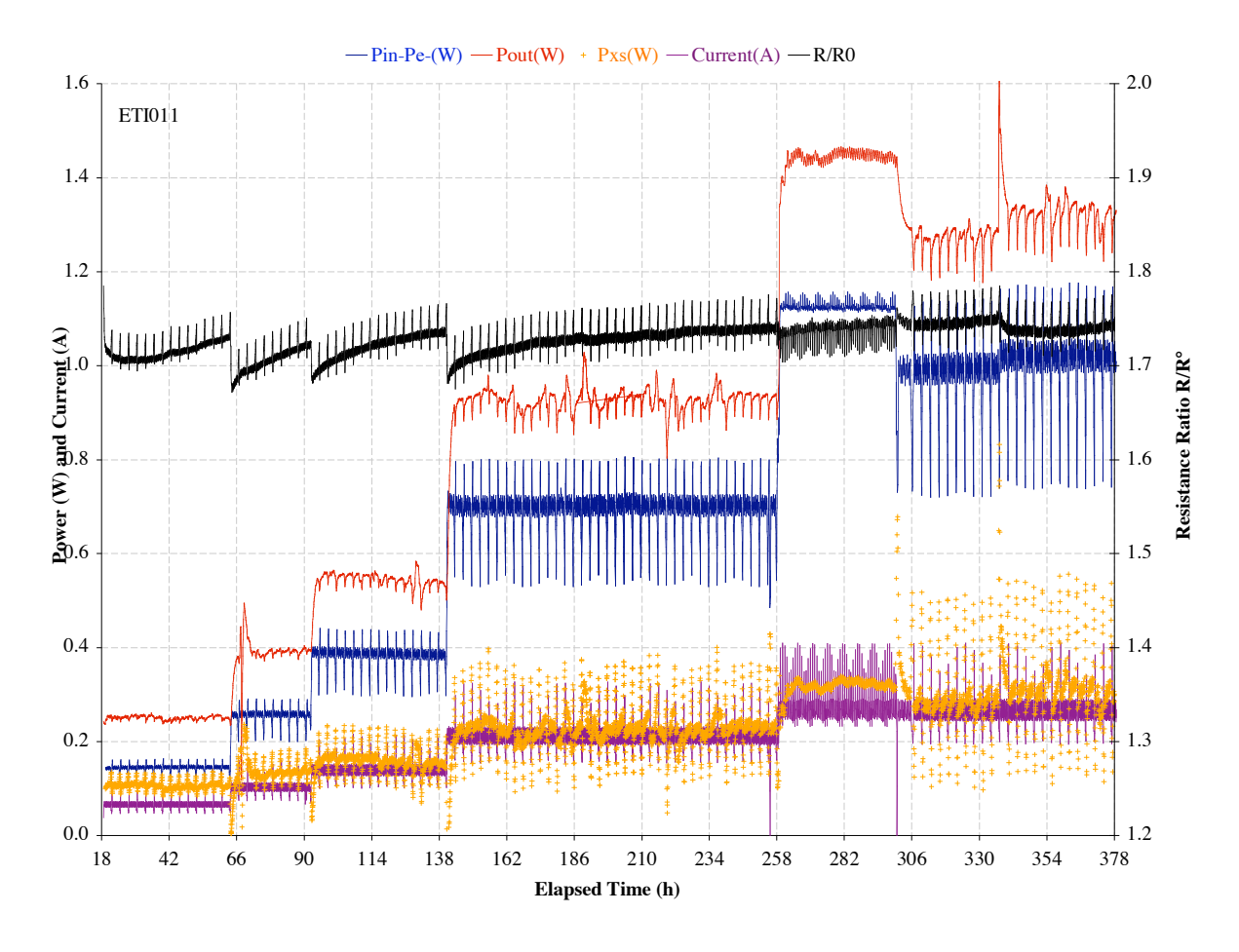


Figure 9. Results of ETI 011-8.

Several features of Figure 8 are of interest:

- 1) The initial tendency of the cathode response to increasing current density is to absorb deuterium (*i.e.*, reduce R/R°) but then to deload with time. The double rate superwave from ~258-300 h appears to benefit loading since the resistance ratio rose spontaneously when the generation rate was restored to its original lower value. The deloading trend with time nevertheless remains unchanged.
- 2) Accompanying the higher rate superwave from ~258-300 h, in addition to higher loading, are markedly higher input and output power and a small but potentially significant increase in excess power. It should be noted here that this result was recognized but technical difficulties of signal generation and data collection prevented us taking advantage of it at that time.¹⁴
- 3) An apparently spontaneous change in the cell conditions resulted in increased voltage, output power, excess power and loading at ~337 h. Since the increases involve both loading (related to absorbed D activity and therefore cathode surface voltage) and cell voltage (an increase of 345 ± 22 mV), one is tempted to attribute the "spontaneous" effect to modification of the cathode surface. Whatever the cause, the loading increased (R/R° decreased from 1.751 ± 0.008 to 1.745 ± 0.12 , corresponding to an average D/Pd increase of 0.0014 or 0.14%), and the excess power increased from 0.30 ± 0.01 to 0.36 ± 0.01 W.

The maximum excess power observed in cell ETI 011 was $\sim 0.36 \pm 0.01$ W or $\sim 30\%$ of P_{ln} .

¹⁴ Because of limited bandwidth in both the digital-to-analog and analog-to-digital conversion. It is recommended in future implementations of this experiment that higher input frequency components and faster data acquisition systems be employed.

SRI DATA ACQUISITION

INTRODUCTION

With satisfactory completion of Steps 1 and 2 of the SRI replication protocol, an attempt was made to replicate Energetics' excess heat observations using a Macintosh-based signal generation and data acquisition system developed independently at SRI. This phase of the program was undertaken in two steps: Joule heater and light water calibrations followed by examination of 15 cathodes from three different sources undergoing superwave electrolysis in heavy water electrolytes.

The results of this campaign are shown in Table 2. The first point of interest is the consistently high and occasionally very high loadings obtained in the cathodes. In previous experiments covering a number of years, we have occasionally been able to approach the loadings shown in Table 2 using well-prepared wire cathodes, but we have never approached these extreme values using foil cathodes, which are much more difficult to control. While it was not our purpose to examine the point systematically, we speculate that the remarkable levels and consistency of loading reported in Table 2 are a result of both the very sophisticated metallurgical control of the palladium cathode before loading that been achieved by ENEA and Energetics, and the use of superwave modulated electrolysis currents.

Consistent with the measured high loadings we also observed highly but not totally reproducible excess heat production. The lack of complete reproducibility has three different origins, discussed more fully below:

A) The three sigma (3σ) calorimetric uncertainty was estimated to be approximately 5% of P_{In}. Of the 15 experiments listed in Table 2, 11 produced excess heat greater than the 3σ experimental uncertainty. As far as we are aware, this level of reproducibility is hitherto unprecedented in the fields of cold fusion or condensed matter nuclear science (CMNS). Failure to obtain systematic replicability in CMNS experiments where success rates in previous years have been more typically 10-30% is frequently attributed to the presence of hidden or uncontrolled variables. If such should be the case, then the increased level of replicability shown in Table 2 may suggest that the use of superwave rather than dc, ac, or pulse perturbation directly or indirectly affects one or more parameters controlling excess heat production. One plausible candidate is the interfacial deuterium flux, known to be a factor in the rate of excess heat production. Both the interfacial deuterium flux and the loading that it controls are strongly enhanced by the presence of superwave cathodic current stimulation.

-

¹⁵ References 15-25.

¹⁶ Reference 19

Table 2. Step 2 Results; SRI Data Acquisition.

ETI	Calor.	Duration	Electrode	Best R/R°	Best D/Pd	Max mW	Pxs %		W/cm ³	MJ/ Mole	eV/ atom
61 57	7a 8a 8b	897 500 1058	L25B-1 Pd-SWNCNT	1.63 N.A.	0.924	105 93	50% 300%	_	4 3	5 4	56 44
58	8c 9a 9b	1356 500 1021	Platinum L25A	1.80 1.69	0.888 0.911	540	200%	485	19	17	187
56	7	335	L24F	1.55	0.940	2095	15%	536	75	19	206
56	8	161	L24D	1.84	0.877	8	4%	1	0	0	0
56	9	232	L25B-2	1.56	0.937	105	3%	24	4	1	9
51	7	500	L25B-1	1.55	0.939	266	12%	176	10	6	68
51	8	500	L25A-2	1.52	0.945	133	5%	14	5	1	5
51	9	500	L19	1.54	0.941	79	43%	28	3	1	11
43	7a	500	L14-2	1.73	0.904	110	80%	65	4	2	25
	7b	741		1.76	0.897	1250	13%	245	45	9	94
43	8a	500	ETI	1.63	0.923	525	5%	65	19	2	25
43	8b	500	L14-3	1.73	0.903	8	1%	2	0	0	1
	9a	658		1.61	0.927			2			
35	7a	536	L17-850	1.35	0.979	1800	12%		64		
	7b	822		1.32	0.986	700	3%	553	25	20	213
35	8a	536	L17-850	0.97	1.055	710	10%		25		
	8b	822		0.95	1.060	2066	13%	313	74	11	120
35	9a	536	JM-900	1.38	0.973	100	1%		4		
	9b	822	-Quench	1.39	0.972 0.944	150 ±	1% 0.049	2	5	0	1

B) Earlier work at SRI performed using 1mm Pd wire rather than 50µm thick foils showed that the excess power measured in a high-precision mass flow calorimeter¹⁷ was proportional to the product of three variables:

$$P_{xs} \alpha \left(\underline{i} - \underline{i}^{\circ}\right) \left(\underline{x} - \underline{x}^{\circ}\right)^{2} |\underline{\delta x}/\underline{\delta t}|$$
 [11]

References 19 and 25.

where i is the electrochemical current or current density and i° a critical threshold (typically 20-50% of i_{Max}), x = D/Pd is the deuterium loading, with x° the threshold loading below which no effect is observed (typically x° \approx 0.875), and $|\delta x/\delta t|$ is the rate of change of loading associated with the flux of D atoms through the interface, irrespective of sign.

Some of the failures to produce excess heat in the experiments summarized in Table 2 can be attributed to a failure to meet simultaneously the conditions of Equation [11]. In general, and particularly for experiments ETI 043-9 and ETI 056-9, this was due to a failure to maintain loading at high current densities, and thus a failure to exceed i° and x° simultaneously, as discussed below.

C) Two different modes of current-driven excess heat production were observed in successful experiments. The first conformed closely with the form of Equation [11], although with some differences from the result previously obtained, ¹⁸ suggesting a systematic difference between thin wire and flat foil cathodes possibly associated with different metallurgy or different surface area ratios. This mode we describe as "typical SRI" heat production or SRI Mode A.

A second mode of behavior was seen in three experiments, all of them exhibiting excess power greater than 100%. This mode is more typical of that reported previously by Energetics, and we describe this as ETI Mode B. In this mode the excess power is relatively insensitive to input power and current. It may be present early in the loading history of a cathode and may persist after cessation of input current. Thus we observe not only an apparent variability in the extent of excess heat produced by an electrode, but also in the mode of heat production and the timing of this heat release.

Experiments were performed in the manner described in the "Experimental" section of "Energetics Data Acquisition," with the exception of the experiment control, data acquisition, and some details of data analysis as described below.

The ETI measurement control and data acquisition system operating in LabView and running on a PC was rewritten from the ground up at SRI to run in the Macintosh operating environment. This change was not made in response to problems detected in the first phase of experimentation, but rather in part to allow for greater flexibility in parameter control and measurement. A complete rewrite also allowed us to view and comprehend better the ETI strategy of data acquisition written in the somewhat opaque LabView code, and thus ensure that the experimental results obtained did not arise from systematic measurement error.

The following variables were measured and recorded for each operating cell as average values in a 1-minute measurement interval.

i) The cell electrolyte temperatures, T_1 , T_2 , and T_3 ; the calorimetric thermal boundary temperatures T_4 and T_5

¹⁸ Reference 19.

¹⁹ References 1-3 and 26.

This is partially accounted for by failure to achieve or maintain the threshold values of equation 11.

- ii) The real and imaginary components of the cathode four terminal axial impedance measured at 1 KHz, Z_{real} and Z_{imag.}
- iii) The product of current and voltage with and without the subtracted thermo-neutral voltage, I $(V - V_{TN})$ and I V.

In addition, the controlled bath temperature and ambient temperatures were also measured and recorded each minute. All the above temperature measurements were made using (nominally) 100 Ω platinum RTDs.²¹ These RTDs were calibrated with respect to a quartz crystal temperature standard.²². Calibrations of the RTDs critical to calorimetry (T₄ and T₅) were made at the beginning and end of each experiment, and occasionally checked during an extended experiment.

Using a strategy similar to that used in 2005, we employed an Apple Power Macintosh G4/733 computer with National Instruments PCI cards (PCI-6143 and PCI-6731) to generate the superwave and measure the instantaneous power. Three Kepco model 50-8 bipolar power supplies were used to supply superwave current to the three cells. National Instruments LabView software (v 7.2 for the Macintosh) was used to perform all data measurement and instrument control tasks.

The three independent superwaves were generated using the PCI-6173 card. The wave was supplied from a file of 180,000 current points output to the power supply at the rate of 200 points/second and immediately repeated. The voltage proportional to superwave current was output to the analog programming input of each cell's respective Kepco power supply. The output of the power supply was connected to the cathode and anode of its respective cell through a 1.000 ohm current shunt. The voltage across the shunt was used to measure the current. All six voltages and currents from the three cells were collected 100 times a second using the PCI-6143 card. The individual products of the instantaneous currents and voltages were averaged and recorded every minute.

One Hewlett Packard 4338A was used the Pd resistance from the three cells. One Keithley model 2001 digital multimeter was used to measure the current and voltage from all three cells. A Keithley model 706 switcher/scanner was used to direct the Pd resistance wires to the 4338A and the 17 temperature sensors to the 2001.

CURRENT PERTURBATION

Electrolysis conditions in the cells were controlled using a computer synthesized superwave signal delivered to the cells by four quadrant Kepco BOP 50-M power supplies operated in controlled current mode. While not rigorously specified mathematically, the rules for generating a superwave require a signal of self-similar character to a kernel function that increases in frequency and amplitude as the amplitude of the kernel increases.

In principle, the self-similar application of this rule up-scale and down-scale to higher and lower frequencies occurs without limit in either direction. In practice we are constrained by our ability to deliver and measure signals. The low frequency limit is imposed by what is a practical

²¹ Omega #PR-11-3-100-1/8-12-E. ²² Hewlett Packard 2804A.

or natural interval in the loading cycle of a PdD cathode. For most of the experiments described below this interval, the cycle or fundamental repetition rate was set at 15 or 20 minutes.

A practical high frequency limit is imposed by the ability of the power supply to deliver and the electrochemical system to accept high-frequency currents. The largely capacitive character of the electrode interfacial impedances demand higher and higher currents with increasing frequency. A second experimental limitation is imposed by our ability to measure accurately the average power input and thus to perform accurate calorimetry. The high frequency limit was constrained by the Nyquist-Shannon sampling theorem²³ to 100 Hz, making the superwave effective frequency range ~1 mHz to ~100 Hz, a dynamic range of ~10⁵.

Superwave perturbations were constructed within the constraints discussed above, using some additional rules relating the maximum and minimum amplitudes discovered by ETI to be effective in promoting loading and excess heat, and the natural 1 minute (16.66 m Hz.) averaging and recording interval. Integral minute intervals were used to prevent aliasing in the measured data. One example of a superwave used in the experiments described below is shown in Figure 10. In this simple example the kernel is a sine squared function with a fundamental period of 15 minutes. Five levels of nesting are used, each 15 times higher in frequency than the preceding to yield a 1-minute periodicity consistent with the measurement input averaging interval, and higher terms.

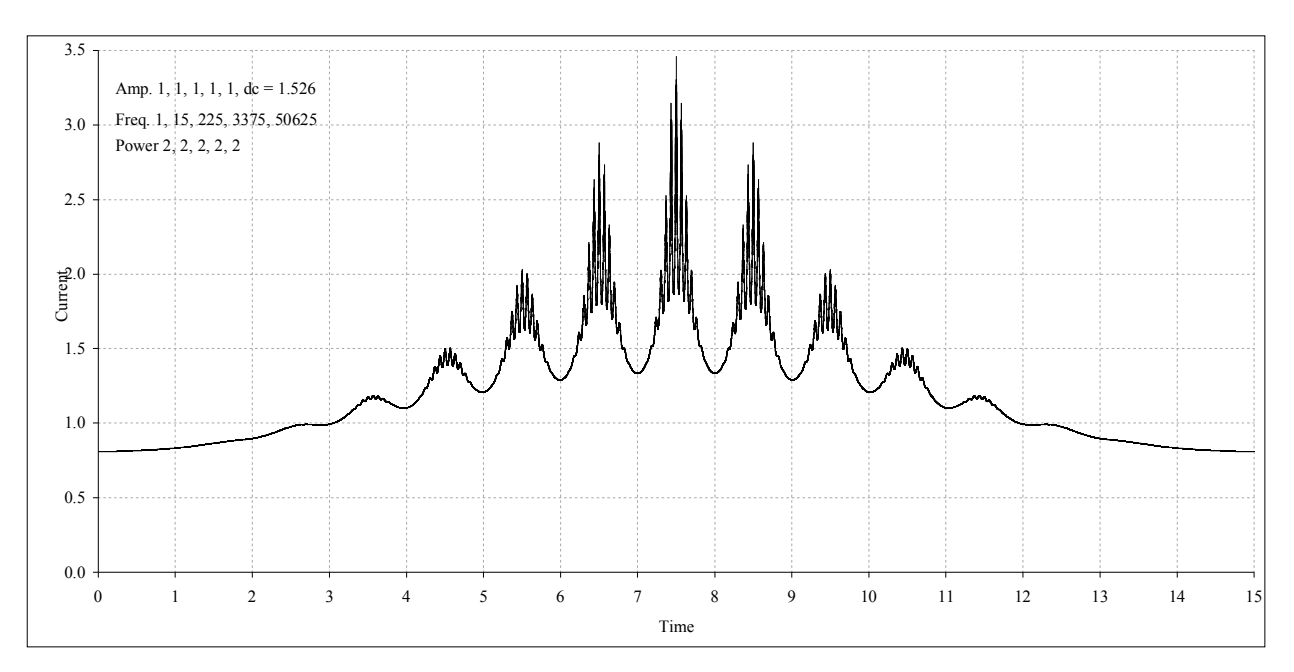


Figure 10. Fifth-order superwave.

²³ Exact reconstruction of a continuous-time baseband signal from its samples is possible if the signal is bandlimited and the sampling frequency is greater than twice the signal bandwidth.

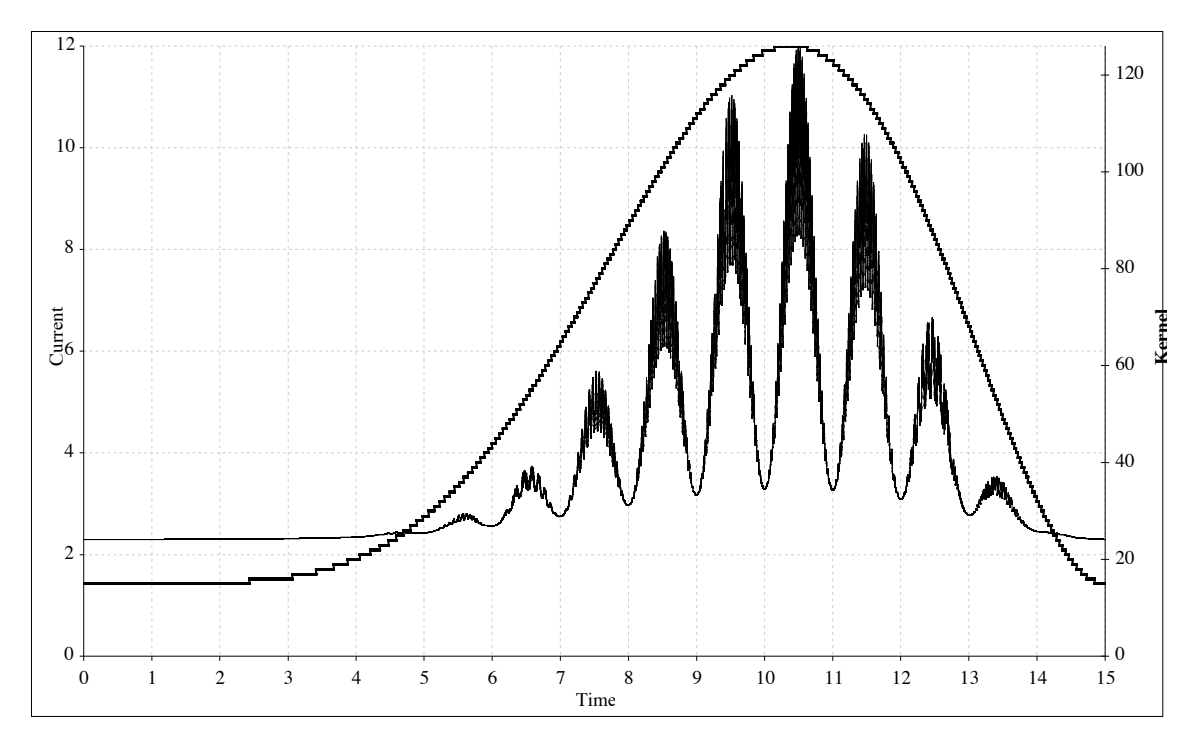


Figure 11. Asymmetric superwave.

Although it is not possible to resolve the higher frequency components in Figure 10, the general intention is to exercise all frequencies over as wide a range as possible with the greatest excitation amplitude at the highest frequencies and *vice versa*. More elaborate functions can and have been used. Figure 11 shows an example with frequencies restricted to 50 Hz and also with five nested levels, but with an asymmetric kernel. Obviously this can be run either forward or backwards to produce a slow uptake and rapid release of deuterium from the cathode, or the reverse.

In practice, calculated values such as those plotted in Figures 10 and 11 were read from the hard disk as digital text into a buffer memory within the LabView data acquisition program, and read out as a loop through PCI-6052E digital-to-analog converter with a controlled scale factor to the input of the analog power supply controlling these cells. Data were processed on two time scales: a 1-minute average corresponding to a single excursion between local minima (see Figures 10 and 11) and a 15- or 20-minute average mirroring the period and looped repetition rate of the generating function.

NON-STEADY-STATE ANALYSIS

Because of their coinciding periods, most of the high-frequency components of the generating function are averaged in the 1-minute data acquisition interval. Nevertheless, the 1-minute averaged input power varies considerably through the looping interval so that the calorimeter is always seeking its steady-state output power in accordance with Equation [9]. Without correction for varying $\delta P_{In}/\delta t$, the calorimetric data show considerable scatter as seen in Figures 7-9. Although this scatter is not random, its presence makes it not possible to operate the calorimeter at the desired sensitivity level of 1 or 2%.

Equation [9] shows two exponential time constants in the response of P_{Out} to a stepped change in P_{In} . A relatively rapid exchange of heat occurs between the electrodes and the inner integrating T_4 boundary, with time constant $\mid 1 \geq 5$ min. A slower equilibration occurs in the temperature difference between the T_4 and T_5 boundaries as the calorimeter seeks to balance P_{In} and P_{Out} after a change in P_{In} . The time constant of this second process was measured to be about 53 min.

Because of the short time constant compared with input looping period, the consequences of τ_1 have little effect on calorimetric precision. This is not true for τ_2 for which six time constants require ~ 5.5 h to complete. To account for the effects of τ_2 , measured calorimetric individual data points were processed retrospectively by adding the result of the following summation:

$$\Delta P = \sum_{\Delta t = 0}^{360} \Delta P_{\text{In},\Delta t} \left(1 - e^{-\Delta t/\tau_2} \right)$$
 [12]

That is, the output power was corrected using the sum of the exponential decay response to each stepped change in P_{In} from the preceding 360 1-minute measurement intervals (6 h) of P_{In} . At this point the response of P_{Out} has achieved 99.9% of its steady-state value for $\tau_2 = 0.88$ h. This analysis was applied to all data sets discussed below.

For some data sets, particularly those in which the bath temperature was changed, corrections were also made for the effect on P_{Out} caused by the heat capacity and changing temperature of the cell contents. The mathematical form of this correction is given by equation 10, which is repeated here for convenience.

$$\Delta P_{\text{Out}} = M_{\text{D}_2\text{O}} C_{\text{p},\text{D}_2\text{O}} \Delta \overline{T} / \Delta t + M_{\text{Al}} C_{\text{p},\text{Al}} \Delta T_4 / \Delta t$$
 [10]

In practice, because both \overline{T} (the average temperature of the cell contents) and T_4 are slow-moving functions of time, $\Delta \overline{T}/\Delta t$ and $\Delta T_4/\Delta t$ can both be calculated as the slope at the respective time series functions, $\delta T/\delta t$, at each point in the data series.

It is important to remember that the form of the non-steady-state corrections is such that, while these can significantly improve calorimetric precision, they do not affect the accuracy of total excess energy generation. The round trip integral effect of both the $\delta P/\delta t$ and $\delta T/\delta t$ corrections expressed by Equations [10] and [12] is zero for the same initial and final conditions.

ETI 035

The first set of three heavy water cells using the SRI data acquisition and new calibrations employed two ENEA cathodes and one prepared by ETI, as shown in the table below.

Calorimeter	Electrode	Anneal	Etch
7	L17 ENEA	850°C	60s HNO _{3 +} 120s 50% Aqua Regia + 15s HNO ₃
8	L17 ENEA	850°C	60s HNO ₃
9	ETI	900°C Rapid quench	60s HNO _{3 +} 120s 50% Aqua Regia + <5s HNO ₃

Each cell was operated for a period of 822 h (34 days) using a variety of superwave inputs for both loading and unloading as parameters suitable to maximize loading and excess heat effects were explored. Both the ENEA cathodes loaded extremely well. Both these cells also exhibited excess heat of the form previously described as SRI (Mode A) with a maximum value of \sim 1W and 10-15% of P_{In} .

Figure 12 plots the resistance ratio and calculated loading for ETI 035-7 for a period of 22 days during the course of the experiment. Points in the upper set referenced to the right axis indicate the resistance ratio $R/R^{\circ*}$, where R is the measured four-terminal axial resistance and $R^{\circ*}$ is the initial resistance ratio at t=0 before application of cathodic current, corrected by the instantaneous cell electrolyte temperature \overline{T} = average $[T_1:T_3]$. The bottom points are the calculated loading²⁴ referred to the left axis.

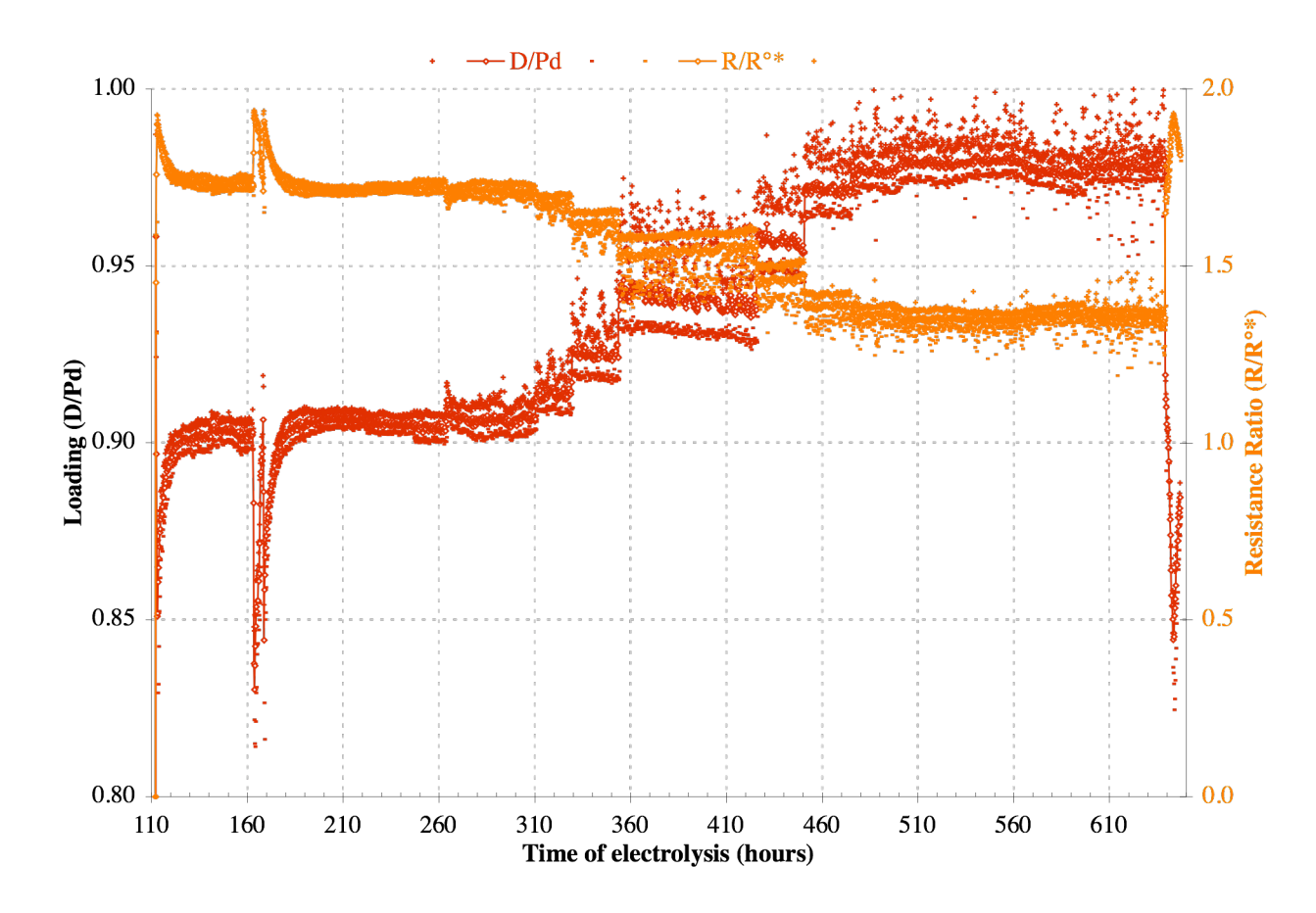


Figure 12. ETI 035-7 Loading and Resistance Ratio.

-

²⁴ Reference 4.

All data in Figure 12 were obtained by applying a superwave stimulus with fundamental period 15 or 20 min. Superwaves also were used to partially deload the cathode just before 112 h and again at \sim 164 h. The purpose of these deloadings was to remove surface films and enhance deuterium uptake. A dc anodic current was used in the final deload at \sim 640 h in order to redefine the position of the resistance maximum (expected²⁴ to be R/R°* = 1.96).

Three points are plotted for each data set: the maximum, average, and minimum values in the 15- or 20-min superwave period. Two significant features can be observed in Figure 12:

- i) The minimum average resistance ratio, measured on the right side of the resistance maximum R/R°* = 1.34, corresponds to a loading D/Pd over 0.98. This extreme value has rarely been seen in heavy water electrolysis, and to our knowledge never before with foil rather than wire cathodes. The combination of superwave loading and ENEA metallurgy results in a lattice condition that is of considerable interest in the study of possible condensed matter nuclear effects, but which may also have broader implications in the field of hydrogen loading in metals.
- ii) The dynamic range in the resistance and loading is also remarkable. The difference between the minimum and maximum loading values in the measurement interval reflects a flux of D atoms across the cathode interface. This flux, driven by the superwave excitation, is also believed to be closely associated with SRI Mode A excess heat production. This net deuterium exchange flux $|i_D|^{26}$ reaches a maximum of 9 ± 1 mA cm⁻² at an average electrochemical current density of 58 mA cm⁻². Thus approximately 15% of the current is causing D atoms to move through the interface into and out of the cathode.

The form of excess heat production previously observed at SRI and described above as "SRI Mode A" conforms approximately to the equation

$$P_{xs} = M (x - x^{\circ})^{2} (i - i^{\circ}) |i_{D}|$$
 [13]

where M is the proportionality constant, $|i_D|$, the flux of D across the interface, replaces $\delta x/\delta t$, and the other parameters are as defined for equation [11]. This form of excess heat production was observed for cells ETI 035-7 and -8, while cell ETI 035-9 demonstrated a good thermal balance.

Figure 13 plots the input current and power, and the output and excess power and energy for cell ETI 035-8 in an interval of \sim 11.5 h of power cycling. The inset shows the region of high current density where excess power was observed at t > 400 h. Although the maximum excess power in this interval is only \sim 9% of P_{In} , the accumulated energy integrated up to 640 h when the event was terminated by reducing the current density, was over 310 kJ. This is far larger than

_

²⁵ The value measured for the twin cathode in ETI 035-8 was even higher. Due to experimental problems this latter resistance was measured in a three- rather than four-terminal mode and is thus subject to greater uncertainty. With this caveat, the maximum measured loading in ETI 035-8 was D/Pd = 1.06 ± 0.02 .

²⁶ The magnitude value $|i_D|$ is calculated from the maximum and minimum values of the molar deuterium loading in the palladium electrode determined from the measured resistance ratio in the superwave excitation period (15 or 20 min).

can be accounted for by chemical effects.²⁷ The black points in Figure 13 labeled "Predicted" are calculated from Equation [13] using $x^{\circ} = 0.875$ D/Pd, $i^{\circ} = 35$ mA cm⁻², i_{D} is calculated from the average rate of change of loading in the superwave interval (15 or 20 min) and M = 50. With the exception of i°, which is about 5 times smaller current threshold, these numbers conform closely with those observed previously²⁸ for 1 mm Pd wire cathodes. A salient difference, however, is that in previous cases at SRI the loading variability measured with dc electrolysis was a natural phenomenon not expected and not fully under experimental control, while in this case fluxing is induced by superwave perturbation.

Figure 14 plots the observed excess power and that predicted from Equation 13 for cells ETI 035-7 and -8. Although there is expected and evident scatter, the two populations of observed and "predicted" excess power are consistent within, but not between, experiments. For ETI 035-7 the slope of P_{xs} vs P_{In} is considerably higher, with higher threshold value.

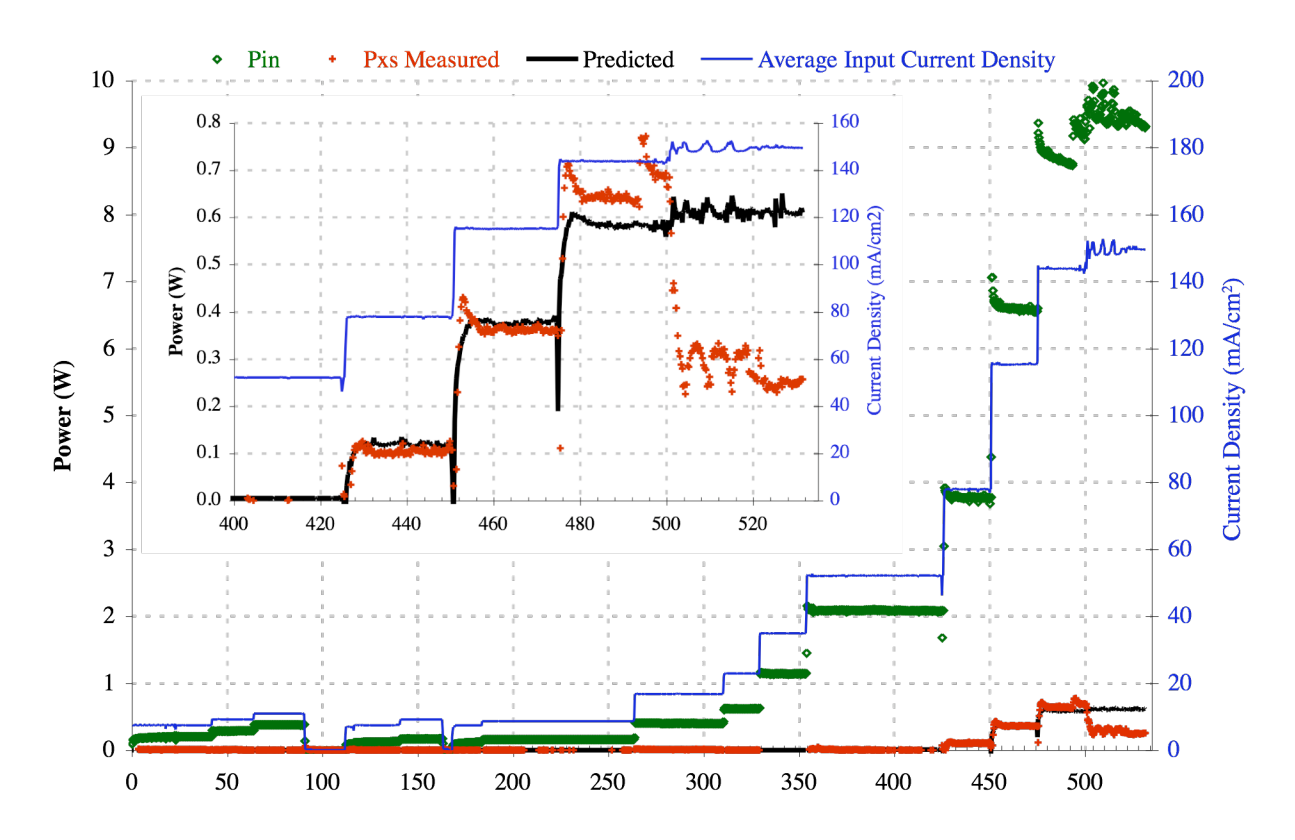


Figure 13. ETI 035-8 Power and Current Density.

 $^{^{27}}$ 316 kJ/4.9mM of Pd = 65 MJ/Mole or ~ 700 eV per Pd atom. 28 References 19 and 25.

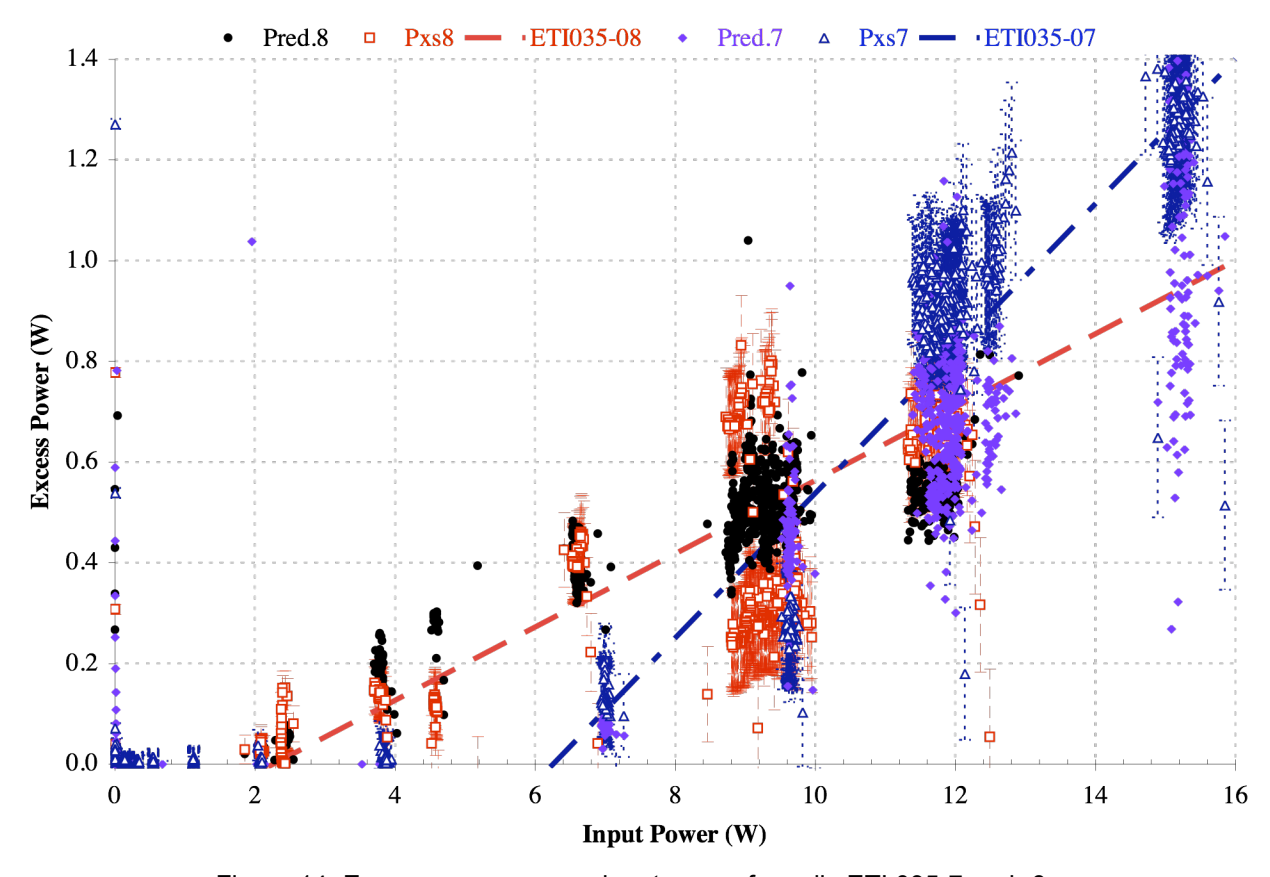


Figure 14. Excess power versus input power for cells ETI 035-7 and -8.

Table 3 presents the values of the coefficients of Equation 13, M, x° , i° , and the average value of $|i_D|$, and P_{In} , for cells ETI 035-7 and -8. It is clear from these values that the late onset of excess power in cell -7 is due to the high current threshold, but that the relatively high slope of the excess power with input power (14%) is due to the high value of M that overcomes the lower average value of the net deuterium exchange flux.

Table 3. Coefficient values for Equation 13

Coefficient	ETI 035-7	ETI 035-8	Units
M	1000	50	
X°	0.875	0.875	D/Pd
i°	115	35	mA cm ⁻²
Average i _D	2.0	6.5	mA cm ⁻²
$ extbf{P}_{ ext{IN}}^{\circ}$	6.1	2.1	W

The electrodes in cells ETI 035-7 and -8 were nominally identical. It is thus not obvious why the proportionality constant M has such divergent values. Since it is well established that the excess heat effect is highly localized to a very small fraction of the available surface, ²⁹ we speculate that M reflects the fraction of the cathode area (and thus volume) participating in excess heat production. At this point we have no independent experimental support for this hypothesis.

More encouraging is the observation that the loading threshold, x° , for the two nominally identical cathodes is the same: D/Pd ≈ 0.875 . This value is essentially the same as that previously observed for 1-mm-dia. Pd wire cathodes³⁰ and appears to be characteristic of the D-Pd system.

The third experiment in this set, ETI 035-9, was operated with a cathode prepared using a commercial Johnson Matthey foil, annealed at 900°C and rapidly quenched. Using superwaves this cathode also loaded to a high level; not as high as the ENEA foils used in ETI 035-7 and ETI 035-8, but certainly exceeding the threshold of excess power initiation $x^{\circ} \approx 0.875$, discussed above. Nevertheless, this cell produced zero or unmeasurably low values of excess power in the range of input power up to 19 W.

Figure 15 plots the measured resistance ratio R/R°* and calculated loading, D/Pd, for an interval of 200 h up to the end of experiment ETI 035-9. At ~640 h a small dc anodic current was applied to partially deload the cathode from its well loaded condition. Following restoration of the superwave cathodic current, the cathode reloaded rapidly to impressive values shown by the upper data sets in Figure 14, referenced to the left axis.

Despite attaining average loading values exceeding D/Pd = 0.94, the cell did not at this time or any other exhibit evidence of excess heat. Figure 16 shows the input current density and input power, and the excess power and energy for the same time interval as in Figure 15. Power is referenced to the left axis and current density (in mA cm⁻²) and excess energy (kJ) to the right axis. Within measurement uncertainty, the value of P_{xs} is zero. If we attempt to correlate P_{xs} with Equation [13] using $x^{\circ} = 0.875$ and average values of i° and $|i_D|$ (75 and 4 mA cm⁻²), we find that the multiplicative constant M must be 10 or less. In other words, and in terms of Equation [13], the cathode used in ETI 035-9 must be 100 times less active than -7, or 5 times less active than cathode -8, or even less. It is not clear whether this is an effect of decreased active area or some more complex property or defect in the loaded electrode.

The results shown in Figures 15 and 16 are anomalous. They are the only case in the history of SRI experimentation in which excess heat was not obtained, at some level, from a cathode that attained and maintained such high loading levels with large interfacial flux dynamics. It is important to understand this case as it may provide insight into other unsuccessful experiments and therefore into the apparent irreproducibility of the effect. At this time the only clue offered in Figure 15 is the tendency of the electrode to lose the average loading gained following each current step. Further analysis will be undertaken. This case is discussed further in the discussion of Figure 42 on pages 78 and 79 of this report.

-

²⁹ References 15 and 27 - 30.

³⁰ Reference 19.

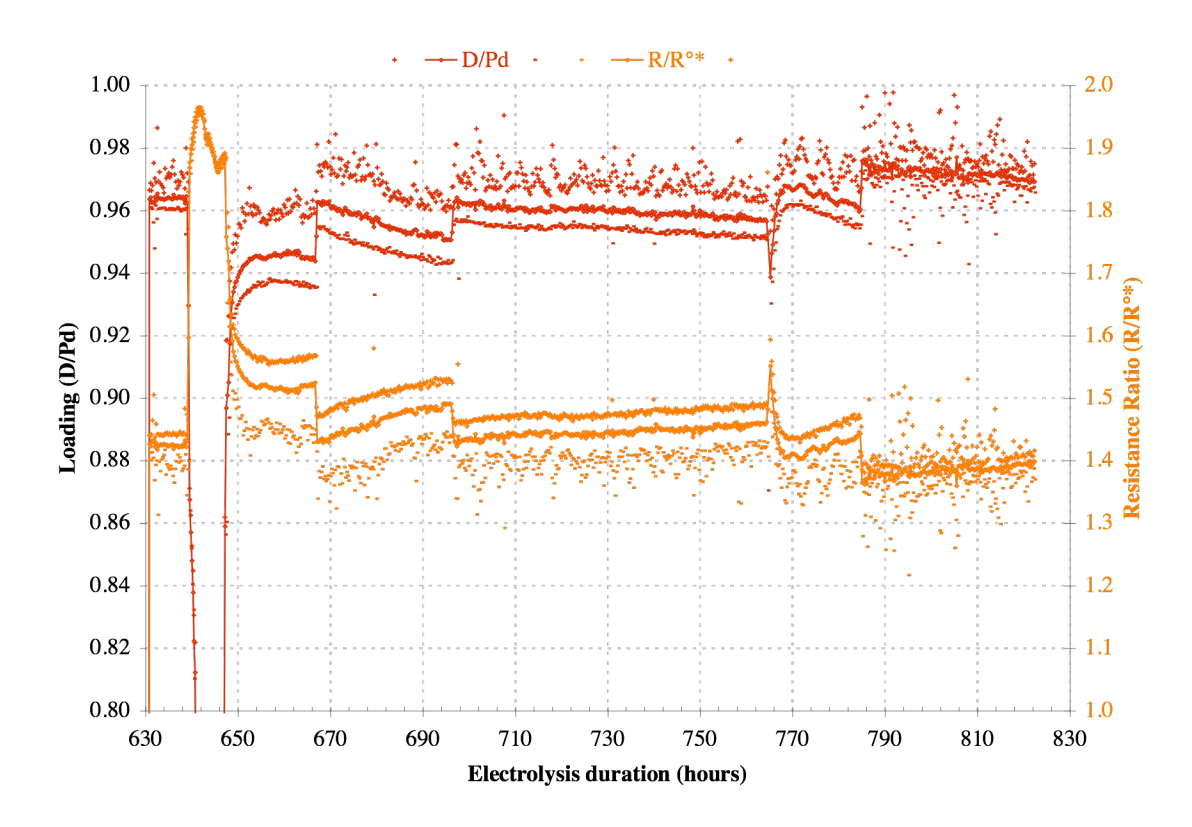


Figure 15. ETI 035-9 resistance and loading.

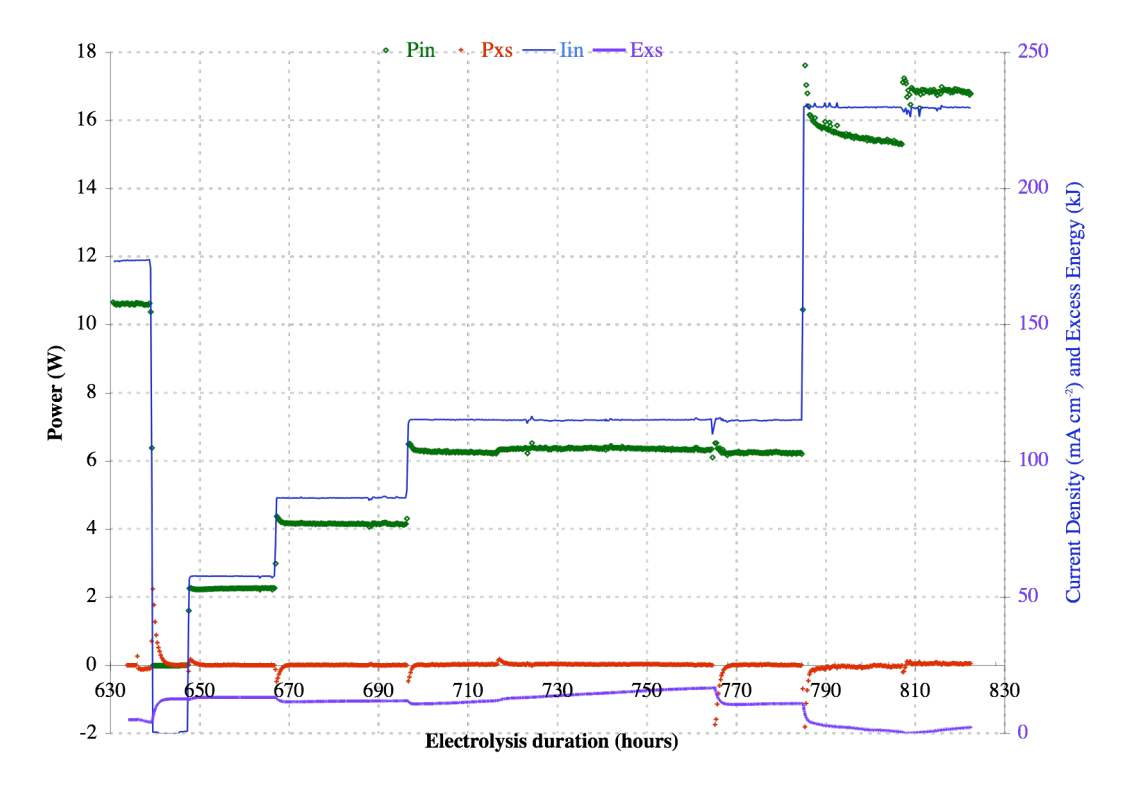


Figure 16. ETI 035-9 input and excess power, current density, and excess energy.

ETI 043

The three cathodes used in the second set of heavy water cells were as described in the following table.

Calorimeter	Electrode	Anneal	Etch
7	L14(2) ENEA	30 min @ 400°C + 60 min @ 850°C	60s HNO _{3 +} 120s 100% Aqua Regia
8	ETI	120 min @ 900°C + rapid quench	60s HNO ₃₊ 120s 100% Aqua Regia
9	L14(3) ENEA	30 min @ 400°C + 60 min @ 850°C	60s HNO _{3 +} 120s 100% Aqua Regia

Although they were selected for their similar treatment and history, the ENEA L14 cathodes used in ETI 043 loaded less easily and less well than the L17 cathodes used in ETI 033 (see above), despite using the same superwave input. Figure 17 shows three attempts to load the cathode in cell ETI 043-7 with anodic strips at 148 and 332 h. The efficacy of these strips can be seen in decreasing resistance ratio and increased loading, but the maximum loading at 500 h was only slightly above 90% (D/Pd = 0.903).

Figure 18 shows the excess power associated with these various loading attempts. The first series of current steps to \sim 20 mA cm⁻² resulted in a maximum loading of 0.893, barely exceeding the threshold value of 0.875 discussed above. Up to 148 h the P_{xs} data show considerable scatter due to a noisy calorimetric sensor (replaced at this point), but no excess power. Following the first strip. the second series of current steps showed evidence of improved loading and a small amount of excess power at very low current densities. The maximum excess power observed was 113 mW at 19 mA cm⁻² and a maximum loading of 0.895. The maximum percentage excess power was 80% at 6.5 mA cm⁻². A second strip and third attempt resulted in slightly improved loading but a rapid decline in excess power.

While the excess power seen in ETI 043-7 is evidently real, and conforms approximately to the Mode A behavior predicted by Equation [13], in the interval 148 < t < 332 h, there is clearly a temporal effect, and the current density threshold i° must be very low. For this interval only, i° ≈ 2 mA cm $^{-2}$ x° ≈ 0.875 and M $\approx 50,000$, with an average $|i_D|\approx 1$ mA cm $^{-2}$. This may suggest a highly active cathode with low threshold and large active area, the failure to produce large excess heat simply being the inability to achieve high loading.

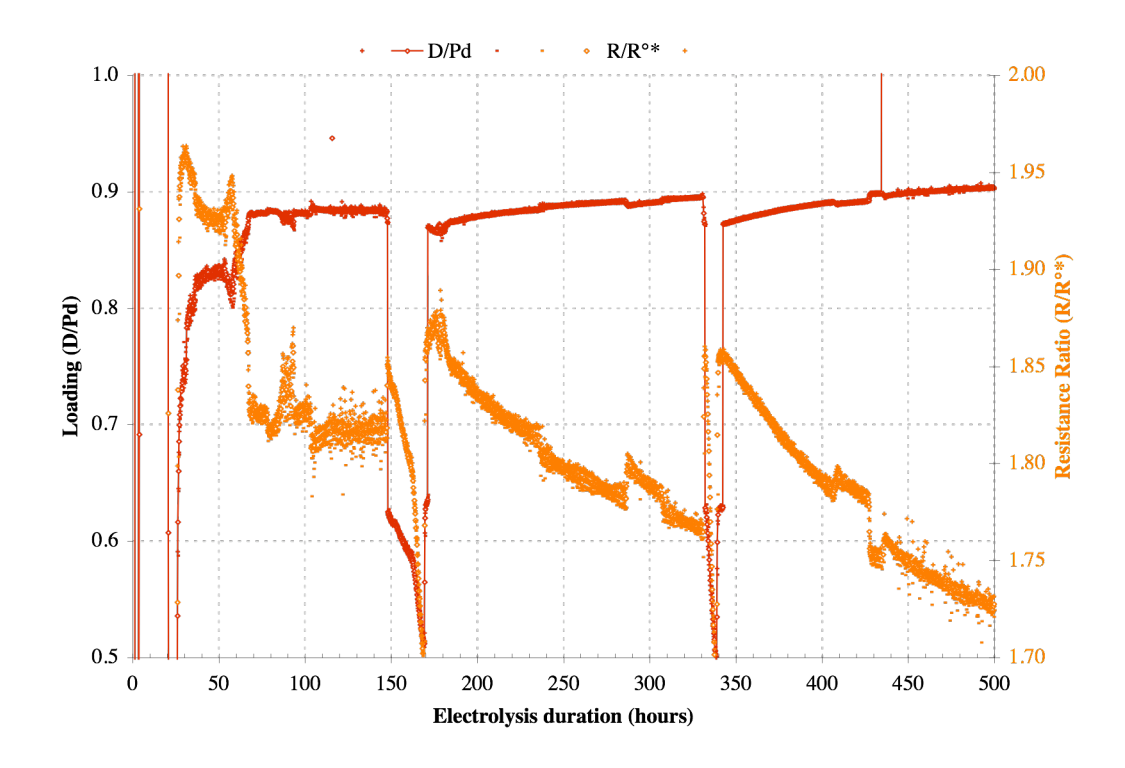


Figure 17. ETI 043-7 Loading and resistance ratio.

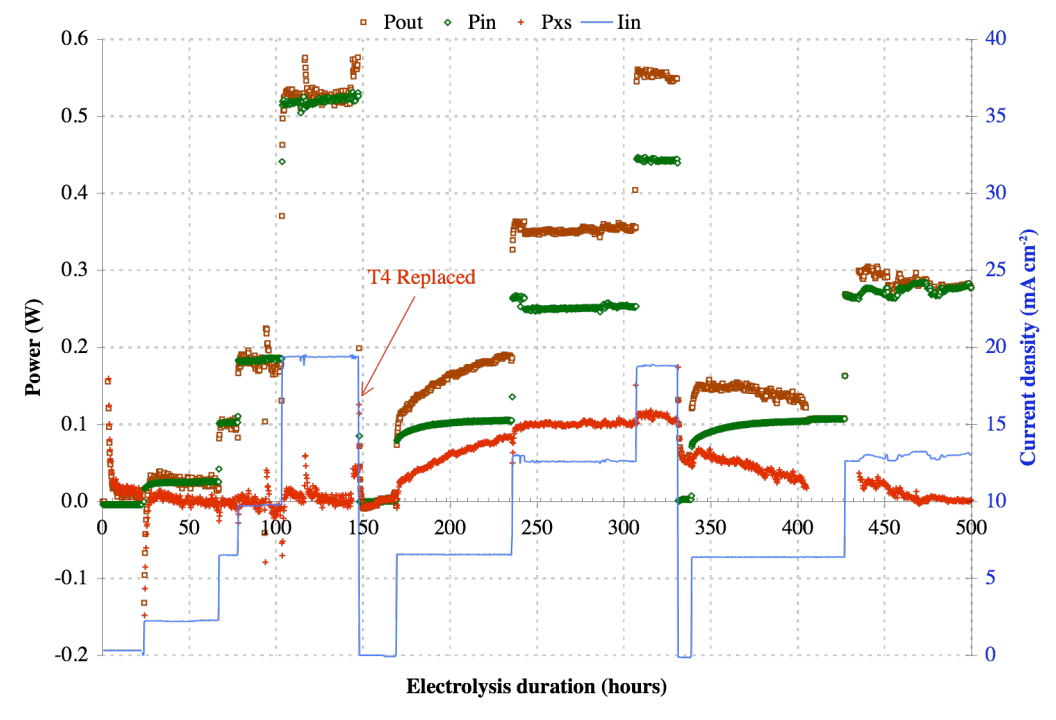


Figure 18. ETI 043-7 loading and resistance ratio.

Unfortunately, this is not a complete description because at approximately the same current stimulation, but at lower and higher loading during the first and third current steps, this cathode evidenced zero or very low and decreasing levels of excess heat. In the fourth set of current steps and current densities up to \sim 140 mA cm⁻² (not shown), loadings up to D/Pd \sim 0.9 were obtained with excess power at 10% levels (\approx 1W).

The excess power behavior observed in cell ETI 043-7 was not observed in the cells operated in parallel, ETI 043-8 and ETI 043-9. At current densities up to 20 mA cm⁻², these latter cells exhibited a maximum loading of 0.92 and 0.90, respectively, but zero or insignificant excess power. At higher input, current cell ETI 043-8 showed a small SRI Mode A type behavior with maximum excess power $\approx 5\%$ (≈ 500 mW) with $x^{\circ} \approx 0.875$, $i^{\circ} \approx 50$ mA cm⁻², $M \approx 2000$ and average $|i_{D}| \approx 1$ mA cm⁻².

Cell ETI 043-9 showed poor loading (\leq 09) at all current densities up to 20 mA cm⁻², but the loading responded positively at higher current densities up to 140 mA cm⁻². Figure 19 shows the current density in mA cm⁻² on the right axis, and input, output and excess power in W on the left axis for the final week of experiment ETI 043-9. The calorimeter is clearly in good thermal balance with excess power zero, while the resistance ratio and loading plotted in Figure 20 respond positively, although slowly, to the increasing current density.

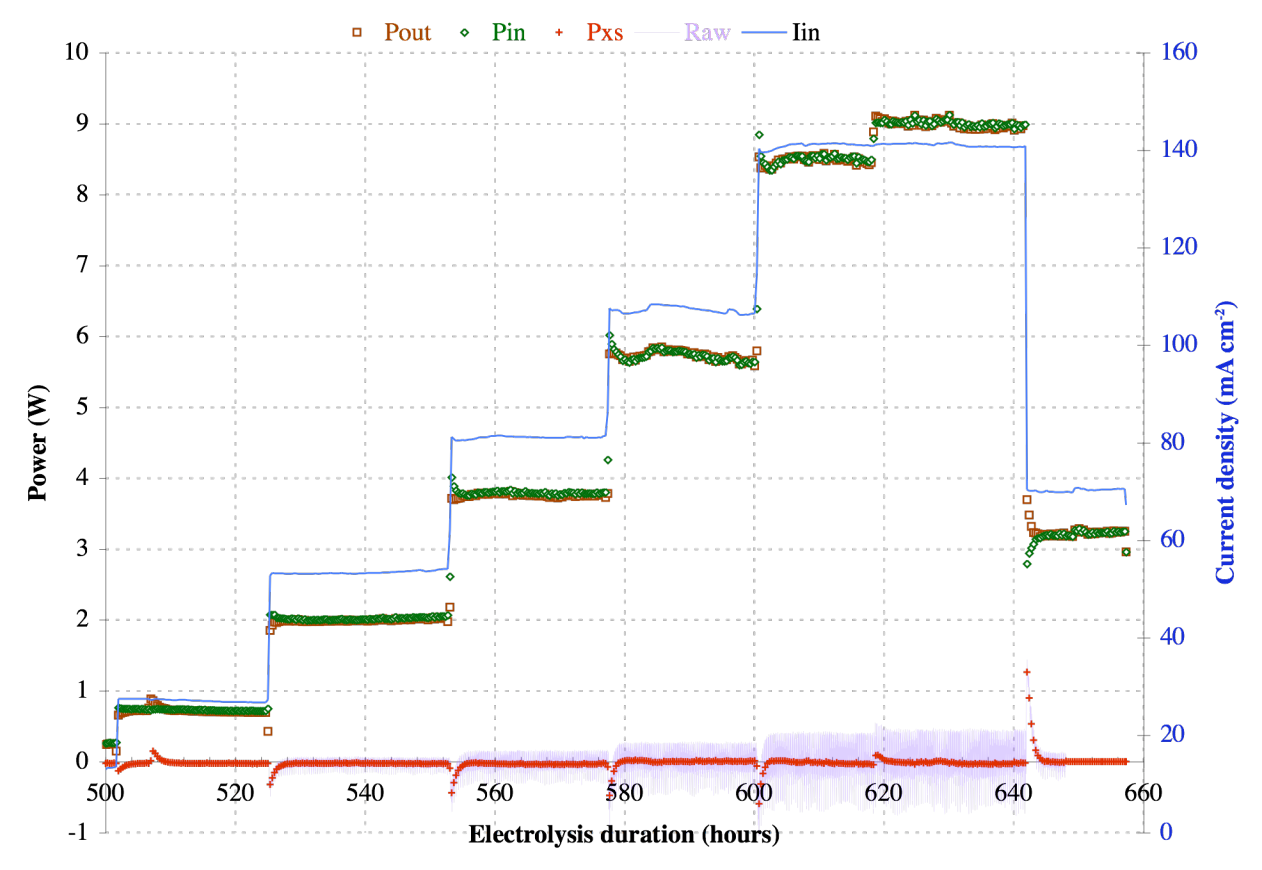


Figure 19. ETI 043-9 power and current density.

In Figure 19 raw excess power data consisting of instantaneous one minute data points <u>uncorrected</u> for non steady state effects are shown in purple. These can be seen to straddle the red "+" excess power points that have been corrected for departures from the steady state and averaged in the 15 minute interval superwave current perturbation.

One factor in the absence of excess power at high loading and current density may be the relatively low value of net interfacial deuterium flux. This can be seen in Figure 20 as the unusually small spread between the maximum (+) and minimum (-) values of the loading during the 15-min superwave cycle. Somewhat unexpectedly, the maximum loading seen in Figure 19, D/Pd = 0.926, was obtained after the current density was <u>reduced</u> from 140 to 70 mA cm⁻². The average value of $|i_D|$ in the interval plotted is 0.63 mA cm⁻².

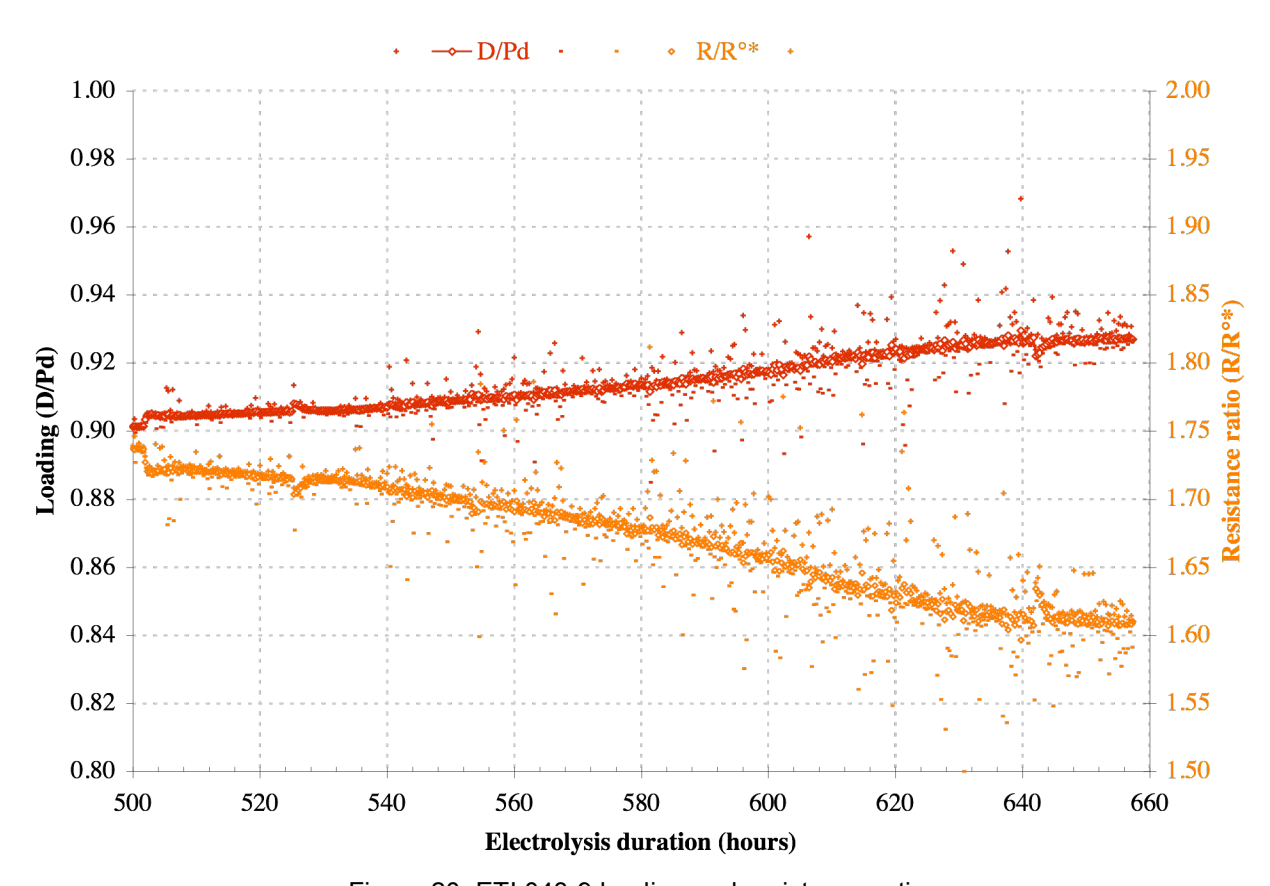


Figure 20. ETI 043-9 loading and resistance ratio.

ETI 051

The third set of heavy water cells using SRI data acquisition were operated at two bath temperatures in order to test possible influences of electrolyte temperature on calorimetry, loading, and excess heat production. The cathodes were as described in the following table.

Calorimeter	Electrode	Anneal	Etch
7	L25B-1 ENEA	30 min @ 400°C + 60 min @ 850°C	60s HNO ₃₊ 120s 100% Aqua Regia
8	L25A-1 ENEA	30 min @ 400°C + 60 min @ 850°C	60s HNO ₃₊ 210s 50% Aqua Regia
9	L18 ENEA	30 min @ 400°C + 60 min @ 850°C	60s HNO ₃₊ 60s 100% Aqua Regia

For the first 312 h these cells were operated at a constant bath temperature of 3°C. The controlled temperature set point of the bath was then raised to 23°C. Figure 21 plots on the left axis the response of the input, output, and excess power, in watts, to input current density and bath temperature (mA cm⁻² and °C on the right axis) for cell ETI 051-7. Figure 22 plots the resulting resistance ratio and loading.

The first thing to note in Figure 22 is the very dynamic nature of the loading response to steps in current density. The uptake of deuterium is strong and immediate, but is followed in each instance after a period of ~12 h by a sustained decline in loading. In one instance (at ~45 h) this loading reversal itself re-reversed. This behavior suggests the presence of a dilute impurity species capable of depositing on the surface and modifying the kinetic balance of atom absorption and recombination. An alternative possibility, and one that has been previously studied at length, ³¹ is that the high loading itself is causing mechanical damage, opening fissures in the lattice and prompting deloading. Whatever the cause, the effect is undesirable, since this cathode was evidently capable of loading and potentially of excess heat production.

The second thing to note in Figure 22 is that, at essentially constant current density (44 mA cm⁻²), the loading increased when the bath temperature was raised from 3 to 23°C at 312 h. This trend also reversed itself after about 12 h, so that the final loading at 44 mA cm⁻² and 23°C (D/Pd = 0.914) is very similar to that at 3°C (D/Pd = 0.912). Nevertheless, the initial trend toward higher loading at higher temperature is not expected and is in some ways encouraging. The solubility of hydrogen and deuterium in palladium decreases with increasing temperature, so that for the same kinetically driven deuterium surface activity we expect to see a lower solubility at higher temperature. Clearly the kinetic balance has shifted in such a way that the surface (and thus bulk) deuterium activity is higher at higher temperature and constant current stimulation.

³¹ Reference 20

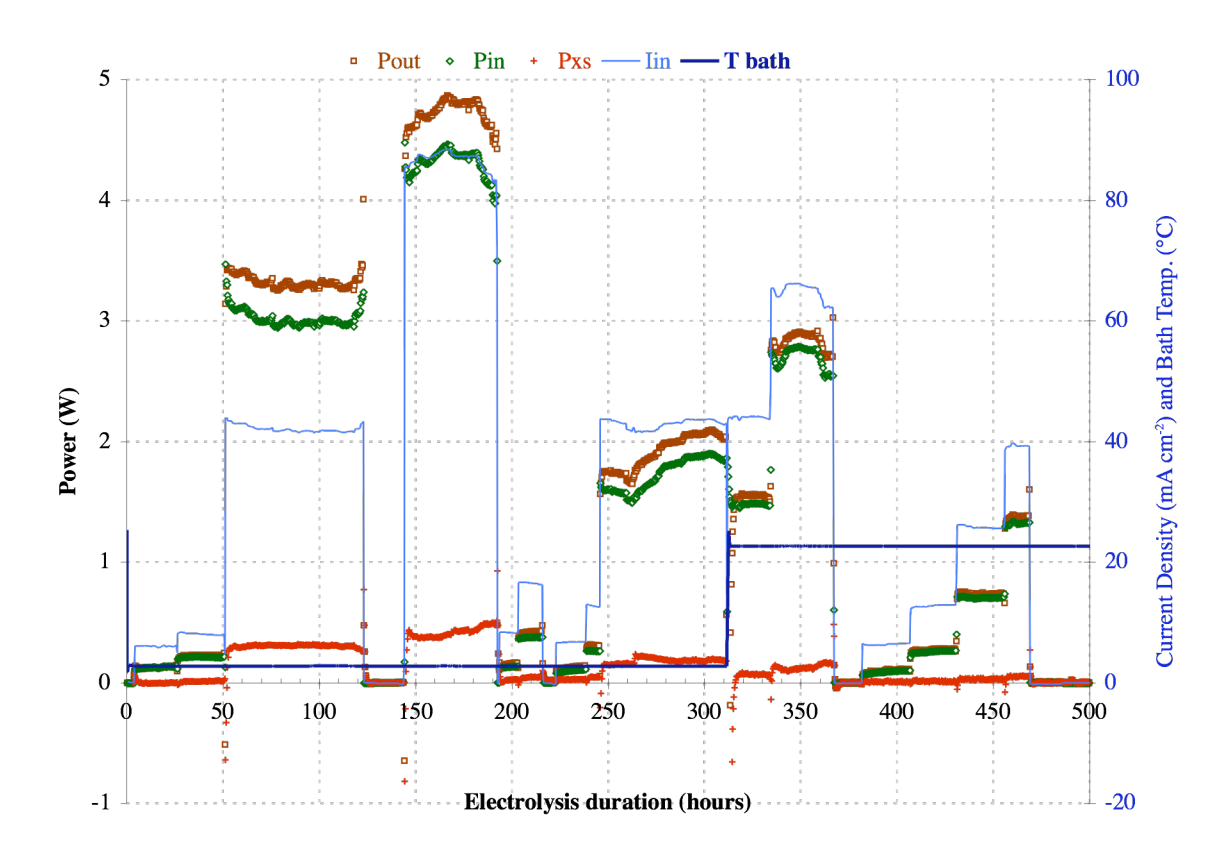


Figure 21. ETI 051-7 power, current density and bath temperature.

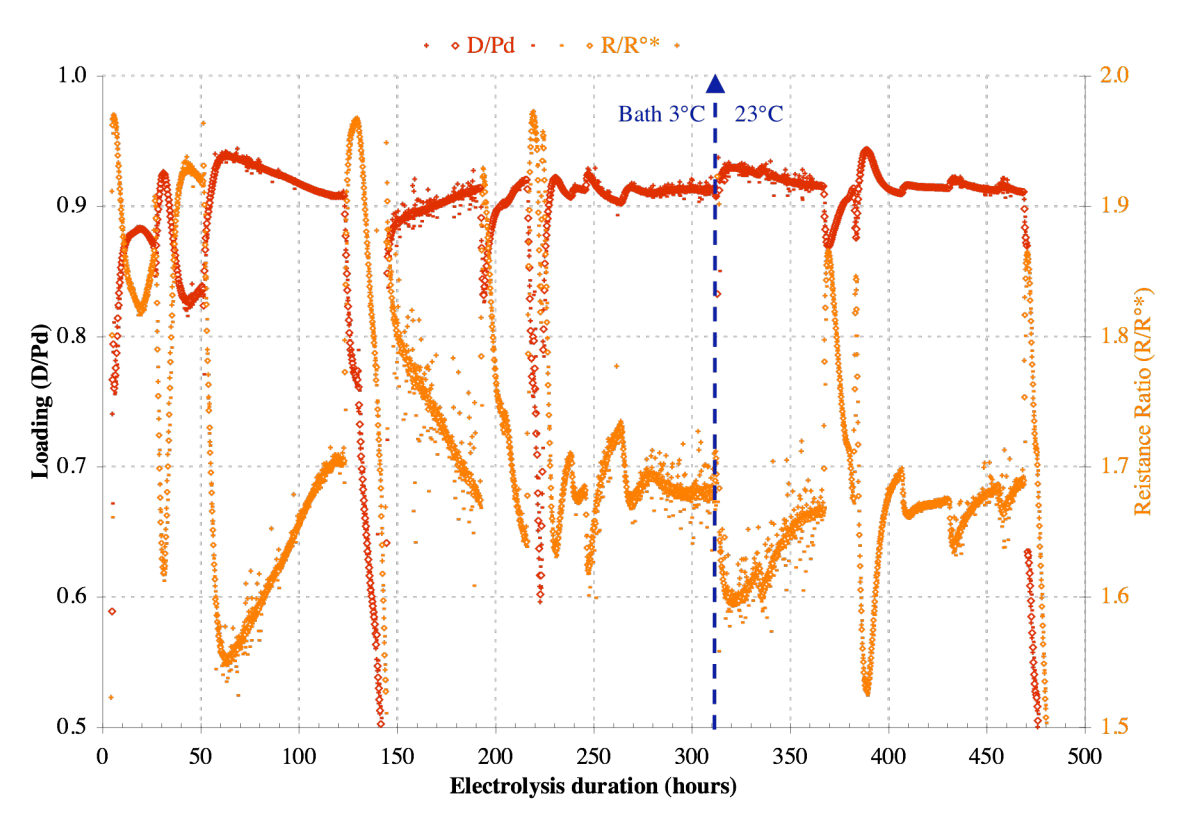


Figure 22. ETI 051-7 loading and resistance ratio.

In the present study the phenomenon of excess heat is of more interest than loading. Figure 21 shows the excess power reaching approximately 12% of P_{ln} (0.488/4.17 W) with the bath at 3°C. The behavior of P_{xs} is very dynamic in this case, but conforms generally with the SRI Mode A (Equation [13]) response, with $x^{\circ} = 0.875$, $i^{\circ} \approx 10$ mA cm⁻² and $M \approx 20000$. This same set of parameters applies at 3° and 23°C. The only exception is the interval between raising the bath temperature at 312 h and reducing the current at 367 h. During this interval with the same threshold coefficient values we would expect to measure an excess power on the order of 1W. In fact, only about 10% of this value was measured.

In the period of the final current steps from 367 to 500 h, the excess power measured conforms closely to Equation [13] with the coefficients listed above. The difference, however, and possibly less encouraging, is that the net deuterium interfacial flux in the last 200 h at 23°C is significantly less than that for the first 312 h at a bath temperature of 3°C. This change in $|i_D|$ is responsible for the lower predicted (and observed) value of P_{xs} . In the interval 0 < t < 312 h, the average value of $|i_D|$ is 0.69 mA cm⁻², a relatively small number if one recalls that for ETI 035-7 the maximum value of this parameter was 9 mA cm⁻². However, in the interval 367 < t < 500 h the average value of $|i_D|$ is 0.22 mA, less than one-third of the value at low temperature.

Given the highly variable nature of our results, it is obviously not yet appropriate to attempt to draw general conclusions. Measurement and production of excess heat at sub-ambient temperatures is both experimentally more difficult and practically less valuable. The general consensus in the CMNS community is that the phenomenon of excess heat generation has a positive temperature coefficient over temperatures at least up to 100°C^{32} and possibly higher. In a single experiment we have observed two counteracting trends, both unexpected:

- i) <u>Increasing the temperature</u> of a well-loaded cathode at constant current density results in <u>increased loading</u>.
- ii) Over a range of current densities and in a similar range of loading, the net interfacial deuterium flux is significantly less at 23° than at 3°C.

Cell ETI 051-8 achieved poor loading at room temperature and rather small levels of excess power (\leq 5%). Consistent with our observation for ETI 051-7, the loading obtained at a bath temperature of 23°C was significantly and consistently <u>higher</u> than at 3°C, although the initial trend during the heatup at constant current was toward lower loading. Despite obtaining a maximum loading of D/Pd = 0.944 at 23°C and 70 mA cm⁻², no excess power was measured at this temperature. This failure cannot be attributed to a significant reduction in interfacial deuterium flux. At 3°C |i_D| averaged 0.41 mA cm⁻² for ETI 051-7, while at 23°C this number was 0.35 mA cm⁻². Additional factors influenced by temperature must play a role in excess heat production.

The effect of operating temperature on cell ETI 051-9 was less easily observed than for the parallel cells ETI 051-7 and -8. The maximum loading observed was D/Pd = 0.940, similar to the other two cells, but this maximum loading occurred at low rather than high temperature. A very small amount of excess power was observed at the highest current densities (70 and 140 mA cm²) and loadings. This excess power reduced to zero with increase of bath temperature. Again, this reduction in P_{xs} cannot be attributed to a reduction in interfacial deuterium flux. At 3°C, $|i_D|$

³² References 31-33.

³³ References 34 and 35

averaged 0.47 mA cm $^{-2}$ while at 23°C $|i_D|$ averaged 0.51 mA cm $^{-2}$. While both are relatively small, the interfacial dynamics at high temperature was greater while the excess power was less.

ETI 056

The fourth set of heavy water cells were operated for 232 h at a bath temperature of 23°C, which was lowered to 3°C and then raised to 4°C at 330 h. The cathodes were as described in the following table

Calorimeter	Electrode	Anneal	Etch
7	L24F ENEA	30 min @ 400°C + 60 min @ 850°C	60s HNO ₃₊ 40 s 50% Aqua Regia + 5 sec HNO ₃
8	L24D ENEA	30 min @ 400°C + 60 min @ 850°C	60s HNO ₃₊ 60 s 50% Aqua Regia + 5 sec HNO ₃
9	L25B-2 ENEA	30 min @ 400°C + 60 min @ 850°C	60s HNO _{3 +} 120 s 50% Aqua Regia + 5 sec HNO ₃

ETI 056-7 operated for 335 h and experienced a drop in bath temperature at 232 h. This drop at a constant current of ~ 110 mA cm⁻² resulted in a <u>deloading</u> of the cathode with decreasing temperature from D/Pd = 0.924 to 0.895. A subsequent attempt to partially strip and reload the cathode at low temperature resulted in poor loading and no further excess heat.

At the highest current densities (80 and 110 mA cm⁻²), and at both 23° and 3°C, cell ETI 056-7 exhibited an interesting dynamic excess power response with a maximum P_{xs} of over 2W and $\approx 15\%$ of P_{In} . Figure 23 plots input and excess power in watts on the left axis versus current density and bath temperature in mA cm⁻² and °C on the right axis. Figure 24 plots the resulting resistance ratio and loading. Note particularly the resistance and loading transition after the drop in bath temperature at 232 h.

Despite this significant drop in loading with temperature, the excess power in Figure 23 makes a strong increase from ~ 0.6 to ~ 2.0 W and then declines apparently spontaneously at constant current. The excess power data up to the temperature step conform with the SRI Mode A expectation of Equation 13 reasonably well, with $x^{\circ}\approx 0.875$, $i^{\circ}\approx 50$ mA cm $^{-2}$ and M ≈ 5000 . As for ETI 051-7, the fitting factors at low temperature differ from those at ambient temperature. Because P_{xs} was observed at the lower temperature for just one current density, and also because of the strong spontaneous variability of P_{xs} at that current density, we cannot independently assess the Equation 10 parameters at a bath temperature of 3°C. Nevertheless, the parameters obtained at 23° considerably underestimate the excess power at 3°C.

Just as for ETI 051-7, part of this underestimate can be attributed to increased deuterium interfacial flux at lower temperature. For the data in Figure 24 at 23°C, the average value of $|i_D| \approx 0.56$ mA cm⁻²; at 3° the average value of $|i_0| \approx 1.41$ mA cm⁻². Again a factor of approximately 3

increase in the net interfacial D flux is observed from high to low temperature. Because of the substantial decrease in loading with decrease in temperature, however, this increase in $|i_D|$ is not sufficient to account for the Equation 13 underestimate of P_{xs} .

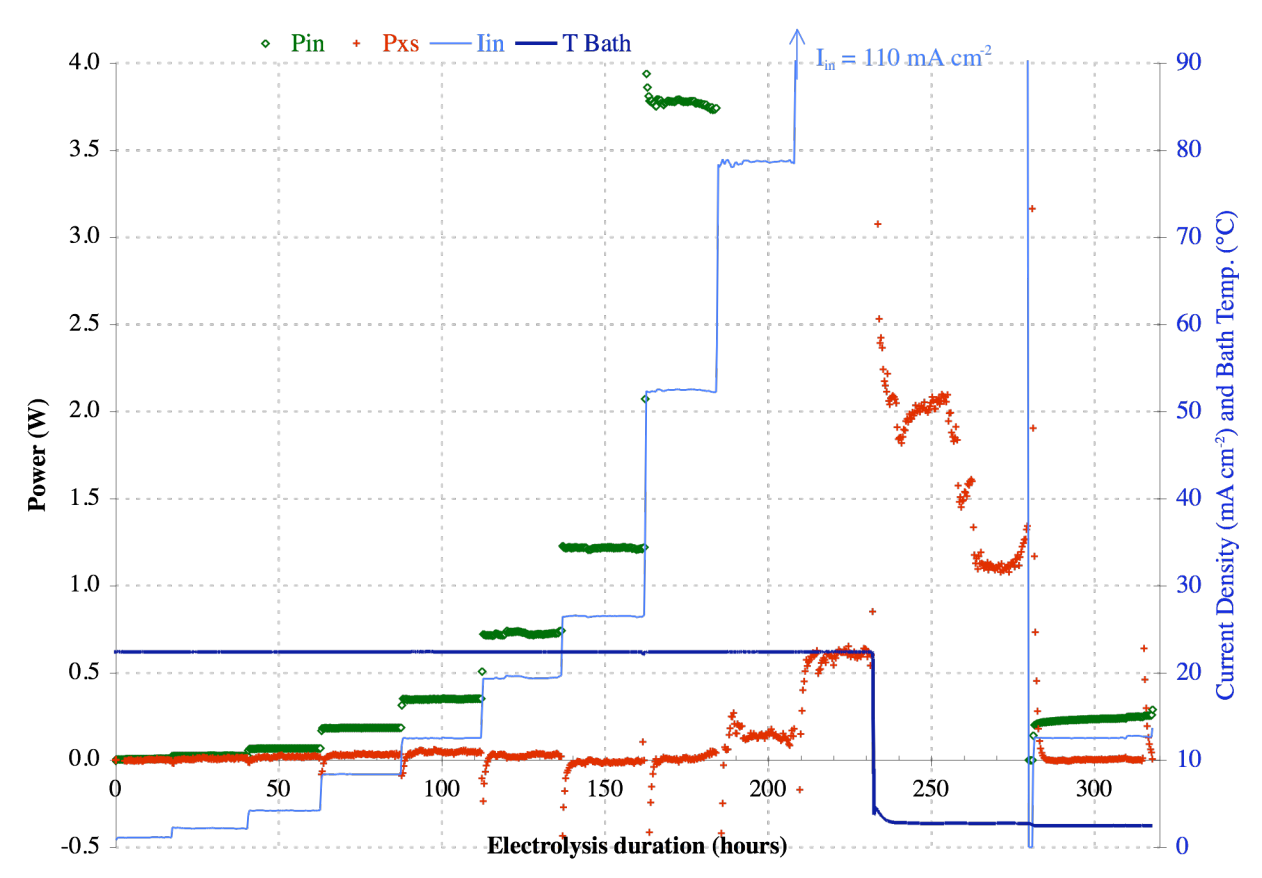


Figure 23. ETI 056-7 power, current density and bath temperature.

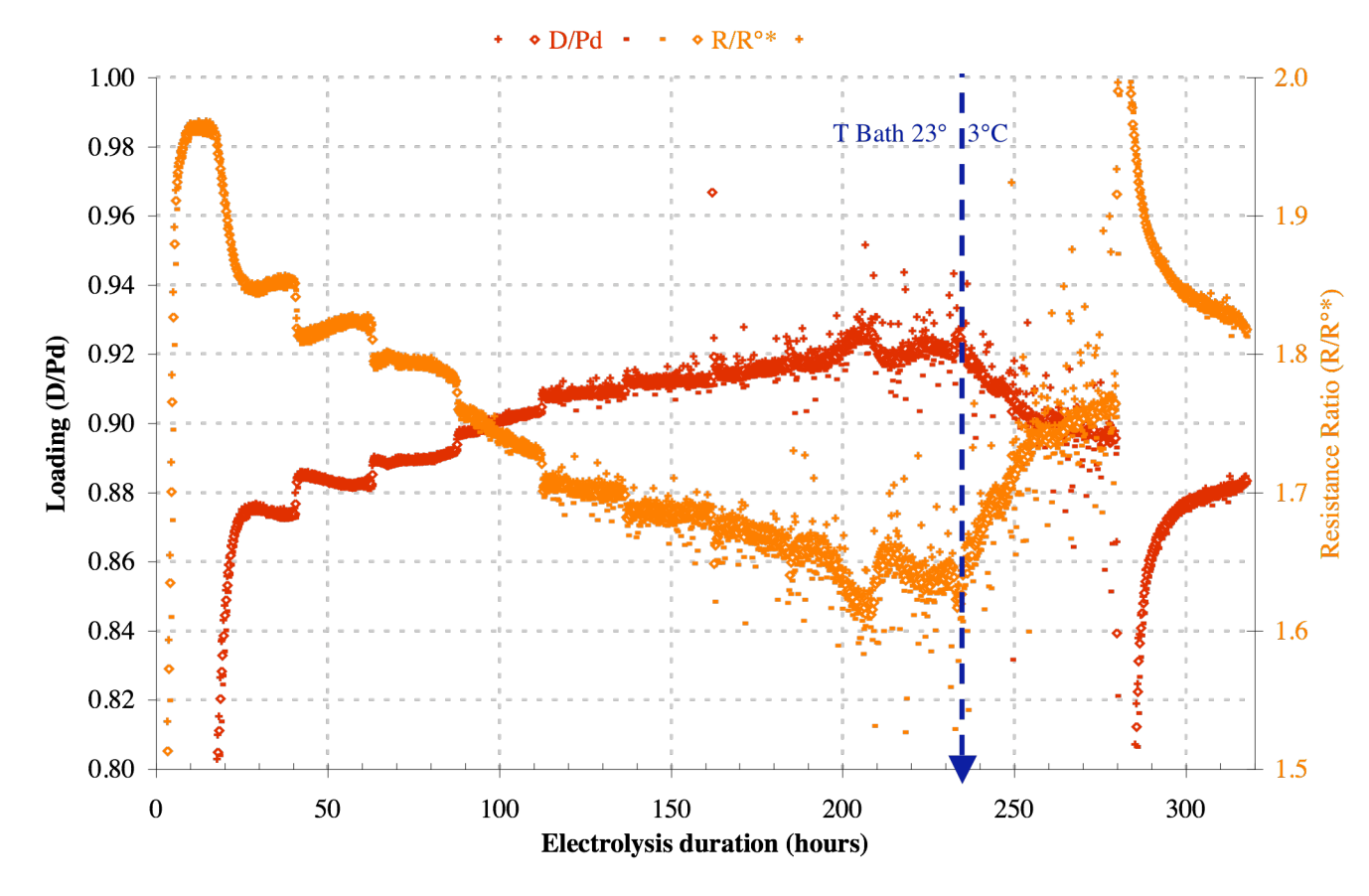


Figure 24. ETI 056-7 loading and resistance ratio.

From a study of two cells where significant excess power survived a transition in bath temperature we are able to make three observations:

- i) The loading of a well-loaded cathode can be significantly higher at higher temperature and the same current density.
- ii) The net interfacial deuterium flux can be significantly lower at higher temperature and the same electrochemical current density.
- iii) The combination of these two factors is insufficient to explain observed higher power excess at lower temperature.

Cell ETI 056-8 was operated for only 168 h, and since it exhibited poor loading, poor response to current steps, and very little or no excess heat, the electrode assembly was removed and replaced with ETI 057-8.

Cell ETI 056-9 was operated for 232 h until the reduction in T_{Bath} . The cathode experienced reasonably good loading in response to current steps up to 27 mA cm⁻². The maximum loading obtained was D/Pd = 0.938. This loading did not hold and declined with time slowly and more precipitously when the current density was doubled to 54 mA cm⁻².

A very small amount of excess power was observed at the highest current density and loading. The maximum value measured was 105 ± 15 mW, or about 3% of P_{In} . Although observed at only two current values and with small and rather scattered excess power data, the

form of the excess power response conformed roughly to the Mode A expectation of Equation [13], with $x^{\circ} \approx 0.875$, $i^{\circ} \approx 20$ mA cm⁻², $M \approx 4000$ and the average value of $|i_D| \approx 1.49$ mA cm⁻².

The relatively low current density threshold and relatively high value of $|i_D|$ suggest that, had the electrode been capable of sustaining loading at higher current density, it may have been able to produce significant levels of excess heat. Because of the low observed values, excess power, and the inability of the cathode to sustain loading, the electrode assembly was removed and replaced with ETI 058-9.

ETI 057, 58 and 61

A different strategy was adopted for this final set of three cells. Rather than a complete removal of electrodes and electrolyte and refurbishment of cells, new electrode assemblies comprising anode/cathode/anode "sandwiches" were used to replace the old (051 series) electrodes without replacement of electrolyte. This method was attempted with two primary purposes: to save time in cell turnaround, which otherwise could take up to a week, and in the hope that minor trace impurities (including protons³⁴) would have been scavenged from the electrolyte by extended electrolysis with respect to the removed electrodes.

This different approach meant that the three cathodes were not started at the same times. Because of the varying degrees of success in the ETI 056 series, ETI 057-8 was started first, ETI 058-9 second, and ETI 061-7 third. The cathodes were as described in the following table.

Calorimeter	Electrode	Anneal	Etch
7	L25B-1 ENEA	30 min @ 400°C + 60 min @ 850°C	60s HNO ₃ + 120s 100% Aqua Regia
8	Pd-SWCNT-Pd	60 min @ 300°C	None
9	L25A ENEA	30 min @ 400°C + 60 min @ 850°C	$60s HNO_3 + 210s 30\%$ Aqua Regia + $5s HNO_3$

Because of the significance of the results of these three cells, and their significant departure from the behaviors of the preceding 21 cells, each experiment will be dealt with in some detail. One important starting difference for the set of cells initiated with pre-electrolyzed electrolyte is that each of them exhibited excess power directly or very early following application of cathodic current density. In practice we are calorimetrically blinded for the initial period of 6-8 h because of the thermal time constant of the calorimeter and the thermal equilibration of the electrode assembly having been introduced to the cell at room temperature. Nevertheless, the three cells—ETI 057-8, ETI 058-9 and ETI 061-7—all exhibited clearly measurable excess power within 10 h of initial current application. This is a far shorter initiation time than any previously observed at SRI with any kind of heavy water electrolysis cell.

³⁴ An alternate possibility is that instead of reducing the electrolyte inventory of protons by selective absorption in the "sacrificed" cathodes, the "light water" fraction in the cells was increased by extended operation in non-hermetic cells and the opening and handling associated with the installation of new electrodes.

ETI 058-9. Evidence of this early initiation of excess power can be seen most clearly in the data for cell ETI 058-9. Figure 25 plots the normalized resistance ratio and calculated loading for this cell as a function of time for the first 500 h of the experiment. Although not easily discerned in the figure, the cathode loaded very rapidly at the starting average current density of ~ 7 mA cm⁻², passing over the resistance ratio maximum in only 1.6 h of electrolysis, initially obtaining a rather impressive loading of D/Pd ≈ 0.932 in only 3.2 h of superwave electrolysis.

The loading trend thereafter was declining values of D/Pd. A brief strip³⁵ was undertaken at \sim 47 h that successfully reversed this trend and improved the average loading. The transient step to higher loading D/Pd \approx 0.9 (with exponential relaxation) at \sim 244 h appears to have been spontaneous. At \sim 410 h the current was reversed and the electrode fully stripped.

Figure 26 plots input power, output power, and excess power in watts on the left axis, and percentage excess power as dark blue points on the right axis. Although relatively small in absolute terms, the initial value of excess power (\sim 30 mW) is already larger than the power input (\sim 200 mW), resulting in a percentage excess of about 160%. Following the short strip at \sim 47 h, the input power decreases, presumably due to the removal of a cathode surface film, and the loading and excess power both increase, resulting in over 200% excess power.

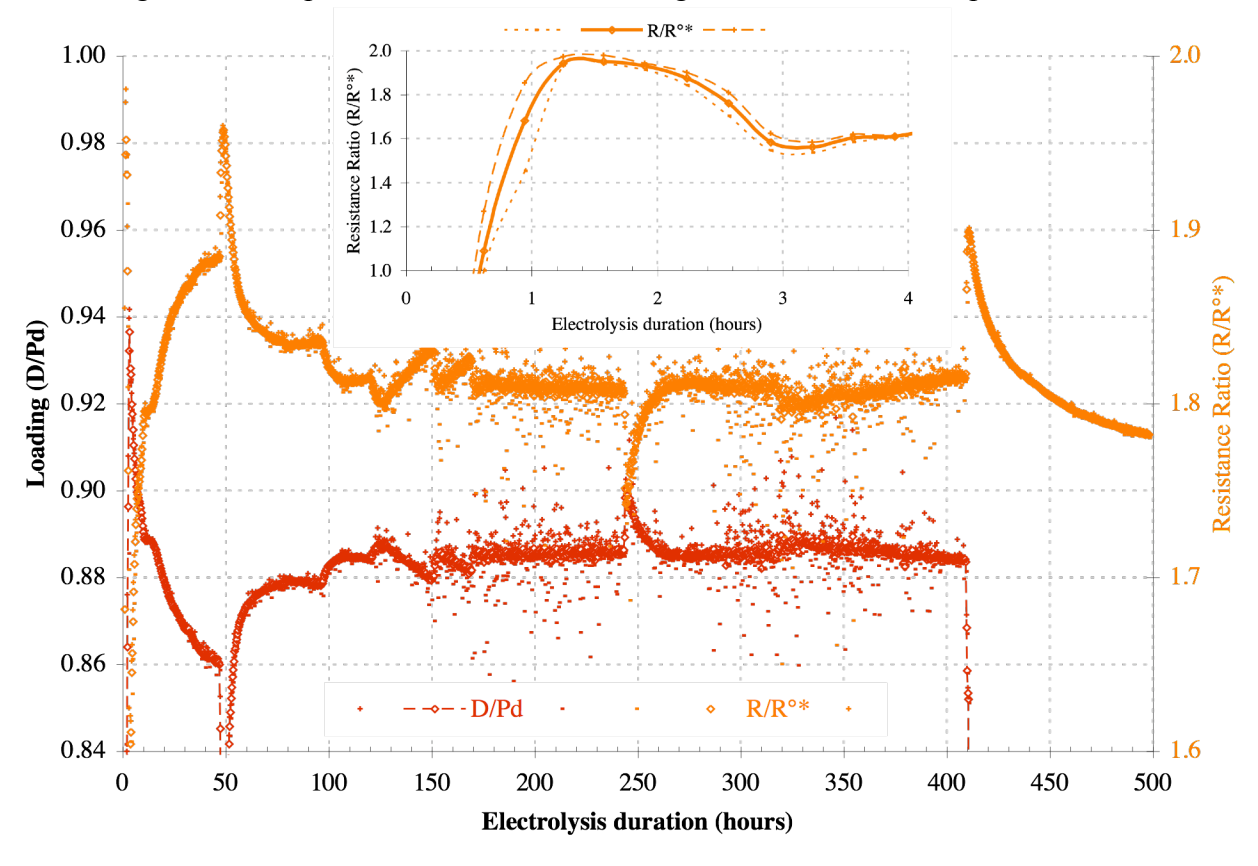


Figure 25. ETI 058-9 loading and resistance ratio.

_

³⁵ This strip was accompanied by a decrease in bath temperature from ~ 3.05 °C to ~ 2.79 °C.

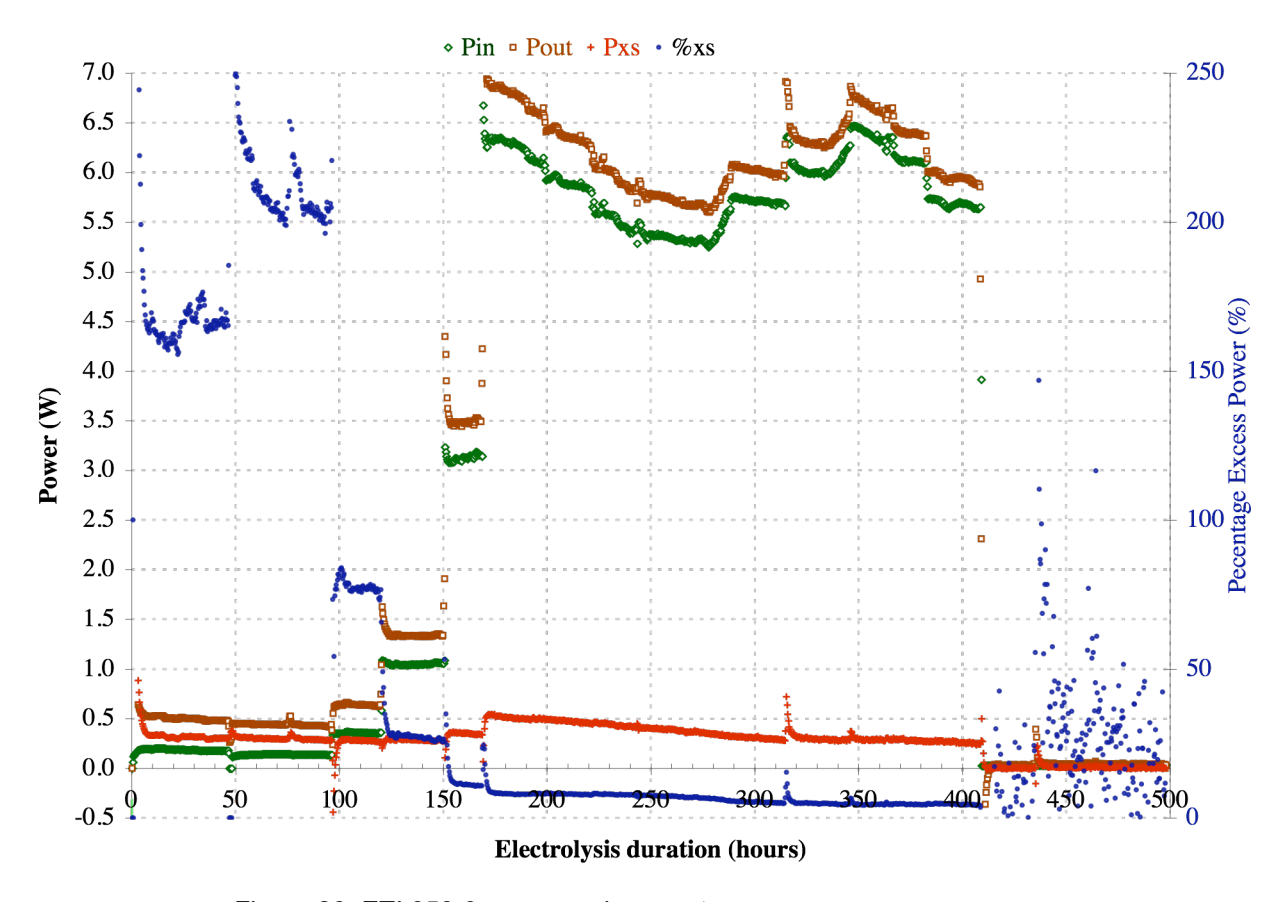


Figure 26. ETI 058-9 power and percentage excess power.

Attempts were made to increase the excess power by doubling the current density at \sim 97, 121, and 151 h, and a final step from 54 to 85 mA cm⁻² at \sim 170 h. As can be seen in Figure 26, these increases in current stimulation resulted in small increases in excess power but superimposed on a general declining trend. At \sim 170 h the decision was made to fix the current density at an average value of \sim 85 mA cm⁻² (20 min) to observe the system response.

Figure 27 presents the data in Figure 26 with a larger vertical scale. The declining trend in P_{xs} and percentage excess are clear. This trend is not directly correlated with the loading, however, which is on average essentially constant from the last current step at ~170 h to the current reversal at ~410 h. The apparently spontaneous increase in loading at ~244 h seen in Figure 25 results in no observable change in excess power on the excess power trend seen in Figure 27. However, the two sharp bursts of excess power seen in Figure 27 at ~316 and 347 h, which appear to arrest and then transiently reverse the decline of P_{xs} with time, do appear to correlate with small stepped increases in the average loading seen in Figure 25.

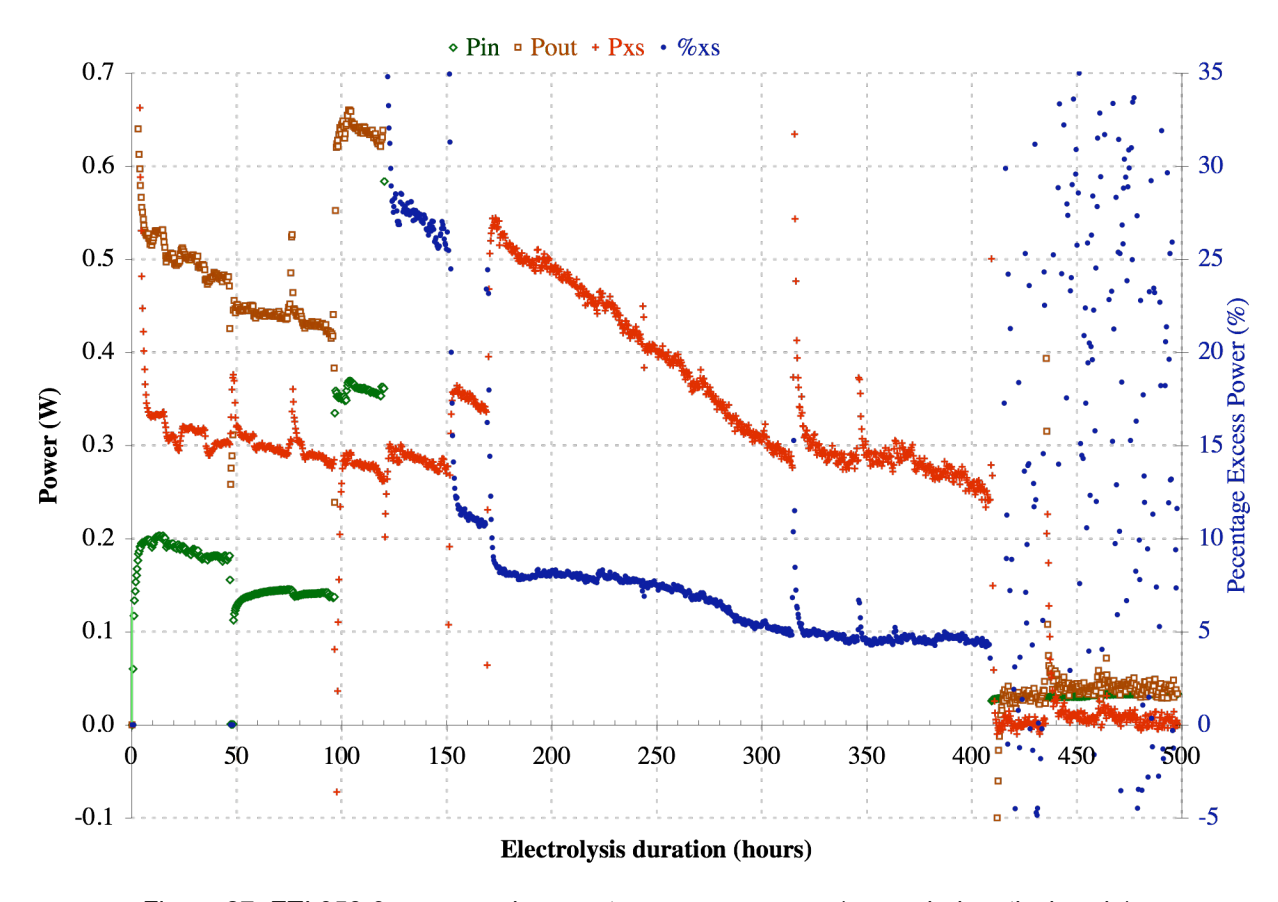


Figure 27. ETI 058-9 power and percentage excess power (expanded vertical scale).

With reversal of current at ~410 h, the output power achieves an average value equal to the input, and the excess power falls to zero. The total excess energy measured to this point was 490 ± 10 kJ, while the total energy input was 5400 ± 50 kJ. For the entire experiment we observe nearly 10% excess energy with a maximum of over 200% excess power lasting for some 50 h.

We have no prior experience with the appearance of excess power effectively at time zero, and this deserves further discussion. Because of the nature of the calorimeter, a simple explanation for a non-zero initial value of excess power is a miscalibration of one or the other of the two calorimetric temperature sensors, T_4 or T_5 , with respect to each other (*i.e.*, an error in ΔT). Several observations make this speculation unlikely:

- 1) These sensors were apparently well calibrated before the experiment during the experiment with ETI 051-9.
- 2) The calorimeter appeared to respond sensibly to controlled power steps during the experiment.
- 3) The calorimeter maintained an accurate thermal balance for the last 90 h of experiment ETI 058-9.
- 4) Post-test calibration of the sensors showed no changes in resistance value or indications of problems.

A more sophisticated argument that the excess heat source in ETI 058-9 was accurately measured and associated with the cathode can be made using data from the additional cell temperature sensors. Three 2-terminal RTDs were used to measure temperatures in the electrolyte at three different positions with respect to the anode/cathode assembly. An additional 4-terminal RTD was used to measure the temperature of the bath cooling water (in addition to the quartz crystal temperature standard). We expect these four sensors in addition to the two calorimetric temperature sensors to maintain an approximately linear gradient between the hottest (T_2 adjacent to and above the electrode assembly) to T_{Bath} (the ultimate heat sink).

Although somewhat complicated to interpret and slightly approximate, the data shown in Figure 28 tend to confirm that the heat source in cell ETI 058-9 behaves consistently in the presence and absence of excess heat. Figure 28 plots the temperature measured in various 6-h intervals centered in the series name value for the six temperature sensors specified, as a function of thermal resistance or distance of the sensor from the heat sink (T_{Bath}). T_2 was given a "distance" of 1 (arbitrary unit). The remaining distances were evaluated by minimum regression of the line for maximum P_{Out} at 177 ± 3 h in Figure 27.

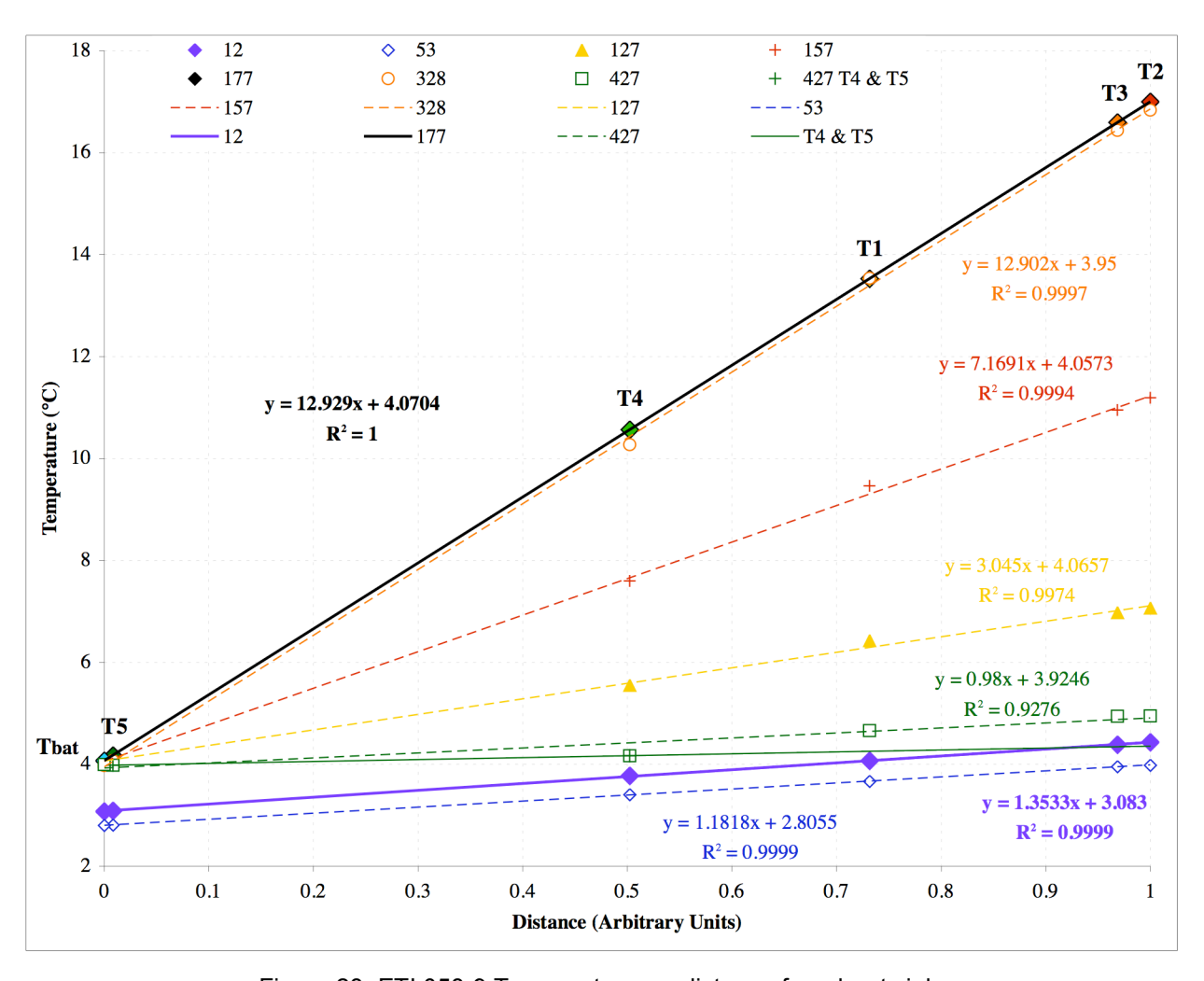


Figure 28. ETI 058-9 Temperature vs. distance from heat sink.

This exercise is interesting in itself as it shows that almost exactly one-half of the temperature drop occurs in the designated alumina thermal barrier between T_4 and T_5 , since the T_4 "distance" is only 0.502. Half of the temperature drop therefore occurs in the electrolyte inside the cell. In other words, the ΔT from T_2 to T_{Bath} is roughly twice the calorimetric ΔT ; the maximum temperature at the cathode is necessarily even higher.

The distance values for the temperatures measured at $t = 177 \pm 3$ h (at $P_{Out} = 6.33 \pm 0.33$ W) apply at $t = 12 \pm 3$ h ($P_{Out} = 0.53 \pm 0.01$ W) and all intermediate values of output power. The output power at 12 and 53 h is mostly P_{xs} (163 ± 3 and 331 ± 9 percent excess, respectively), while the output power at 177 and 328 h is mostly the electrochemical input ($P_{xs} = 8.2 \pm 0.2$ and 4.9 ± 0.1 percent excess, respectively). Had there been an error in measuring P_{xs} we would expect to see the calorimetric sensor points displaced from the temperature gradient line, indicating miscalibration of sensors T_4 and/or T_5 . In fact, the regression fitting coefficients R^2 for all lines $12 \le t \le 328$ are extremely good. Absent such deviation, we are forced to conclude that temperatures T_4 and T_5 are measured accurately, and that therefore cell ETI 058-9 exhibited excess heat from the beginning of rational calorimetry roughly 6 h after experiment initiation until the cathode was forcibly stripped after 410 h of cell operation.

A final point is worth noting. Two lines are drawn in green in Figure 28 for the data set of 427 ± 3 h obtained during the time that the cathode was under reverse bias (*i.e.*, Pt cathode vs. Pd anode). The regression line through all data shows a less good fit, with the errant point being the calorimetric sensor T_4 . The solid line drawn only through T_4 and T_5 exhibits a smaller slope consistent with the net input power. We interpret this departure from the behavior discussed above as a manifestation of very much poorer mixing in the cell when operating with large-area outer cathodes and a small-area inner anode. We can rationalize this change in mixing behavior quite simply as being the consequence of a different bubble pattern. Twice the volume of gas $(2D_2)$ evolved on the smaller, single, inner cathode is expected to produce a stronger upwelling mixing vector. Replacing this vector with a bubble source (O_2) of half the intensity, possibly somewhat opposed by a now stronger D_2 evolution outside, is likely to reduce net convection. This putative change in convection pattern does not affect calorimeter accuracy, which is controlled by the thermal conductivity of the alumina thermal barrier layer between the isothermal boundaries T_4 and T_5 , and not by the temperature drop in the electrolyte or mixing conditions therein.

In the absence of further technical input we conclude that the excess power and energy performance characteristics of cell ETI 058-9 must be considered as important and worthy of further study. This cell apparently produced $P_{xs} > 500$ mW and > 200% of P_{ln} for a period of nearly 50 h, and an integrated $E_{xs} = 490 \pm 10$ kJ, corresponding to over 9% of the integrated electrochemical input energy, and an energy density of ~ 200 eV/Pd atom. It is worth noting, however, that this excess heat event does not conform to Equation 13, which characterizes the SRI Mode A behavior. Until we have a better understanding, we will characterize the results of cell ETI 058-9 as "Mode B."

The phenomenological differences between Mode B and Mode A behavior can be summarized as follows:

1) Mode B excess heat initiates within 6 h of application of cathodic current (or 4 h of maximum loading), whereas Mode A behavior requires a longer initiation time, typically several hundreds of hours.

- 2) Mode B excess heat responds sluggishly to input cathodic current density and, so far, exhibits no obvious current density threshold.
- 3) Mode B excess heat has not been observed at D/Pd loadings less than the threshold typical of Mode A behavior (D/Pd ≈ 0.875) and appears to respond at least transiently to increased average loading; however, a threshold value has not been observed.

Insufficient data exist to evaluate the dependence of Mode B excess heat on net interfacial deuterium ion flux. However, the interfacial flux in the interval shown in Figures 25-27 is very small ($|I_D| \approx 0.5 \text{ mA cm}^{-2}$) compared with the values measured in association with Mode A behavior ($|I_D|$ up to $\sim 10 \text{ mA cm}^{-2}$).

ETI 061-7. The next cell started in this series was ETI 061-7. Figure 29 shows the resistance ratio and loading behavior of this cell as a function of time during the first 300 h of the experiment. In contrast with the preceding cell (ETI 058-9), Figure 29 exhibits a higher loading, higher net interfacial flux but slower attainment of initial loading compared with Figure 25. For cell ETI 061-7 the resistance maximum was not obtained until \sim 6 h after initial current application compared with \sim 2 h for the previous cell. Figure 29 shows the maximum loading of ETI 061-7 steadily increasing with time, steps in current density and extended anodic strips (at \sim 168 and 263 h) with a maximum loading of D/Pd \approx 0.926 obtained at \sim 500 h, compared with \sim 3 h for ETI 058-9.

Despite this very clear difference in loading behavior, cell ETI 061-7 also showed evidence of excess heat production at low current density in the early hours of the experiment. Figure 30 plots input, output and excess power in watts on the left axis and percentage excess power on the right axis. While not as dramatic as Figure 26, Figure 30 shows excess power averaging of \sim 50% for two periods of approximately 40 h each, one at the beginning of the experiment and one building apparently spontaneously at \sim 310 h.

This result provides some supporting evidence for the existence of a Mode B behavior and for the unexpected early onset of excess power in cell ETI 058-9. The excess power was nevertheless rather small, in absolute amount less than 100 mW for the first ~300 h of the experiment. In an effort to confirm this amount and verify the calorimeter performance, the cell was operated at very small dc anodic bias between 168 and 188 h. During this time, the electrode deloaded (Figure 29) and the excess power reduced as expected. However, the 20-h period at effectively zero input power revealed a small drift downward of calorimetric sensor T₄. The data in Figure 30 have been corrected for this drift with the assertion that no excess power was present during the period of low loading and small anodic bias from 168-188 h. Data to the left of 168 h in Figure 30 should therefore be treated with caution, although the step down in excess power with removal of cathodic bias indicates that at least 50 mW of excess power was present immediately preceding this point.

_

³⁶ The scales of Figures 25 [ETI 058-9] and 29 [ETI 061-7] are the same with the left loading axis displaced to separate the resistance and loading curves.

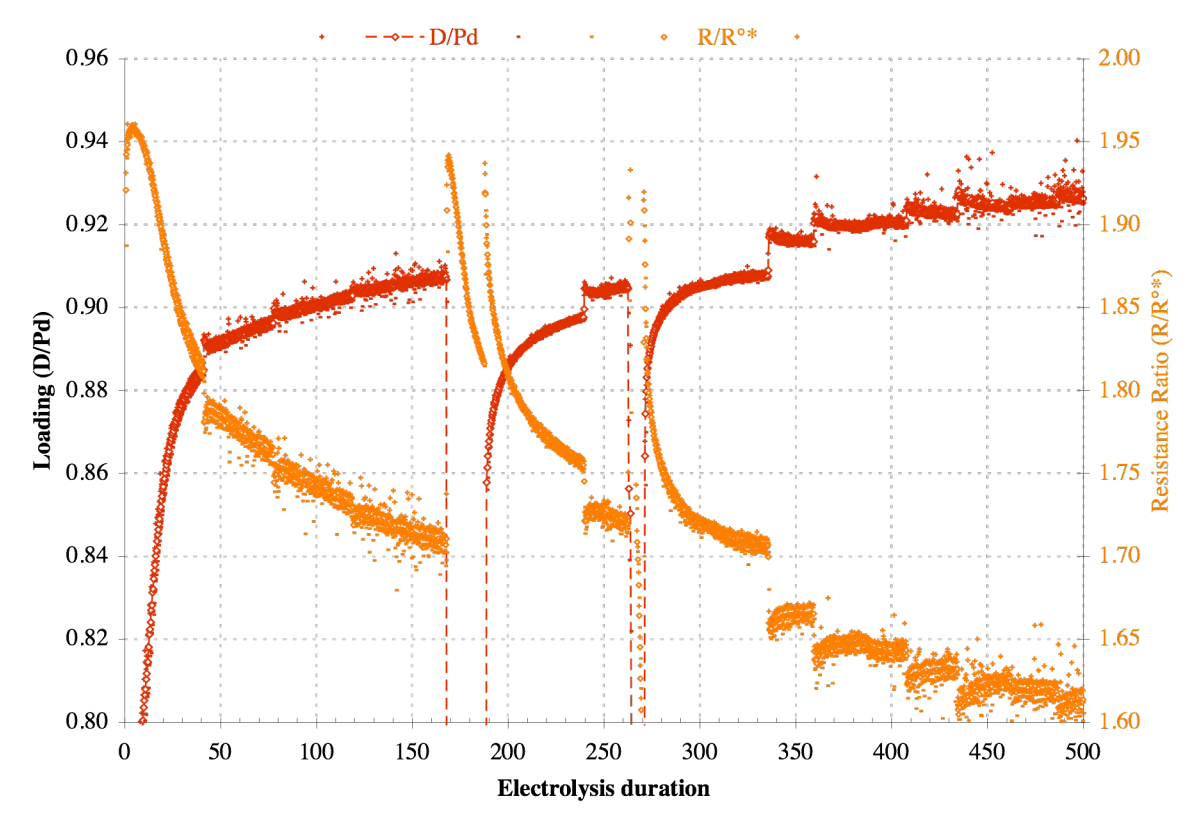


Figure 29. ETI 061-7 loading and resistance ratio.

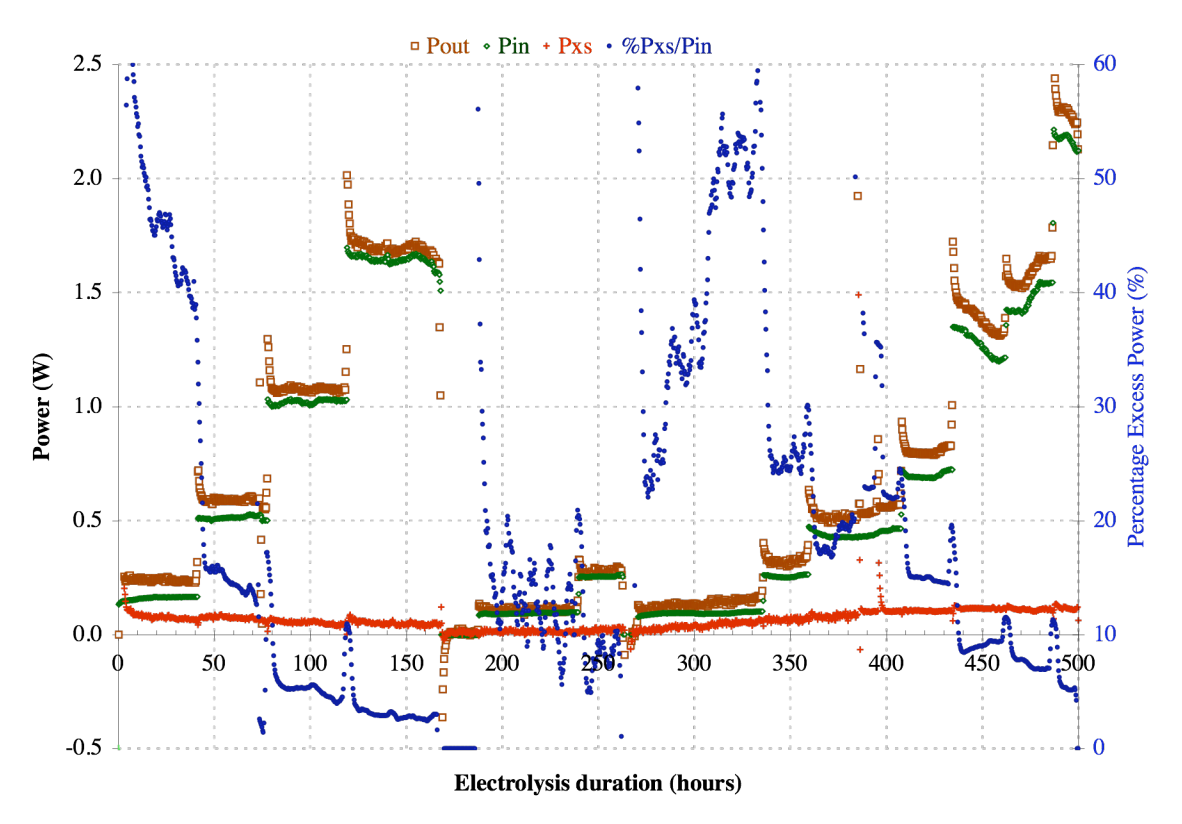


Figure 30. ETI 061-7 power and percentage excess power.

At later times, the cell was exercised with "normal superwave" current steps. The cathode loaded very well, the calorimeter operated as intended, and the cell exhibited P_{xs} up to 120 mW and over 50% of P_{In} . This small effect was more characteristic of Mode B than Mode A behavior in that P_{xs} did not exhibit a current density threshold or dependence.

An attempt was made later in the experiment to test directly for Mode A behavior at current densities above 100 mA cm⁻² and loading D/Pd > 0.92. Figure 31 plots the resistance ratio and loading before and following a brief current strip at ~ 555 h. Figure 32 plots the input, output, and excess power (W) on the left axis and average electrochemical current density (mA cm⁻²), percentage excess power, and excess energy integrated over the entire experiment (kJ) on the right axis. What is seen in Figure 31 is a rather well-behaved null calorimetric result, with $P_{xs} \le 1\%$ and a wide dynamic range of power input. Only at the highest current density (104 mA cm⁻²) and highest loading (D/Pd = 0.925) is there any significant departure of the output from the input power (a maximum P_{xs} of ~2.5%). The total excess energy integrated in this experiment was ~130 kJ, most of which was produced during the first 500 h of cell operation.

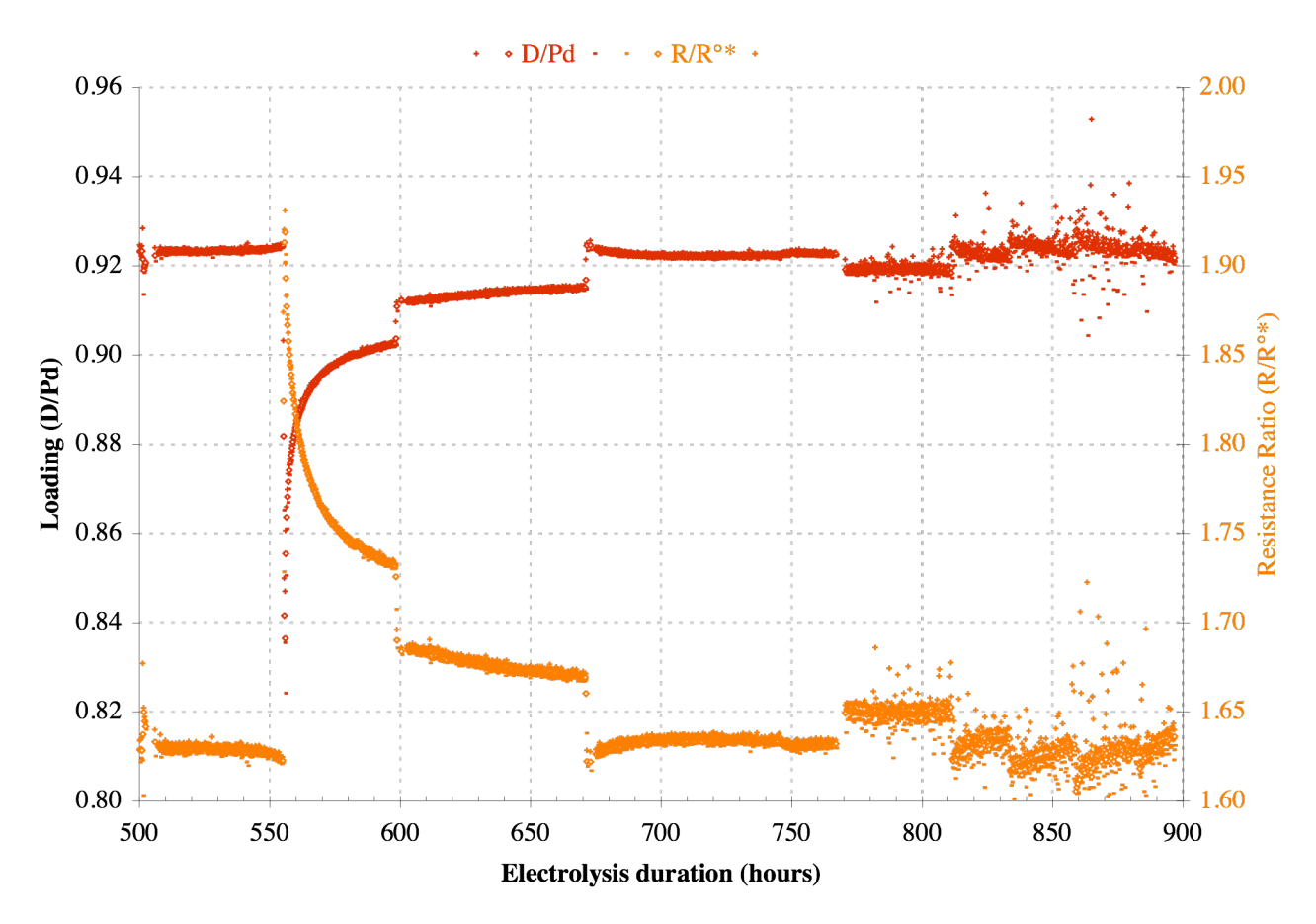


Figure 31. ETI 061-7 Loading and resistance ratio after 500 h.

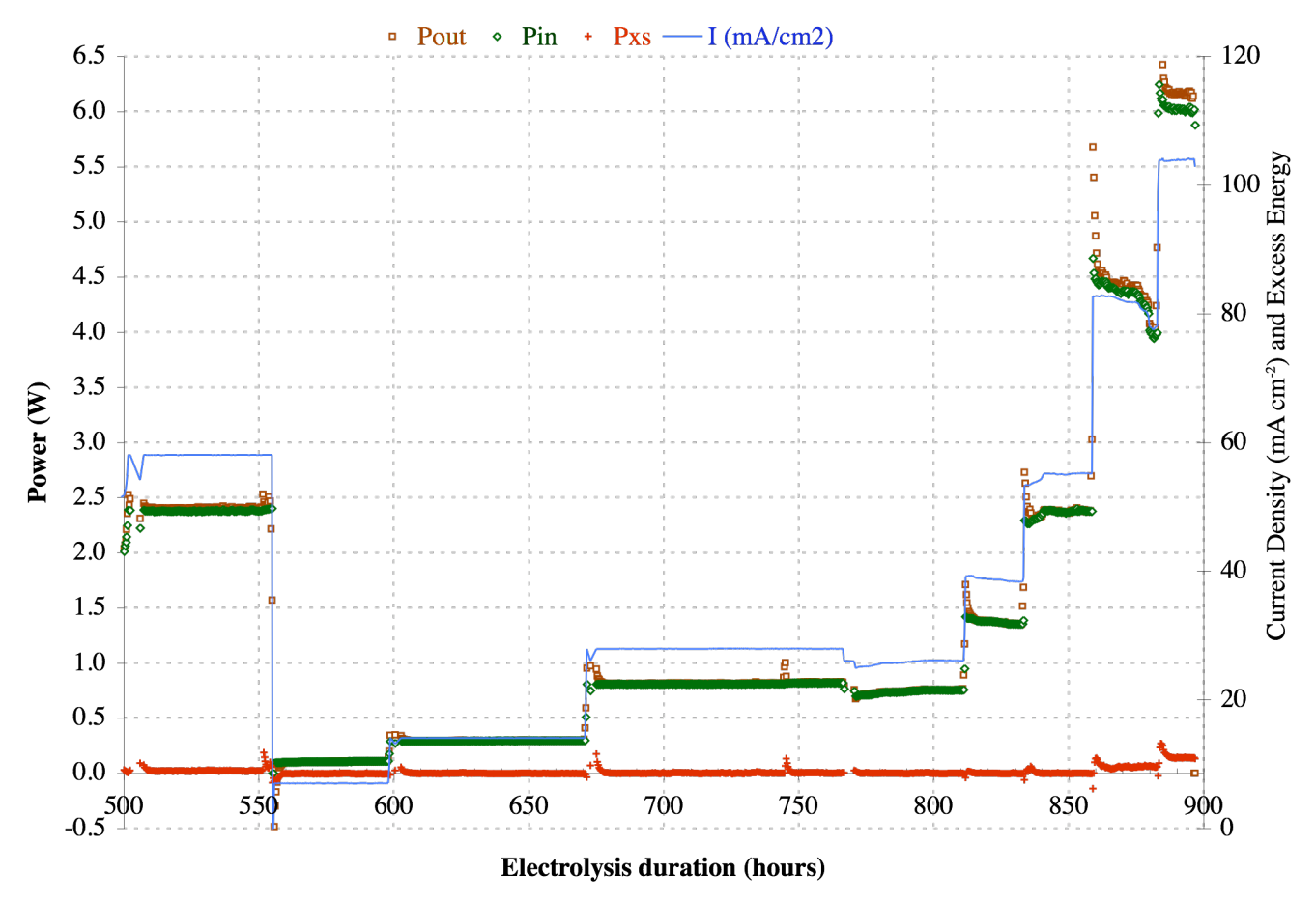


Figure 32. ETI 061-7 power and percentage excess power after 500 h.

ETI 057-8. Discussion of cell ETI 057-8 has been reserved until last because this was in many ways the most unusual cathode with in several ways the most unusual results. The cathode was constructed 37 from 50 μm Pd foil (JM), coated with single-wall carbon nano tubes (CNI HiPco® super purified) using electrophoresis (1.4 mg on one side and 2.7 mg on the other side), and finally coated with 0.9 μm of electrodeposited Pd.

Because of the method of construction, four terminal resistance measurements were not attempted with this composite cathode and thus we have no information concerning cathode loading. Figure 33 plots input, output and excess power (W) on the left axis and excess energy (kJ) on the right axis. Experiment ETI 057-8 was started with a calorimetric bath temperature of 22.46 \pm 0.05°C. The initial value of P_{xs} at 4 mA cm⁻² is small and uncertain (\sim 10 \pm 3 mW) but, based on prior calibration of sensors T_4 and T_5 , apparently nonzero. A concern was raised that this small amount of initial excess may be due to misorientation of the anode/cathode structure with respect to the calorimetric sensors and the cooling bath. At 22 h marked by the leftmost arrow in Figure 33, calorimeter 8 was rotated 90° in the bath. No immediate effect was seen in the temperature sensors and the current density was then doubled to an average value of \sim 8 mA cm⁻² approximately 30 min later.

-

³⁷ Reference 36.

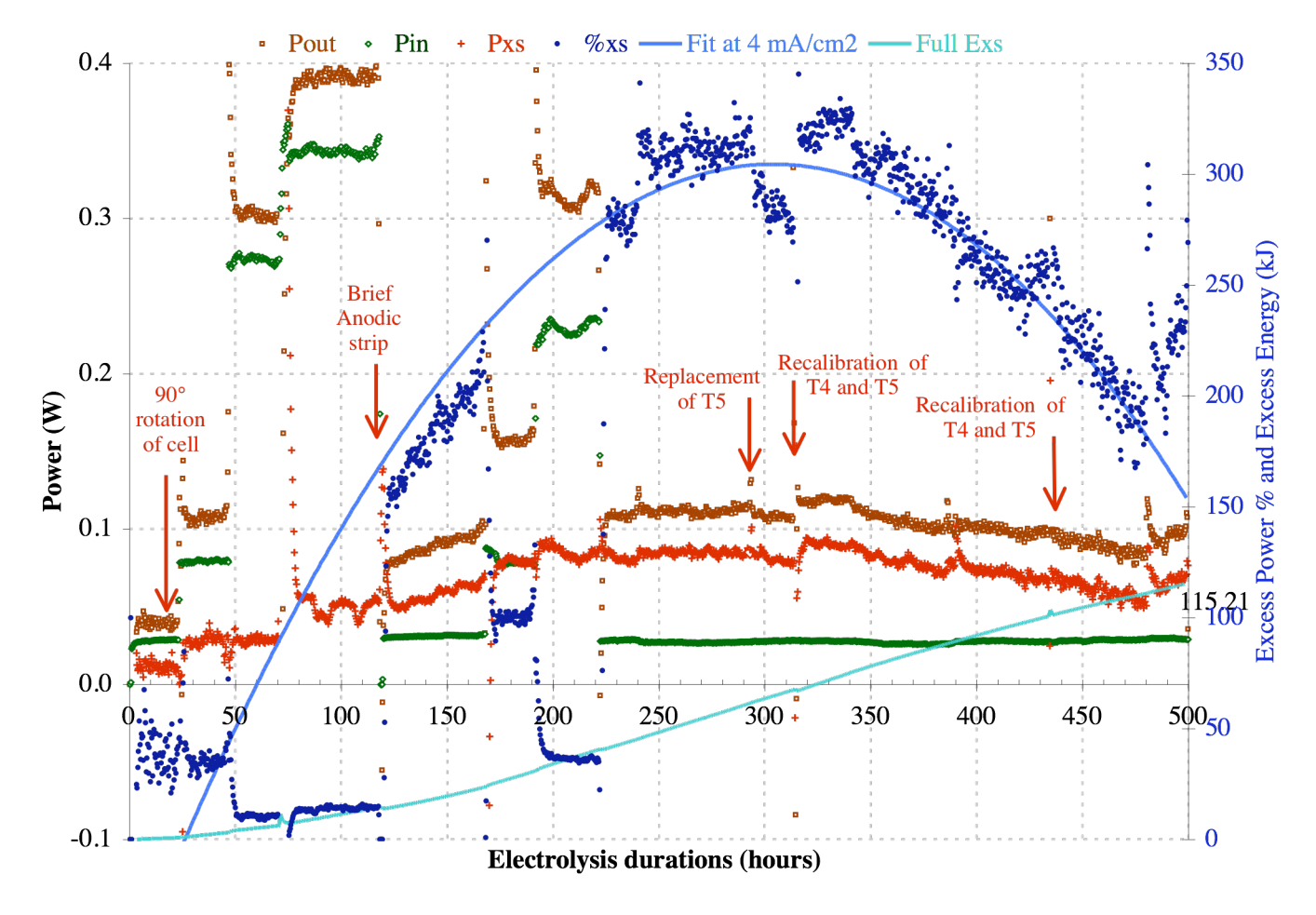


Figure 33. ETI 057-8 power and percentage excess power.

Doubling of the current input resulted in a factor of \sim 3 increase in both the input and output power, with the result that the excess power was maintained constant at $40 \pm 15\%$ of P_{In} . Anticipating a further increase in P_{xs} , the input current density was doubled again at \sim 47 h to \sim 16.5 mA cm⁻². Rather than increase, the excess power did not respond (immediately) to this current step and held constant at 30 ± 5 mW (now only 10% of P_{In} .

The sequence of steps and responses outlined above, while disappointing in their effect on the absolute value of P_{xs} and our ability to influence this with current, provides a good defense against potential systematic errors of calorimeter calibration due to either a dc offset error (ΔT_{error}) or an error in the multiplication factor that converts $\Delta T_{measured}$ (= $T_4 - T_5$) into output power. The second step from 8 to 16 mA cm⁻² resulted in no change of P_{xs} , so the multiplication factor is accurate. If the multiplication factor is accurate, then the increase in P_{xs} with the first step cannot be due to a putative ΔT_{error} .

At ~ 70 h the calorimetric bath temperature was lowered from ~ 23 to $\sim 3^{\circ}C$. The result can be seen in Figure 33 as a significant increase in P_{In} (presumably due to increases in both the interfacial kinetic and electrolyte resistances). P_{xs} increased proportionately even more from ~ 30 to ~ 60 mW with the percentage excess increasing from approximately 10% to a value of 15% of P_{In} .

Because of the apparently better performance of the excess heat at low temperature and low current, and uncertainty about the state of the cathode surface and loading, cell ETI 057-8 was subjected to a 1.5 h anodic strip at 118.5 h and the current density returned to \sim 4 mA cm⁻² at 120 h. The duration of this step was too short to allow thermal re-equilibrium at the lower input power. By the time the calorimeter regained its steady state output the excess power, at 4 mA cm⁻² after the strip, was essentially unchanged from its previous value at 16 mA cm⁻² (50 ± 10 mW). However, because of the approximately 10-fold decrease in P_{In} , this new value of P_{xs} represents roughly a 150% effect rather than 15%.

The cell was left with a 20-min superwave cycle of average current density 4 mA cm $^{-2}$ for 48 h. During this time the excess power increased apparently spontaneously to ~ 70 mW, while the input power remained essentially constant. At the end of this 2-day period the excess was $\sim 210\%$ of the input power.

Another attempt was made to increase excess power by doubling the average cathodic current density to 8 mA cm⁻² at \sim 170h, and again to 16 mA cm⁻² at \sim 193 h. Both attempts resulted in small increases in P_{xs} to a maximum value of \sim 95 mW. The increase in the denominator, P_{In} , resulted in a decrease in the percentage excess to \sim 100 and \sim 40% at 8 and 16 mA cm⁻² perturbation.

In the pursuit of high percentages it was decided to reduce the current density back to 4 mA cm⁻² and make long-term observations of the behavior of the calorimeter. This was begun at 223 h. Of major concern in observing a small excess power caused by an even smaller input power is maintenance of the calibration of the calorimetric sensors, T_4 and T_5 , relative to each other. The bath and quartz crystal temperature sensors provide a check on T_5 since at low output power all three sensors should measure very similar values (see Figure 28). In the period 128 < t < 168 h there was an indication of a drift in T_5 that has been corrected in Figure 33.

To increase confidence in the measured calorimetric temperatures, sensor T_5 was replaced at 295 h. Both T_4 and T_5 were recalibrated by removing them from the calorimeter and strapping them together to the quartz crystal temperature standard at 316 and 434 h. A small calibration change in the (previously uncalibrated) new sensor at 316 h resulted in a small increase in ΔT , and thus P_{xx} seen in Figure 33.

It seems likely that a small miscalibration of sensor T_4 resulted in an anomalously low value of P_{xs} in the interval 295 < t < 316 h. No other errors were indicated by recalibrations, and the excess power reaching a maximum of 95 mW and 330% of P_{In} shown in Figure 33 appears to be a robust signal outside the various measurement uncertainties.

Not only does this signal appear real, it appears to have temporal structure. The solid parabolic line in Figure 33 is a best fit to the data for percentage excess power collected at a bath temperature of 3.8°C and at an average cathodic current density of 4 mA cm⁻². While this line has no theoretical significance, it does suggest that, left uninterrupted, the excess power from this cathode may have risen from zero to a maximum and fallen back toward zero following a somewhat parabolic trajectory.

This relatively simple phenomenological observation may have sufficed had the experiment finished at this point. In an attempt to observe a threshold onset and maximize the percentage excess power, we reduced the current density progressively toward and to zero. The results of this exercise are shown in Figure 34. The steps in P_{In} reflect the stepped reduction of the average

cathodic current density from 4, 2, 1.5, 1, 0.5, and finally to 0 mA cm⁻² at 675 h after experiment initiation. At this point the cathode was electrically disconnected from the power supply.

The first thing to note in Figure 34 is that the excess power appears to rise independently of current density decreases. The second troubling feature is that the excess power maintains itself at an almost constant value of 50 ± 20 mW for ~ 160 h <u>after</u> cessation of all input current. At this point, P_{xs} began to decline for a further ~ 160 h until it was decided to terminate the cell while the putative excess power was present, in an attempt to detect nuclear emissions.

The questions directed to the excess power data in Figure 33 apply also to Figure 34. Can the temperature measurements T_4 and T_5 be trusted? In the complete absence of input power, with no possibility of net sustained chemical reaction, then a sensor temperature T_4 elevated above T_5 can be interpreted only by invoking an anomalous "excess" heat source. Further checks were undertaken given the very unusual result of Figure 34.

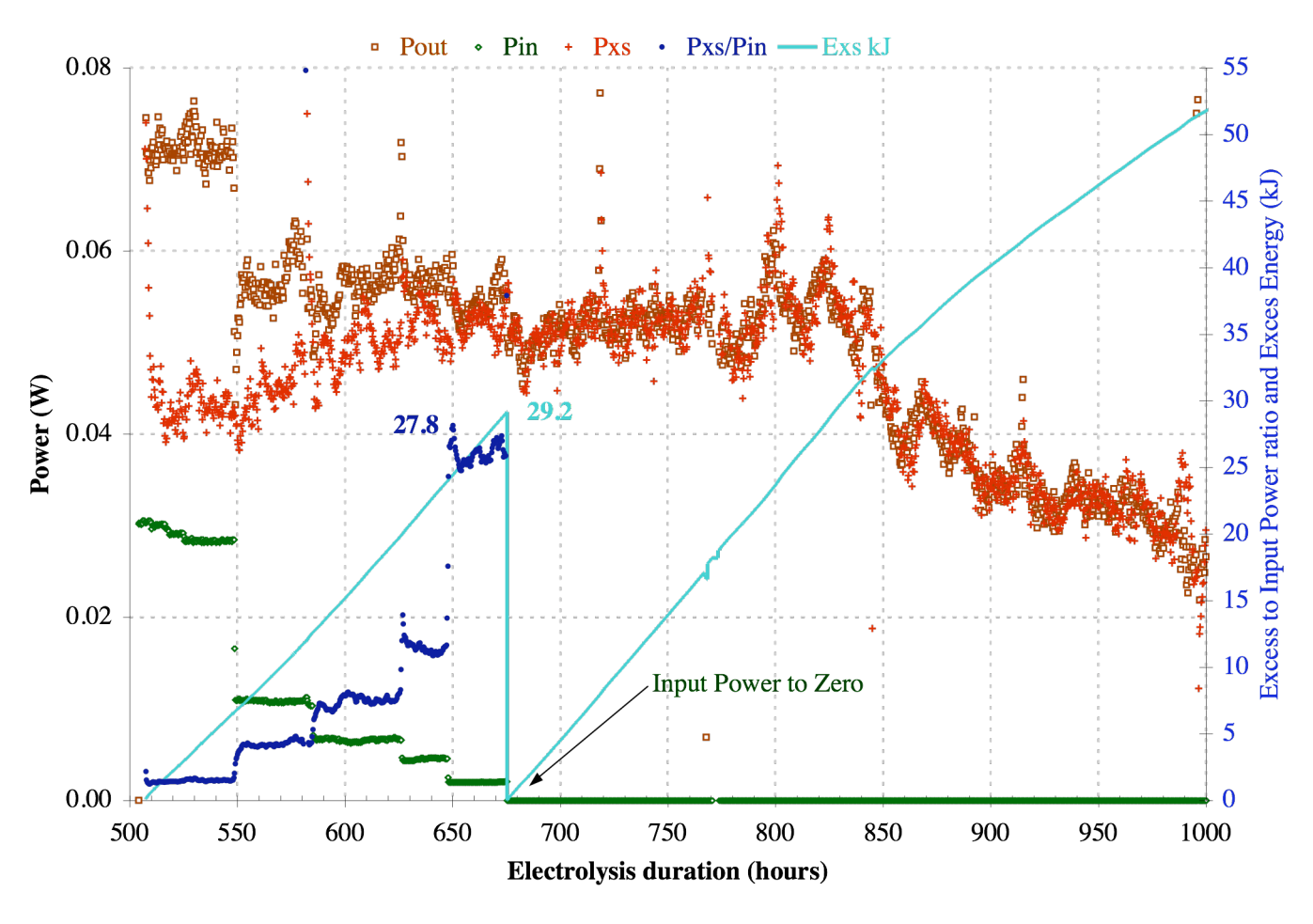


Figure 34. ETI 057-8 power and excess/input power ratio.

In addition to the sensor replacements and calibrations described above in reference to Figure 33, the following steps were taken to ensure that sensors T_4 and T_5 were accurate:

- 1. At 480 h the data acquisition for Cell 8–T₅ and Cell 7–T₅ were interchanged to ensure that mismeasurement of temperature was not the result of added resistance in the digital multiplexer (in other words, to check if a systematic error could be transferred between the Cell 8 and Cell 7 data collection systems).
- 2. At 503 h a third T₅ sensor was installed in Cell 8. This sensor was calibrated (together with another RTD sensor) versus the quartz crystal temperature (QCT) standard in a common bath in the range 3.767 to 3.990°C.
- 3. At 582 h the T_4 and T_5 sensors (in all three cells) were removed from the cells and calibrated with respect to the QCT standard at 4.818 4.829°C.
- 4. At 652 h the T_4 and T_5 were removed from Cells 8 and 9 and calibrated with respect to the QCT at 4.038° C.
- 5. At 844.98 h sensors T₄ and T₅ were removed from Cells 8 and 9 and calibrated with respect to the QCT at 4.035°C.
- 6. At 845.03 h sensors T₄ and T₅ were returned to Cell 8 with positions reversed. In this way any systematic error associated with the measurement of temperature of either sensor should have an effect of opposite sign.

None of the steps described above gave any cause for concern about the accuracy of the calorimetric temperature sensing in Cell 8, either for T_4 or T_5 . Obviously no error of multiplication factor could produce the observed result. With diminishing input power and constant (or increasing) excess power, the power multiple P_{xs}/P_{In} increases rapidly. The dark blue circle points in Figure 34 show this value increasing to $P_{xs}/P_{In} = 27.8 \pm 1$ at an average input current density of $i = 0.63 \pm 0.02$ mA cm⁻². When the current and input power are reduced to zero, this ratio obviously loses mathematical significance. Nevertheless, a power gain of 2800%, if real, has very significant theoretical and potential practical importance, in spite of the low absolute value.

At 1059 h, the cell was opened *in-situ* and the cathode was kept immersed in H_2O in front of a Ludlum model 306/42-30 neutron detector. This effort was made with the hope of being able to observe some direct nuclear evidence of the ongoing heat process. No counts above background were recorded during the 16-h exposure.

Because of the heterogeneous character and fragile nature of cathode ETI 057-8, resistance measurements were not made so there was no direct measure of the bulk cathode deuterium loading. During the period for which this cathode was at open circuit (after 1058 h), the cell voltage provides a measure of the deuterium surface activity and thus an indirect measure of loading. This number was not recorded automatically but was displayed and frequently noted manually during the "heat after life" episode of cathode ETI 057-8. This cathode maintained a surface voltage > 800 mV (with respect to Pt) for several hundred hours following current cessation, possibly until the experiment was terminated. Such large values indicating high D

_

³⁸ Only the product I*V was averaged and recorded for calorimetric purposes.

surface activity and (potentially) loading have not previously been observed with simple Pd cathodes.

At 1062 h the cell was reassembled using a 50 μ m thick Pt foil of the same area in place of the ETI 057-8 cathode. The cell was allowed to operate open circuit under identical conditions as previously prior to cathodic replacement, in the same electrolyte. The cell was then exercised through a series of current density steps up to 71 mA cm⁻² and then back to zero to confirm the baseline calibration and multiplication factor of the calorimeter.

Figure 35 shows the result of removing and replacing the composite cathode in ETI 057-8 with a similarly sized Pt foil. During the period shown, the cell and calorimeter conditions were held constant: temperature, current density = 0, calorimeter coefficients and temperature sensor calibrations. It is fairly clear from Figure 35 that 20-30 mW more heat was present in the calorimeter with the Pd/C composite cathode than with Pt.

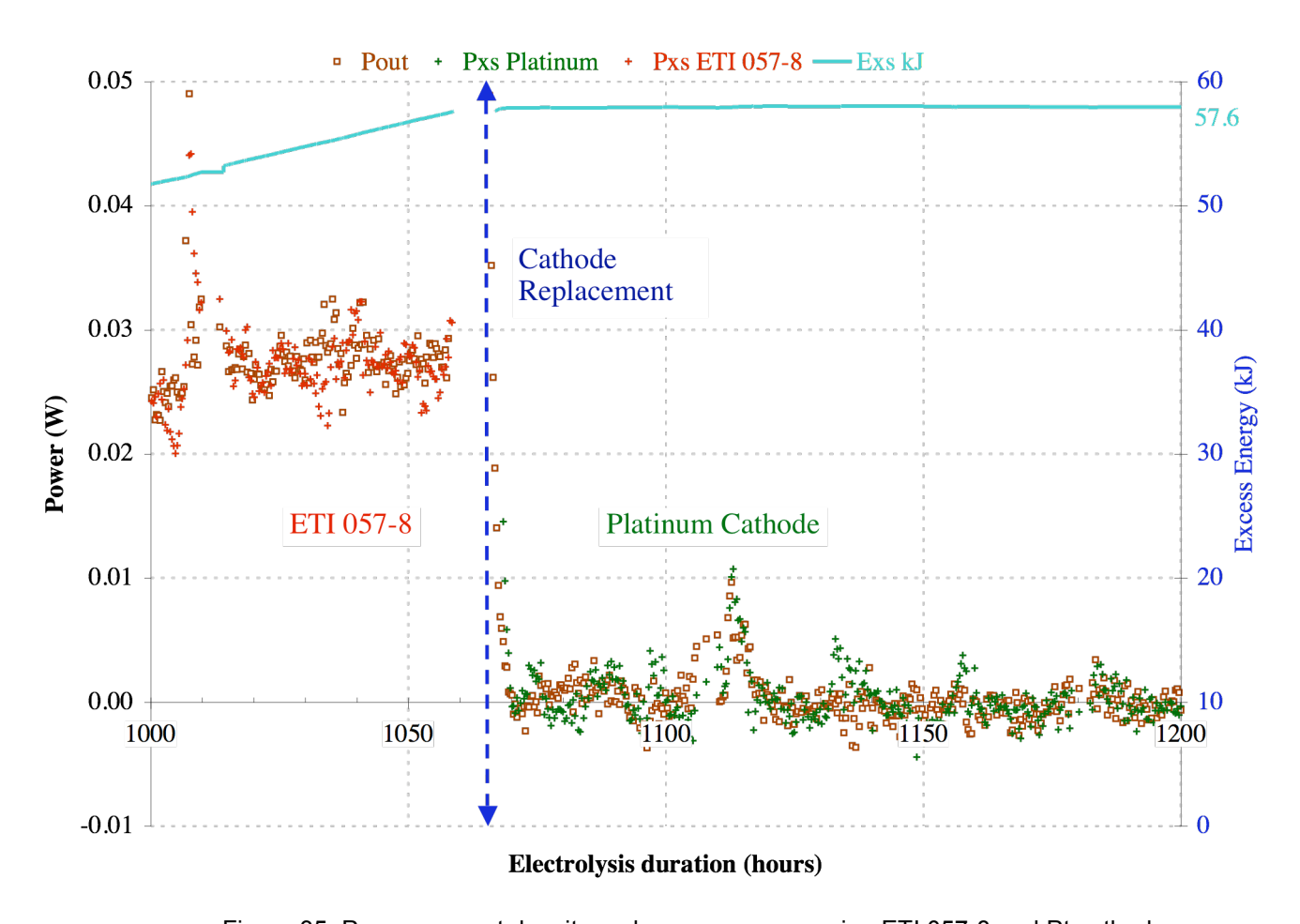


Figure 35. Power, current density and excess energy using ETI 057-8 and Pt cathode.

Figure 36 is a continuation of Figure 35 with a different left axis vertical scale, and shows the response of the calorimeter to current density steps to 13, 25, 36, 71 and back to 0 mA cm⁻². The performance of the calorimeter is as expected, the only significant deviation from thermal balance being incomplete correction for the transient behavior of the power input and output. The unsteady behavior of these functions for the platinum electrode at the highest current density is attributable to a poor electrode contact caused by the somewhat impromptu nature of the cell rebuild, since it was not possible to spot weld the Pt wire contact to the substitute Pt cathode.

Despite various checks and interchanging of sensors, a consistent positive temperature difference was measured between the calorimetric, four-terminal RTD sensors T_4 and T_5 . If this difference is due to the presence of a heat source in, at, or near the cathode, then some evidence of it should be reflected in the non-calorimetric electrolyte sensors $T_1 - T_3$. As discussed previously in relation to Figure 28, these sensors display a consistent temperature in relationship to the inner boundary sensor, T_4 , with the temperature drop from the innermost electrolyte sensor, T_2 , to the heat sink, T_{bath} , being twice that from T_4 .

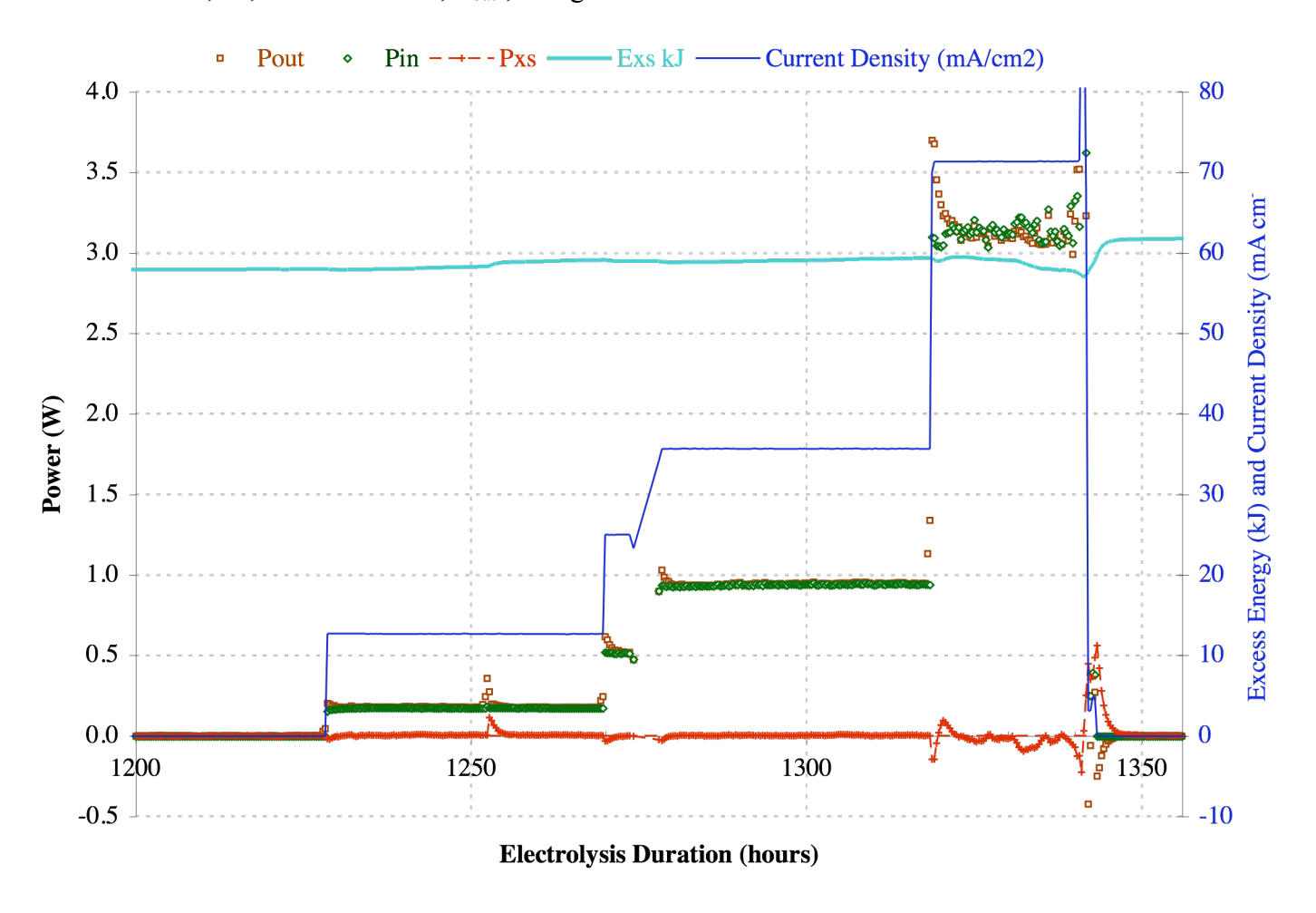


Figure 36. Power, current density and excess energy calibration using Pt cathode.

Figure 37 plots average temperature values from two populations, one 24 h before removal of the cathode, labeled "ETI 057-8", the other 24 h after the cell temperatures have stabilized following replacement of the active cathode with a dummy, labeled "Platinum." The error bars shown are standard deviations of the measured values in the respective 24-hour intervals.

The lines in Figure 37 are constructed as follows:

- 1) The green dashed line at the bottom joins the points $(0, T_{bath})$ and $(1, T_{center})$ with slope determined from twice the difference between T_4 and T_5 . The horizontal positions of all other points on (or near) this line are the relative thermal resistance (or distance) value determined from Figure 28. The gradient in temperature in the cell with the Pt cathode is due to heat leaking into the cell from the higher ambient temperature (23.98 \pm 0.23°C). This effect is small, and is included in the calorimetric evaluation of cell heat output power output. In terms of the relative thermal resistance axis of Figure 37, the position of $T_{Ambient}$ is 369. That is, the ambient heat leaking into the cell to affect the temperature of the calorimetric sensor T_4 (at relative position 0.5) is only 1 part in 737, or 0.14% of that produced by a heat source close to the position of T_2 .
- 2) The solid red line is the position predicted for all sensor temperatures based on the small difference in average bath temperature, and a slope that reflects the small change in average ambient temperature (23.99 ± 0.32°C) inleakage. In other words, if all parameters of the calorimeter and heat flow paths were the same before and after interchanging the ETI 057-8 cathode with the platinum blank, and the only differences were the small changes in ambient and bath temperature, then the measured temperature values should straddle the solid red line. Apparently they do not.
- 3) The dashed red line at the top is a regression fit to the six measured temperatures with the fitting parameters shown. The difference in slope between the dashed and solid lines reflects the presence of an additional heat source located somewhere in the vicinity of T₂ and T₃. Comparing the measured value at T₄ (3.968 ± 0.005°C) with its predicted value (3.934 ± 0.01°C) gives a temperature difference of 0.034 ± 0.01 °C. Since the value of K for this cell was 1 W/K, this temperature difference represents 34 ± 10 mW, very close to the value seen in Figure 35.

While not intended to be statistically rigorous, this exercise tends to confirm that the Cell 8 calorimeter was working in an understandable manner, and that the heat observed using cathode ETI 057-8 after cessation of current input (and presumably before) is real and significant. The population of points represented by the red diamonds in Figure 35 appears to be different from that of the blue squares for the blank unexercised cathodes. The alternative explanation that the difference in populations is due to a systematic error that was corrected by installing a blank cathode seems unlikely. We must therefore confront the possibility that approximately 60 kJ of excess energy was produced in a period lasting some 380 h or 16 days <u>after</u> the removal of the superwave (or any) electrochemical stimulus.

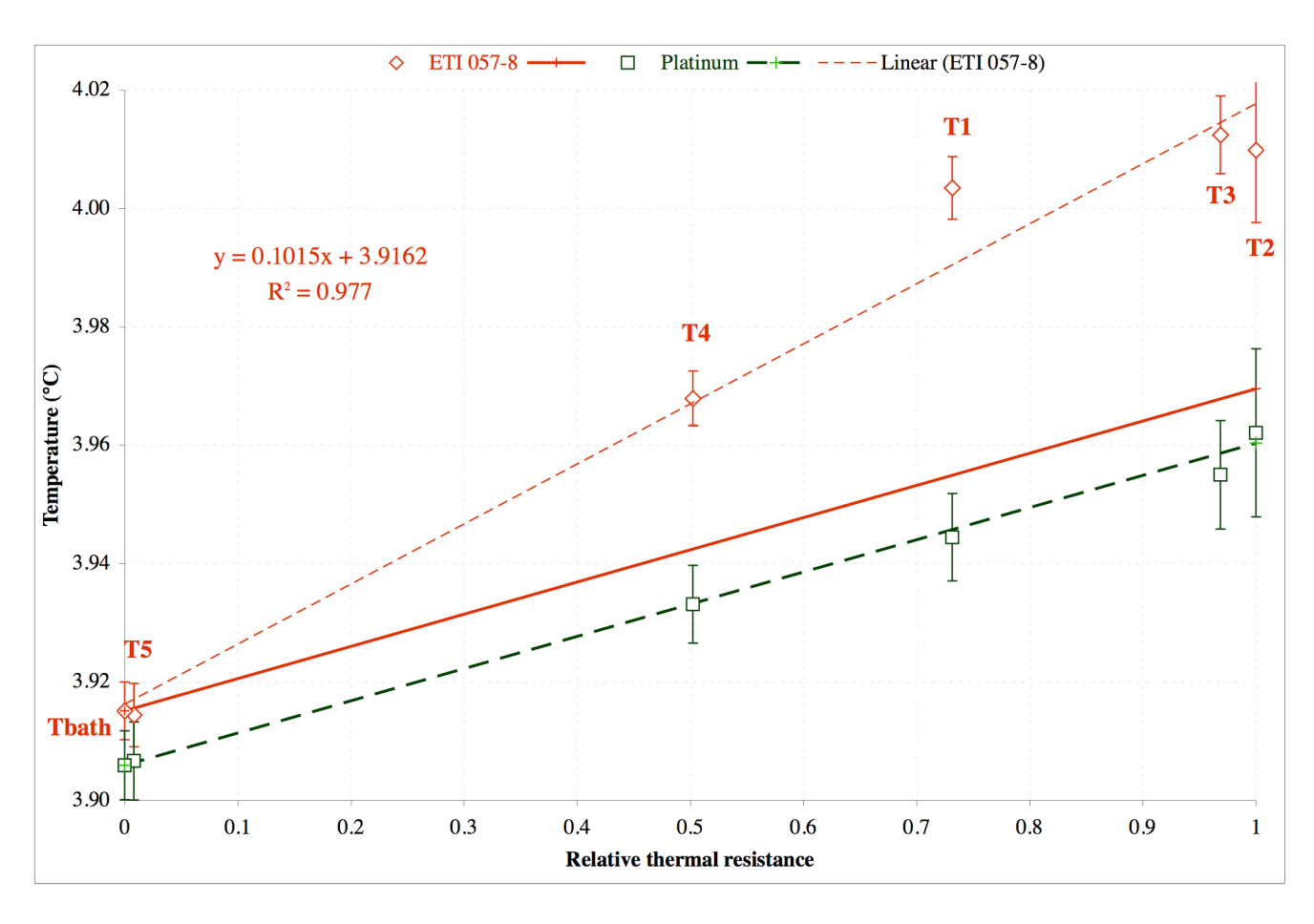


Figure 37. Temperature profile with ETI 057-8 and platinum cathode.

There seems very little reason to doubt the existence of Mode B excess heat in Figure 33, present early in the cell operation, exhibiting no obvious current threshold, and on the whole rather insensitive to net cathodic current density. Figure 34 reveals possibly another mode of excess heat production, heat after cessation of external stimulus that we tentatively call Mode C. The tests and checks performed during the intervals of Figures 34, 35 and 36 also leave little reason to doubt the existence of such behavior, even though we do not expect to see excess heat in a deuterium-loaded lattice not subject to external stimulus.

A possible explanation was proposed by Energetics³⁹ in response to their similar observations of "Mode C" behavior in similarly constructed cathodes. Electrode ETI 057-8 was constructed by layering palladium, single-walled carbon nanotubes (SWCNT), and then palladium again. Figure 38 shows an electron micrograph of the post-test surface of this cathode. Energetics hypothesized that in such an electrode excess heat is generated inside the nanotubes. For this to happen the deuterium in the nanotubes must be at high density (or activity), and there

_

³⁹ E. Greenspan personal communication.

needs to be a flux of deuterium through the nanotubes⁴⁰. These conditions are obtained during the electrolysis, where the superwave stimulus generates high loading and flux. After removal of the cathodic current, a flux of deuterium will be established through the nanotubes, acting as a deuterium atom source to the palladium and into the electrolyte. Evidence of this source and flux is the abnormally high open circuit voltage registered by the Electrode ETI 057-8 cathode. This process may be responsible for the "heat after cessation of external stimulus," although we must treat this as a working hypothesis awaiting further experimentation.

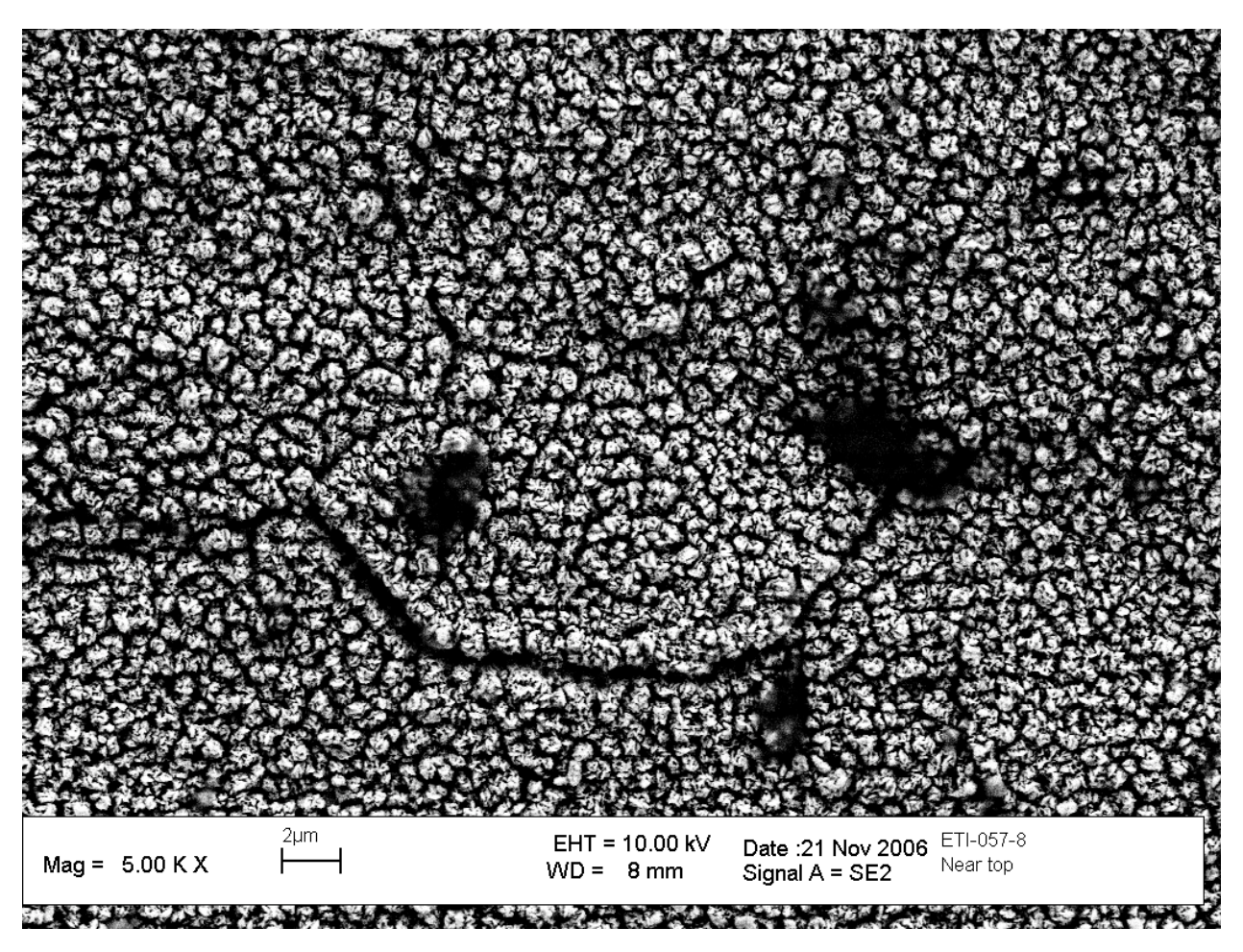


Figure 38. Post-test surface of cathode ETI 057-8 (SEM at NRL).

⁴⁰ In carbon-free palladium it can be postulated that excess heat is produced in similarly sized linear defect structures at the cores of dislocations.

POST TEST ANALYSES

The electrodes were examined by optical microscope at SRI and by SEM at ENEA (Frascati) and NRL. NRL also undertook a preliminary survey for isotopic effects and has prepared a separate report of their microscopic and isotopic studies⁴¹. The Summary and Conclusions of this report are incorporated here for convenience.

NRL SUMMARY

The analysis conducted of the materials provided has revealed some definitive information. ICP-MS⁴² indicates there are some low level impurities present in the solutions used, some consistent with dissolution of stainless steel, and the components of solder, among a few others. No obvious distortions in the isotopic composition of Li or B were measured. The surface of the cathodes has a varied structure, with hillocks, grain boundary grooving and extrusion, precipitates, faceting, nodules, low Z contaminants, and in the case of cathode 057-8, a very porous structure being present. XRD⁴³ suggests that environmental contributions of H can contaminate the cathodes. and that they unload over time to the a phase of Pd(H,D). CNDP⁴⁴ confirms that the surface of the cathode retains Li following electrochemical processing, and suggests the SWCNT cathode may present about a factor of 3 more surface area. Trace element analysis of the cathodes and anodes has not been performed as yet, as this effort is a destructive form of analysis. ICP-MS from etchings of a part of the electrodes will be conducted to compare with impurities found in the solutions. If warranted, Trace Element Accelerator Mass Spectrometry (TEAMS) will be performed as well. Additional SEM of the Pt electrodes, and XRD of the remaining cathodes are still planned.

NRL CONCLUSIONS

The analysis of cathodes, anodes, and solutions has found some common features among them, as well as features preferentially associated with either heat producing or non-heat-producing cathodes. Whether these features are relevant to the performance of the cathodes is uncertain, but they are worthy of further investigation. Some interesting correlations to consider include: large grain boundary grooving observed only on some non-heat-producing cathodes, and small (~100 nm) nodules only on some heat producing cathodes. There does not appear to be any critical correlation between an impurity or isotope enrichment and the production of excess heat. However, the precision and sensitivity applied thus far may not be sufficient to observe such a correlation. It is interesting to note that there are measurable amounts of Li, B, and U in the materials analyzed, that have been previously suggested as important contributors to the mysteries of condensed matter nuclear science.

⁴¹ Reference 37. The image in Figure 38 was obtained in this study.

⁴² Inductively Coupled Plasma – Mass Spectroscopy.

⁴³ X-Ray Diffraction.

⁴⁴ Cold Neutron Depth Profiling.

HELIUM

The major species expected⁴⁵ to be associated with the excess heat as a nuclear product is ⁴He. The electrochemical cells and calorimeters used in this study were not designed to be helium leak tight and no attempt has been made so far to correlate heat and helium production levels. At some future stage, when NRL and ENEA have exhausted their arsenal of diagnostic testing, it is planned to analyze samples of electrolyzed and blank palladium cathodes for both ⁴He and ³He. As this analysis is destructive it will be reserved until last.

TRITIUM

At the conclusion of the experiment series, the initial D_2O and final electrolyte solutions were analyzed for tritium content. Sample volumes of 4.0 ml were withdrawn from the electrolytes and distilled to dryness. A 1.0 ml portion of this distillate was then added to 10.0 ml of BioSafe II⁴⁶ scintillation liquid. These "cocktails" were then counted for 60 min using a Beckman LS 6500 liquid scintillation counter with a count efficiency of 20%. All counting of active samples took place at least 2 h after the sample was placed in the dark sample chamber to preclude any photochemically induced counts. The results of this analysis are shown in Table 4.

No tritium enhancement is expected from non-nuclear reactions for closed cell operation. There is a known separation factor between the concentration ratio of T/D in the gas above an electrolyzing solution of TDO and D_2O , but in a system where all of the electrolysis products are recombined and returned as liquid to the cell, tritium will not accumulate preferentially in one phase or another. The situation in our operating cells is a little more complex, and a number of potential sources and sinks of tritium must be considered:

1. Electrolyte makeup - source. None of the cells sealed hermetically, and loss of D₂O (and TDO) presumably as vapor was observed to occur. Because of the sensitivity of the calorimetry to electrolyte level, a simple arrangement of a passive auto-siphon was used to maintain level in the cell by permitting gravitational bleed from a larger external D₂O reservoir. This arrangement avoids the complexity and potential fragility of level sensors and active controllers, but suffers the disadvantage that the timing of the demand feed is not monitored automatically. The total volume delivered in any interval is known from the change in level of the external reservoir, which is monitored and recorded manually. Each mole of added D₂O brings with it new tritium at its initial concentration in the D₂O.

_

⁴⁵ References 22 and 38-63.

⁴⁶ Research Products International Corp., Mt Prospect, IL.

Table 4. Electrolyte Tritium Results

	DPS	Atoms	Tritium Expect		
Sample	/ml	/vessel	Enhancemen Max.	19%	± 3%
D_2O	2.80 ± 0.3	$3.6E+11 \pm 3.3E+10$	ξ Typical	10%	± 2%
ETI009	8.03 ± 0.3	$1.0E+12 \pm 4.1E+10$	2.866 ± 0.12	187 %	± 4%
ETI011	3.89 ± 0.3	$5.0E+11 \pm 3.3E+10$	1.390 ± 0.09	39%	± 7%
ETI012	3.93 ± 0.3	$5.0E+11 \pm 3.3E+10$	1.402 ± 0.09	40%	± 7%
ETI015	7.74 ± 0.3	$9.9E+11 \pm 4.1E+10$	2.765 ± 0.11	176%	± 4%
ETI016	2.98 ± 0.3	$3.8E+11 \pm 3.3E+10$	$1.40 1.065 \pm 0.09$	7%	± 9%
ETI017	2.93 ± 0.3	$3.8E+11 \pm 3.3E+10$	$1.27 1.048 \pm 0.09$	5%	± 9%
ETI021	2.74 ± 0.3	$3.5E+11 \pm 3.3E+10$	$0.91 0.979 \pm 0.09$	-2%	± 9%
ETI022	2.66 ± 0.3	$3.4E+11 \pm 3.3E+10$	$0.81 0.949 \pm 0.09$	-5%	± 10%
ETI035-7	3.18 ± 0.3	$4.1E+11 \pm 3.3E+10$	$2.36 1.137 \pm 0.09$	14%	± 8%
ETI035-8	3.34 ± 0.3	$4.3E+11 \pm 3.3E+10$	$4.85 1.193 \pm 0.09$	19%	± 8%
ETI035-9	3.53 ± 0.3	$4.5E+11 \pm 3.3E+10$	1.259 ± 0.09	26%	± 7%
ETI043-7	2.73 ± 0.3	$3.5E+11 \pm 3.3E+10$	$0.90 0.976 \pm 0.09$	-2%	± 9%
ETI043-8	2.86 ± 0.3	$3.7E+11 \pm 3.3E+10$	$1.10 1.021 \pm 0.09$	2%	± 9%
ETI043-9	3.01 ± 0.3	$3.9E+11 \pm 3.3E+10$	$1.48 1.074 \pm 0.09$	7%	± 9%
ETI051-7	2.70 ± 0.3	$3.5E+11 \pm 3.5E+10$	$0.86 0.964 \pm 0.10$	-4%	± 10%
ETI051-8	2.53 ± 0.3	$3.2E+11 \pm 3.5E+10$	$0.68 0.902 \pm 0.10$	-10%	± 11%
ETI051-9	2.56 ± 0.3	$3.3E+11 \pm 3.5E+10$	$0.71 0.914 \pm 0.10$	-9%	± 11%
ETI056-7	2.79 ± 0.3	$3.6E+11 \pm 3.5E+10$	$0.99 0.997 \pm 0.10$	0%	± 10%
ETI057-8	2.63 ± 0.3	$3.4E+11 \pm 3.3E+10$	$0.78 0.940 \pm 0.09$	-6%	± 10%
ETI058-9	2.90 ± 0.3	$3.7E+11 \pm 3.3E+10$	$1.19 1.036 \pm 0.09$	4%	± 9%
ETI061-7	2.72 ± 0.3	$3.5E+11 \pm 3.3E+10$	$0.88 0.970 \pm 0.09$	-3%	± 10%

- 2. <u>Gas loss source or sink</u>. D₂, DT and O₂ electrolytically evolved in the cell convect to the recombiner and there recombine to form D₂O and TDO. The rate of this reaction and its exothermicity are such that the species initially produced are D₂O and TDO vapor. The electrolytic separation factor governed by the differential rates of D₂O and TDO electrolytic reduction will determine the ratio concentration of TD:D₂ and TDO:D₂O in the vapor phase of the external recombiner chamber. In the presumed perfect operation of the recombiner, these ratios will be the same. Whether this effect is a source or sink of tritium compared with the makeup source depends on the product of two separation factors:
 - a. The electrochemical separation factor, $\xi_{Electrochem}$. that generates D_2 and DT in the gas phase of the recombiner.
 - b. The gas phase separation of D_2 , DT, D_2O and DTO diffusing (or convecting) out of the recombiner volume and into the ambient, ξ_{Diff} .

3. <u>Solid absorption – source or sink</u>. The solid surfaces into which the various D and T species can come in contact may preferentially adsorb or absorb one or other isotope and therefore act as a source or sink for tritium. The largest volume by far is the PTFE liner of the cell and the ancillary tubing that connects the cell with the recombiner. The two most active volumes are the recombiner itself⁴⁷ and the palladium cathode. Values have been measured experimentally for the liquid:solid separation factor for T/D at an electrolyzing Pd|D₂O interface. This number varies from approximately⁴⁸ 6 to 9, with D greatly preferring to occupy the Pd lattice compared to T. This is clearly a source of tritium enhancement in the electrolyte (or, more specifically, deuterium depletion) but the total number of moles of D in the electrolytic D₂O (25 moles) compared with D in the palladium cathode (at most 2.8 x10⁻³ moles) render this source term negligible⁴⁹.

This situation seems complex, and we clearly do not have sufficient information to determine quantitatively the rate of tritium concentration or sequestration by each of the mechanisms listed above. A glance at the column labeled "Atoms/vessel" in Table 4, which lists the total increase of tritium atoms for each experiment, reveals that, whatever the quantification of the tritium generation rate, it is many orders of magnitude too small to account for the excess heat energy of successful experiments.

We are concerned here with addressing a much simpler question: "Is there plausible evidence to suggest that tritium was produced as a nuclear product in any of the experiments performed in this series?" We will do this by examining the worst possible case leading to maximum tritium enhancement for the inventory of materials used in our experiments: an open pot in which tritium concentration is increased by physical evaporation and fractional distillation of the more volatile D_2O component⁵⁰. This case has the advantage of being well measured and understood, and conservative with respect to tritium generation, as will be discussed later.

Figure 39 plots the expected increase in liquid phase tritium levels normalized to its initial value as a function of the volume of D_2O used to make up the volume lost. Three values are used for the electrochemical separation factor, $\xi_{Electrochem}$, defined as,

$$\xi_{\text{Electrochem.}} = \{ [T]/[D] \}_{\text{Liquid}} / \{ [T]/[D] \}_{\text{Gas}}$$
[14]

⁴⁷ The Hoppecke AquaGen recombiner catalyst has a proprietary composition.

⁴⁸ References 64-74.

⁴⁹ Unpublished evidence from experiments performed previously at SRI indicates that tritium absorbs preferentially in palladium in the high D loading condition so that this very small source term might in fact be a sink for tritium. The results of the present study show the same tendency.

⁵⁰ Electrolytic "evaporation" is a mixed and more complex case as electrolytically produced D₂ and O₂ bubbles leave the cell saturated with D₂O vapor at the temperature of cell operation.

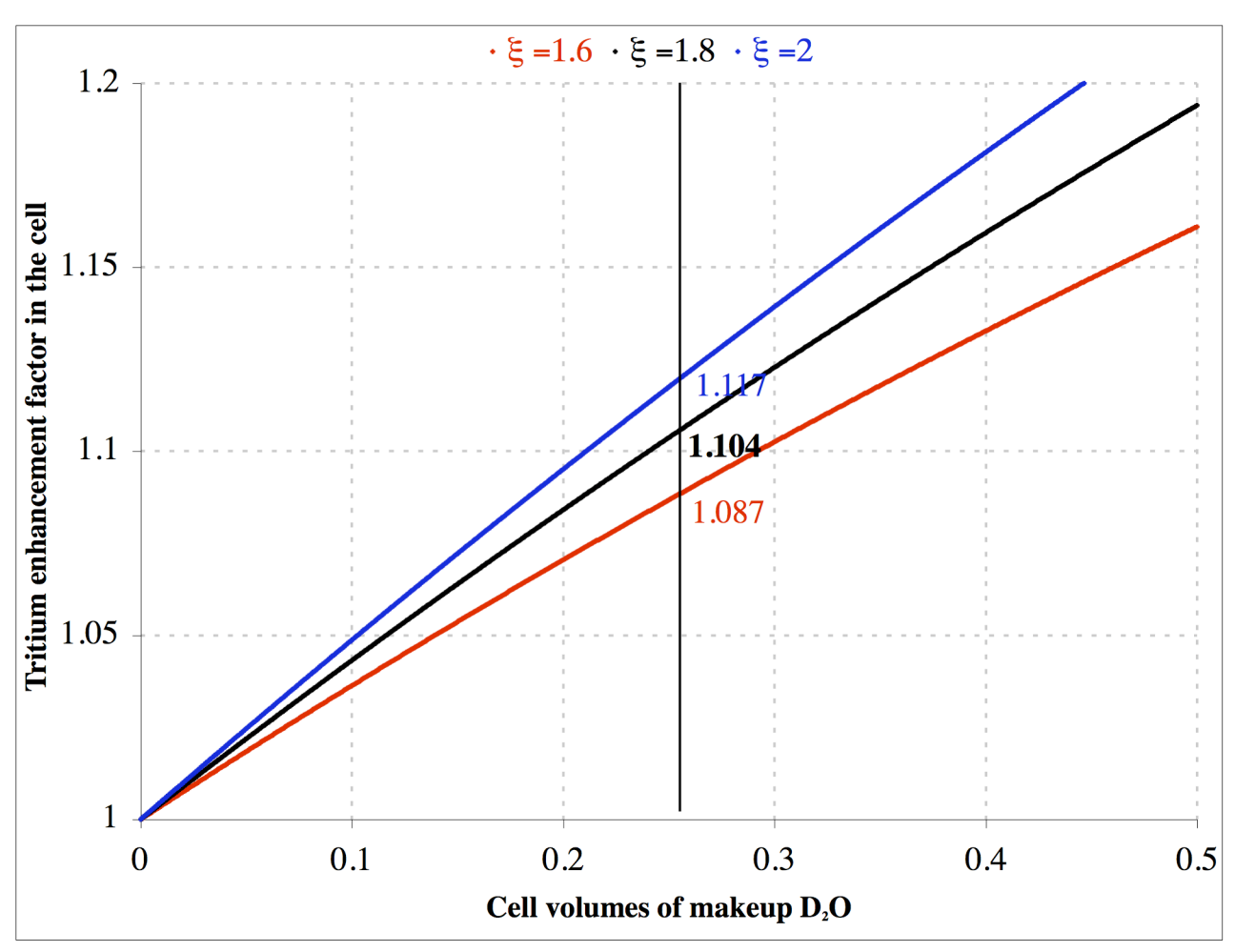


Figure 39. Tritium enhancement factor *versus* makeup D_2O volume as a function of the value of the separation factor, ξ .

The mean value of 1.8 is that quoted and used extensively by Szpak.⁵¹ This value appears to depend somewhat on the nature of the solution, and the boiling.⁵² The upper and lower values of the separation factor (1.6 and 2.0) appear to be plausible bounds. The electrolyte volume of the cells is 230 ml. While only intermittently recorded, the maximum value of makeup D_2O used in the experiments listed in Table 4 was approximately 50% of a cell volume, shown at the right axis of Figure 39. More typically this number was ~25% cell volume, shown by the vertical line with numeric callout in Figure 39. On some occasions the amount of D_2O makeup was even less.

Figure 39 shows that for separation in a freely boiling pot, we expect a tritium enhancement of about 10%, at most roughly twice this. In Table 4 the experiments listed in green fall into this window of possibility, those listed in orange clearly cannot be accounted for by this means of tritium separation, and those in red well exceed the upper limit of 20% at $176 \pm 4\%$ and $187 \pm 4\%$

⁵¹ Reference 75.

⁵² References 76-79

4%. We can reasonably assert that, whatever is causing the tritium enhancement in the 2 or 5 larger cases (orange and red), it is not evaporative boiling of the cell D_2O makeup feed.

This conclusion is confirmed by the fact that 2/3 (14/21) of the cells in Table 4, those listed in blue and black, show no sign of tritium enhancement within the measurement uncertainties. In fact, the two listed in italics in black appear as if the electrolyte tritium levels may have reduced with electrolysis. First we will consider what this means in terms of <u>whatever</u> separation factor and process may be operational, and then we will consider whether this makes physical sense.

Figure 40 plots the tritium enhancement factor for the cell for two different makeup volumes of D_2O (25% and 50%) as a function of separation factor. The data points from Table 4 are plotted in their positions presuming a 25% makeup. In other words, the positions of these points determine the value of separation factor that would be needed to account for the measured final values of tritium concentration, for a cell with 25% makeup (typical for most cells).

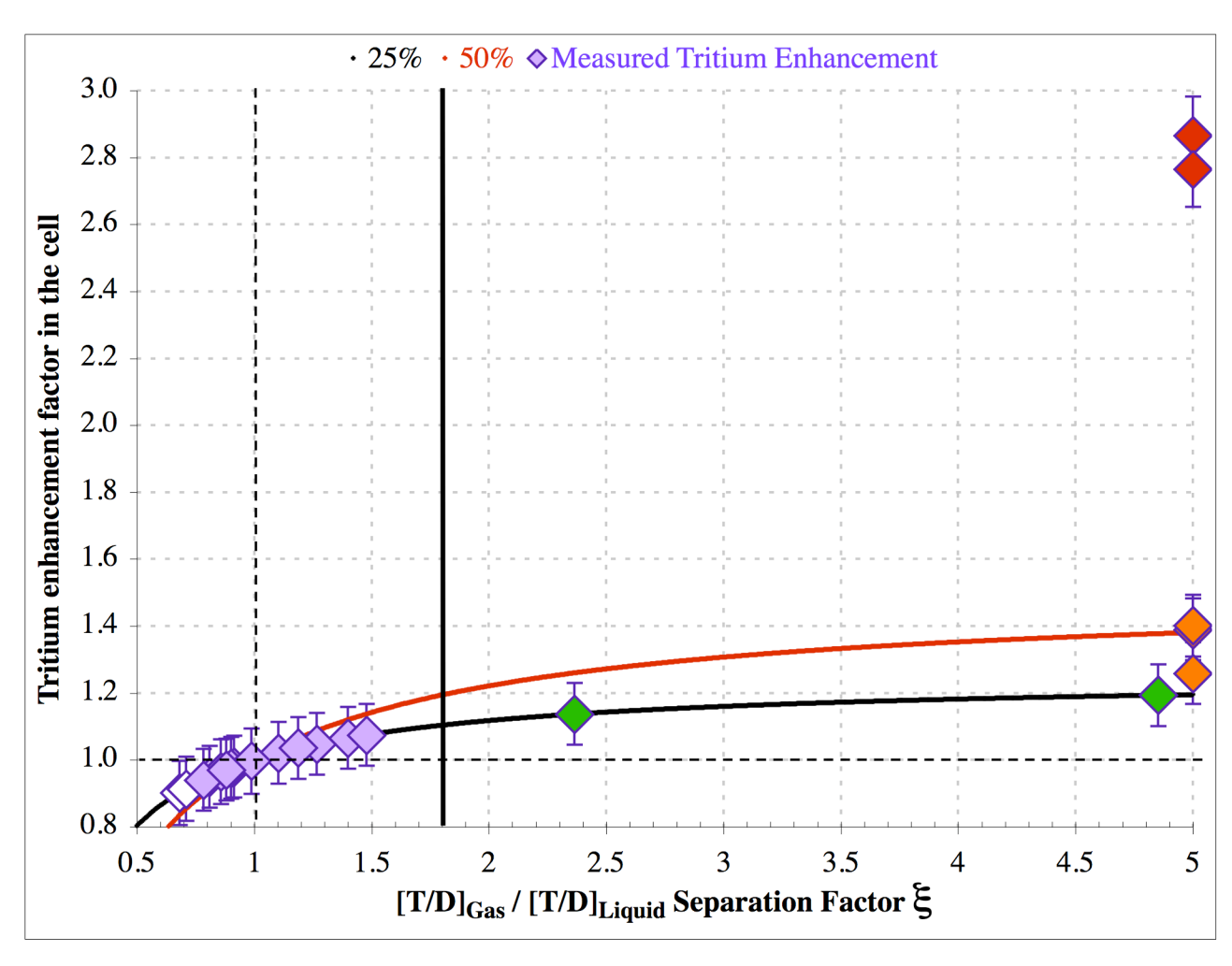


Figure 40. Tritium enhancement factor *versus* separation factor, ξ as a function of the value of makeup D₂O volume.

The data points in green appear at large values of ξ but nevertheless can be accommodated within the uncertainties of tritium analysis and makeup volume. The orange data points require extraordinary values of ξ and cannot be explained at any plausible value of D_2O makeup with $\xi = 1.8$. The red data points cannot be accounted for by any possible value of separation factor. They and the orange points are plotted at $\xi = 5$ simply to include them in the graph.

The unfilled points appear to fall below unity (zero separation) and the values of the blue points cluster not at $\xi = 1.8$ but at a separation factor of $\xi = 1$. This in fact is the expected value for $\xi_{Electrochem.}$ in which isotopic separation is achieved by the selective reduction of D_2O over TDO in reactions

2 [
$$D_2O + e^- -> D_{ads.} + OD^-$$
]
 $D_{ads.} + D_{ads.} -> D_2$ [15]

versus

$$D_2O + e^- \rightarrow D_{ads.} + OD^-$$

$$TDO + e^- \rightarrow T_{ads.} + OD^- \quad (\sim 50\% \text{ of the time})$$

$$D_{ads.} + T_{ads.} \rightarrow DT \qquad [16]$$

The isotope effect in this reaction is very small indeed and may not favor D_2 in the gas phase (i.e. ξ may be less than 1). Fleischmann and Pons in a classic paper⁵³ measured the value of $\xi_{Electrochem}$ in very similar electrolytes to those used in this study, using Pt rather than Pd cathodes to avoid the questions of hydrogen absorption or tritium production. They state "Blank experiments using Pt-cathodes (which have very similar separation factors to Pd) indicate little accumulation of DTO so that $S_{D,T}$ is close to unity under the conditions of our experiments." Experience accumulated in more than 500 similar experiments at SRI in closed and open cells⁵⁴ involving the prolonged electrolysis of 1.0 (and, to a lesser extent, 0.1 and 0.3) molar LiOD solutions and subsequent tritium analysis indicate that the D|T separation factor is unity or very slightly favors D rather than T (i.e., that $\xi \leq 1$).

The reason for this very poor separation can be readily understood by inspecting the second step of Equation [16]. If the electron addition occurs at the D-O bond of TDO, then an adsorbed D atom will form that will very readily associate with a similar D atom to form molecular D_2 , which may form gas bubbles that escape the electrolyte, thus enhancing the electrolyte tritium concentration. Molecular symmetry and our experimental observations, however, suggest that the T-O bond is almost identically susceptible to electron reduction and the overall separation factors balance to approximately unity. Presumably this isotope insensitivity is due to the random

⁵³ Reference 80.

⁵⁴ References 24 and 25.

orientation of the nonlinear T—O—D moiety as it approaches the Pd surface for catalyzed reduction.

The arguments presented in this section, while not completely rigorous, are sufficient to suggest that tritium was produced *de novo* in two or more of the experiments performed. Since our new expectation value of the separation factor is close to unity (no separation of T from D), this number of anomalous results may be as high as 7 out of 21. We must consider a potential source of this "new" tritium.

The circumstances of the apparent tritium producing experiments do not appear to correlate directly with other measured parameters of the experiments: D/Pd loading, excess power and excess energy. Table 5 compares the accumulation and accumulation rate of tritium with the duration, maximum loading, maximum excess power and power gain, and total excess energy of the experiment. The data points clustered around $\xi = 1$ in Figure 39 are all taken individually and as a group as having a tritium generation of $0 \pm 10\%$. In other words, this is the blank group with which the other experiments are compared.

Table 5 Tritium Summary.

	Tritium	Accumi	ılation:		Maximi	ım	Average			
Acc	umulation	Duration	Rate	Max.	Excess	Power	P _{XS} from T	Ratio	Excess	Energy
	(Atoms)	(hours)	T/s	D/Pd	(mW)	% of P _{Ir}	(mW) (mW)		(kJ)	(eV/Pd)
ETI009			2.0E+05	0.895		<2%	1E-04			
ETI015	6.4E+11	1035	1.7E+05	0.895		<2%	1E-04			
ETI012	1.5E+11	939	4.4E+04	0.877		<2%	3E-05			
ETI011	1.4E+11		4.0E+04			30%	22 3E-05	9E+05	80	31
ETI035-9			5.0E+04				1 3E-05	3E+04	2	
	> 17 E 1 T 0	220	5.02.01	0.575	100	170	1 32 03	SETOT	_	1
ETI035-8	7.4E+10	822	2.5E+04	1.060	2066	13%	106 2E-05	7E+06	313	120
ETI035-7			1.8E+04	0.986		3%	187 1E-05	2E+07	553	
ETI016	0	989		0.871		<2%				
ETI017	0	966		0.939	70	25-60%	60		209	80
ETI021	0	412		?	?	?			?	0
ETI022	0	407		?	?	?			?	0
ETI043-7	0	741		0.904	1250	80%	92		245	94
ETI043-8	0	500		0.923	8	5%	36		65	25
ETI043-9	0	658		0.927	0	1%	1		2	1
ETI051-7	0	500		0.939		12%	98		176	68
ETI051-8	0	500		0.945	133	5%	8		14	5
ETI051-9	0	500		0.941		4%	16		28	
ETI056-7	0	335		0.940			444		536	
ETI057-8	0	1058				300%	30		115	
ETI058-9	0	1021		0.888		200%	132		485	
ETI061-7	0	897		0.924	105	50%	45		146	56

Inspection of Table 5 does not reveal any obvious clue as to why tritium accumulated in some experiments, but not in others. Higher rates of accumulation were observed in early cells with poor loading and no excess power, but later cells exhibiting good loading and conspicuous excess power also accumulated tritium. Higher accumulation and accumulation rates occurred in experiments with longer duration, raising the possibility that this effect occurs late in an experiment. However, we are not in a position to judge the time history of tritium production as interim samples were not made. This should certainly be done in future experiments.

In the few cases where significant excess energy and meaningful tritium accumulation were recorded, it is instructive to compare the relative rates based on the supposition that tritium was produced by the nuclear disproportionation of deuterium (²H) in the palladium lattice to produce protium (¹H) and tritium (³H),

$$^{2}H + ^{2}H \rightarrow ^{1}H + ^{3}H$$
 [17]

This is not claimed or considered to occur in these experiments as it occurs in high-energy, isolated, pairwise reaction. Should reaction [17] occur it would produce a neutron flux commensurate with the tritium generation rate shown in Table 5 ($2 \times 10^4 - 2 \times 10^5$ per second). These experiments were monitored for neutrons, and this level of production certainly was not present. Nevertheless, the energetic thermodynamics of reaction [17] are the same as for the d-d reaction in high energy and plasma physics, even if the pathway is different, and we can evaluate the energy expected from the tritium accumulation rate.

The column in Table 5 labeled "Average P_{XS} " lists the average excess power (mW) calculated by dividing the accumulated excess energy by the total experiment duration. This allows easy comparison with the excess heating expected from tritium generation presuming that reaction [17] yields 4.03^{56} MeV / tritium atom produced, shown in the next column of Table 5. The next column to the right, labeled "Ratio," calculates a ratio of the average excess power or integral excess energy observed to that expected from the tritium accumulation measured.

Only one of the values in the "Ratio" column can be treated as significant. For the largest tritium producers (and for experiment ETI 035-9) the uncertainty in excess power measurement is larger than the calculated average value. This uncertainty (several mW) is very much larger than the largest value expected from the highest rate of tritium accumulation, $\sim 0.1~\mu W^{57}$. The experimental uncertainties in tritium measurement for the experiments with two lowest tritium accumulation rates listed in Table 5 shown in green, are so large as to render the denominator of the ratio unreliable.

⁵⁵ This an obvious oversimplification since we have a time history of excess power and know that it does not occur for the entire experiment duration (particularly not at the beginning), and does not occur uniformly in time.

⁵⁶ In high energy reaction, $d + d - > {}^{3}H (3.02 \text{ MeV}) + {}^{1}H (1.01 \text{ MeV}).$

⁵⁷ Such a low heat rates would never be observable in calorimeters of the present design and would present a stern challenge to any calorimetric method.

We are left with only one value of the ratio, shown in bold in Table 5 for experiment ETI 011, where meaningful and believable excess power and excess tritium values were observed simultaneously. This value is $\sim 10^6$ which is the value sometimes⁵⁸ associated with the excess heat / tritium production branching ratios in condensed matter fusion⁵⁹. The relationship between heat and tritium production, and helium and tritium production is, however, very poorly understood in CMNS studies. Numerous experiments that have shown reliable excess heat have shown no measurable increase in tritium, and there are reliable claims for tritium production⁶⁰ where no excess heat was measured.

It is not, in fact, common in CMNS studies to observe a large tritium increase in experiments that also produce large amounts of excess heat, presumably or observably accompanied by ⁴He. The experimental results shown in Figures 3 and 4 for experiment ETE #64 are exceptional in this regard. A sample of the electrolyte used in that experiment by Energetics in Omer, Israel, was analyzed at ENEA (Frascati) and found by conservative estimate ⁶² to have experienced a 750% increase in the starting tritium concentration. The total energy associated with this tritium increase by d-d reaction is less than 1 J compared with 1.1 MJ of excess energy measured by the calorimeter, again a ratio factor of ~10⁶. Clearly, whatever is producing the tritium is a tail phenomenon, and there remains very much more to be understood in the relationship between heat, helium-4, and tritium⁶³.

⁵⁸ Reference 81.

⁵⁹ In high energy and plasma physics, the commonly observed ratios for the three branches of d-d fusion: $d + d \rightarrow {}^{3}He + n$, $d + d \rightarrow {}^{1}H + {}^{3}H$, $d + d \rightarrow {}^{4}He + \gamma$

are, $1:1:10^{-7}$, ${}^{3}He = n:{}^{1}H:{}^{4}He$.

In condensed matter reactions this ratio appears to be more like 10^{-12} : 10^{-6} : 1.

⁶⁰ See chapter 4.4.1 in reference 81 for an overview

⁶¹ References 19, 25, 39-62 and 82, and see chapter 4.4.2 in reference 81 for an overview.

⁶² V. Violante personal communication 2006.

⁶³ The observed presence of <u>both</u> tritium and heat in some ETI cells operated both in Omer and SRI must be considered as unusual. Although highly speculative at this point, one possibility is that the high dynamics of current density and deuterium fluxing caused by superwaves stimulates both of the regimes where tritium and heat normally are produced independently.

SUMMARY AND CONCLUSIONS

INTRODUCTION

A series of experiments was undertaken to replicate isoperibolic calorimetry results obtained from heavy water electrolysis at specially prepared palladium foil cathodes. The original experiments were performed and reported by a private corporation, Energetics LLC. The distinguishing feature of these experiments is their use of complex fractally nested, non-sinusoidal input currents rather than simple dc or pulse electrolysis.

A formal replication protocol involving two steps was adopted. The first was, effectively, a hardware rebuild at SRI by the original experimenters to demonstrate that the experiment was performing as it had initially. This rebuild was then used as a vehicle to communicate any experimental subtleties to the SRI scientists. The second phase employed the same basic hardware with minor modifications and new data acquisition hardware and software; these experiments were operated under SRI scientist control. Three heater calibrations and eight heavy water electrolysis experiments were performed in the first step. Three heater calibrations, three light water calibrations, and fifteen heavy water electrolysis experiments were performed in the second step.

The Energetics calorimeters and cells were found to be well designed and calibrated, and capable of steady baseline operation in the absence of excess heat. The three sigma (3σ) calorimetric uncertainty was estimated to be approximately 5% of the input power under normal input conditions. Of the fifteen experiments performed in Step 2, eleven produced excess heat at or above the 3σ experimental uncertainty. As far as we are aware, this level of reproducibility is hitherto unprecedented in the fields of cold fusion or condensed matter nuclear science (CMNS). This high level of reproducibility is attributable to two conspicuous differences between Energetics experiments and all those that preceded them:

- i. Very high deuterium atom loadings that result from superwave cathodization of appropriately prepared palladium foils.
- ii. The extraordinarily high interfacial flux of deuterium in and out through the palladium cathode surface that results from superwave stimulus.

HEAT EFFECTS

Excess power was observed to have three phenomenologically different forms that we tentatively identify as Modes A - C. The general features of these different modes are as follows.

Mode A. Behavior conforms closely to Equation [13], reproduced here,

$$P_{xs} = M (x - x^{\circ})^{2} (i - i^{\circ}) |i_{D}|$$
 [13]

where M is a proportionality constant, i is the electrochemical current or current density and i° a critical threshold typically 20-50% of i_{max} , x = D/Pd is the deuterium atom loading and x^{o} the threshold loading below which no excess heat is observed – typically $x^{o} \approx 0.875$, and $|i_{D}|$ is the flux of D across the interface expressed as a current density.

This form was first recognized⁶⁴ in excess heat experiments conducted with 1 mm diameter palladium wire cathodes. The 50- μ m thick foils used in the experiments described in this report show similarities but also systematic differences with Pd wires in the constants of Equation [13]. The loading threshold observed in both cases is very similar with $x^{\circ} \approx 0.875$. For the foils examined in this study the current density thresholds, i° , were a factor of 5-10 lower than for 1 mm wires although this may be a result of the lesser degree of current uniformity for the foil geometry. For geometric reasons associated with anode-cathode areas and spacing, the accessible range of current density for foil electrolysis is very much less than for wires. Probably more a result of the superwave stimulus than geometric effects the interfacial flux term, $|\delta x/\delta t|$, was up to an order of magnitude larger in the present study compared with previous dc electrolysis of palladium wires.

This combination of factors led to excess power effects of 5-50% of the input power, very consistent with previous excess heat results at SRI and elsewhere. Although the proportionality constant of Equation [13] is not well specified and probably reflects some properties of surface heterogeneity, this equation permits explanation of experiments that do not produce heat excess. The failure to meet and maintain the current, loading, and flux criteria simultaneously results in a failure to observe Mode A excess heat.

Mode B. A second mode of behavior was seen in three experiments and in all of those exhibiting excess power greater than 100%. This mode is more typical of that reported previously by Energetics⁶⁶ and we describe this as ETI Mode B. In this mode the excess power is relatively insensitive to input power and current, and may be present early in the loading history of a cathode.

The phenomenological differences between Mode A and Mode B behavior can be summarized as follows:

- i) Mode B excess heat initiates within 6 h of application of cathodic current (or 4 h of maximum loading), whereas Mode A behavior requires a longer initiation time, typically several hundreds of hours.
- ii) Mode B excess heat responds sluggishly to input cathodic current density and, so far, exhibits no obvious current density threshold.
- iii) Mode B excess heat has not been observed at D/Pd loadings less than the threshold typical of Mode A behavior (D/Pd ≈ 0.875) and appears to respond at least transiently to increased average loading

Insufficient data exist to evaluate the dependence of Mode B excess heat on net interfacial deuterium ion flux. However, the interfacial flux in the intervals of Mode B behavior observed in this study is very small ($|i_D| < 1 \text{ mA cm}^{-2}$) compared with the values measured in association with Mode A behavior ($|i_D|$ up to $\sim 10 \text{ mA cm}^{-2}$).

An apparent excess power that is flat with respect to input power may signal a miscalibration of one or other of the calorimetric temperature sensors. Numerous precautions

_

⁶⁴ Reference 19.

⁶⁵ Reference 81.

⁶⁶ References 1-3.

were taken during the course of and following each experiment to guard against such a systematic error. Simple precautions included recalibration and replacement of calorimetric (and other) temperature sensors, interchange of temperature sensor position, post test calibration, and examining the temperature response of all sensors to identify the position of the heat source.

Particularly close attention was paid to one case of Mode B heat excess with the following conclusion: "In the absence of further technical input we conclude that the excess power and energy performance characteristics of cell ETI 058-9 must be considered as important and worthy of further study. This cell apparently produced $P_{xs} > 500$ mW and > 200% of P_{In} for a period of nearly 50 h, and an integrated $E_{xs} = 490 \pm 10$ kJ corresponding to over 9% of the integrated electrochemical input energy, and a specific energy of ~ 200 eV/Pd atom."

Because of the relative insensitivity of Mode B heat excess to input current density and therefore power, the ratio values can be very large. In this study we have observed Mode B power excess of ~50%, 80%, 200% and 300% of the input power, at absolute values of a few hundred mW. These results are consistent with similar results obtained at ENEA (Frascati)⁶⁷ and with many of results obtained by Energetics in Omer. As impressive as they are, these results are dwarfed in ratio and absolute terms by the more spectacular results obtained in Omer and shown in Figures 3 and 4 of this report.

Mode C. After a considerable period of closely studied Mode B excess heat production, a single cathode constructed differently from all others continued to display a sustained temperature difference between the inside and outside of the calorimetric cell <u>after</u> the cessation of all input power. Similar effects have been observed in the CMNS field previously. SRI reported such a result in 1993⁷⁰ and referred to it as "heat after life"; Fleischmann and Pons⁷¹ had previously noted such an effect and coined the term "heat after death". Numerous other researchers have subsequently observed and commented⁷² on this rather unexpected effect. Setting aside issues of life and death, we call the apparent continuation of heat production with no input current Mode C.

The concerns of temperature sensor miscalibration expressed above for our Mode B observations obviously pertain to Mode C, although without input power the checks are somewhat simplified. All of the tests described above for Mode B excess heat were applied to our sustained observation of Mode C behavior lasting some 380 h in cell ETI 057-8, and no errors were found that caused us to doubt the accuracy of the temperature measurements.

Two further tests were performed. Both the calorimetric sensor positions and data acquisition channels were interchanged separately to ensure that systematic error did not reside in the temperature sensors or in the electronics associated with temperature measurement. Finally, the apparent heat-producing cathode was removed and substituted with a blank platinum electrode of similar geometry. This test resulted in the output power going to its expected value of zero and the proposition that a systematic error was corrected by installing a blank cathode

71

6

⁶⁷ References 83 and 84.

⁶⁸ ETI internal report (unpublished), 2006.

⁶⁹ Reference 2.

⁷⁰ Reference 18.

⁷¹ References 85 and 86.

⁷² References 1 and 87 - 93.

seems unlikely. We must therefore confront the possibility that approximately 60 kJ of excess energy was produced in a period lasting some 380 h or 16 days <u>after</u> the removal of the superwave (or any) electrochemical stimulus.

The cathode exhibiting Mode C behavior, Electrode ETI 057-8, was made of single-walled carbon nanotubes (SWCNT) sandwiched between thin Pd layers electrodeposited on top of 50 micron Pd foil. We understand that excess heat production requires high loading as a thermodynamic precondition, and some sort of stimulus to produce the effect. In Modes A and B we propose that electrochemistry provides the loading, and the exchange flux of deuterium through the interface provides the stimulation. For the Pd-SWCNT-Pd electrode it is possible that these two conditions were met and sustained after the cessation of the electrochemical current by the deloading of D from the Pd foil, that is a relatively large reservoir of D, through the nanotubes. Alternatively, the nanotubes may perform the role of both deuterium reservoir and flux channel. Evidence of this D flux is provided by the abnormally high open circuit voltage registered by the electrode ETI 057-8 cathode for an extended period (days or weeks) after this cathode was disconnected from the current supply.

NUCLEAR EFFECTS

The major species generally anticipated⁷³ to be associated with the excess heat as a nuclear product is ⁴He. The electrochemical cells and calorimeters used in this study were not designed to be helium leak tight, and no attempt has been made so far to correlate heat and helium production levels. At some future stage we intend to analyze samples of electrolyzed and blank palladium cathodes for both helium isotopes: ⁴He and ³He. As this analysis is destructive it will be reserved until last but a very significant fraction of any helium produced and residing in the palladium is expected to remain "frozen" in the lattice for subsequent analysis.

In 5 of 23 experiments performed, post test analyses revealed a significant increase in the electrolyte tritium concentration that cannot be accounted for by electrolytic or vapor separation of the heavier isotope. The circumstances of the apparent tritium-producing experiments do not appear to correlate directly with other measured parameters of the experiments: D/Pd loading, excess power and excess energy. The two largest tritium increases (187±4% and 176±4%) were for experiments that exhibited relatively poor loading (D/Pd \approx 0.895, barely above the threshold value of $x^{o} \approx 0.875$). These two experiments also exhibited no excess heat within measurement uncertainty (\sim 2%).

Anti-correlation of tritium and excess heat production is not unexpected. It is not common in CMNS studies to observe large tritium increase in experiments that also produce large amounts of excess heat presumably or observably accompanied by 4 He. In one case in our experimental series (ETI011), meaningful excess power and excess tritium values were observed simultaneously. From this case we can calculate a ratio of the energy predicted for tritium produced from deuterium nuclear disproportionation, compared with the integral excess energy measured in the experiment. The value of this ratio is $\sim 10^{-6}$ which is the approximate value commonly associated with the tritium / helium product branching ratios in condensed matter fusion 74 .

-

⁷³ References 22, 39-62 and see chapter 4 in reference 81.

⁷⁴ Reference 81

Experiments demonstrated an increase in both the reproducibility and signal amplitude as a consequence of a material science effort performed in parallel⁷⁵ to improve the performances of the electrodes. The results indicate significant probability of achieving further strong improvement. Additional study should be carried out along these lines to better identify a possible correlation between the surface characteristics of the specimens and their behavior. In future work the state of the material should also be correlated to the production of nuclear ash (predominantly ⁴He, ³He and tritium).

IMPROVED CELL DESIGN

A shortcoming in the present work was our inability to measure helium, particularly ⁴He, in real time or at all in the gas phase of the experiment. The design of this generation of Energetics cells using plastic and PTFE parts and elastomeric seals rendered the calorimeters not completely hermetic and substantially helium permeable. Various strategies were considered to circumvent this limitation but none could be implemented easily or without significant compromise to the calorimetry.

The ability to measure ⁴He temporally and quantitatively correlated with excess heat production provides one of the greatest assurance that the excess heat derives not only from a non-chemical source but from a <u>particular</u> nuclear reaction⁷⁶. In an incompletely sealed system it is not possible to retain and analyze quantitatively product ⁴He released to the gas phase, or to exclude ambient background ⁴He from the measurements. Experiments may therefore suffer from an underestimate or overestimate of product ⁴He rendering the measurement meaningless.

As noted above, the Energetics isoperibolic calorimeter proved to be a capable instrument, well designed and constructed, and adequate for the quantification of 5%-500% levels of excess power. This is not, however, a first principles calorimeter and requires separate and individual calibration of internal constants. The need for calibration invites the criticism that the appearance of excess heat is due to a unidirectional change in a calibration constant (which then reversed itself before post test calibration). This criticism may seem stretched and we have no evidence or even suspicion that this indeed occurred. Nevertheless such a criticism is more easily avoided than rebutted since this would necessitate semi-continuous calibration.

A final limitation of the current experimental series was exposed in our discussion of the tritium enhancement results. The use of an external recombiner and the need for makeup D_2O makes the accurate quantification of tritium increase much more difficult. It must be stressed that no physically reasonable values for D_2O makeup and T/D separation factor can account for the large percentage increase seen in at least two experiments. But again it is preferable to render the situation simple by employing a recombiner inside a completely sealed system so that all products are retained for analysis rather than relying on a limited mathematical "proof". The use of an external recombiner also introduces a calorimetric complexity associated with the chemical heat conveyed out of the calorimeter with the evolving D_2 and O_2 that is better avoided.

_

⁷⁵ The materials science study of the effects of surface morphology on excess heat production were performed in collaboration with ENEA (Frascati) and the University of Rome (La Sapienza).

⁷⁶ d + d -> ⁴He + 24 MeV of lattice heat. Although we can measure the heat and potentially the product helium, we do not consider it practical at this stage to measure the loss of reactant deuterium.

The three suggested improvements above have been incorporated in a new electrochemical cell – calorimeter design that we propose to employ in the planned Phase II of this program. This design resulted from discussions between Energetics, ENEA, and SRI scientists in a meeting convened for this purpose. Energetics has taken the lead in engineering development, which ENEA staff are supporting with finite element calculations of internal temperature distributions and heat flow, and SRI staff are supporting with their calorimetry expertise. The current design, scheduled for proof testing in Omer and Frascati, is shown in Figure 41 Its core, including Teflon beaker, anodes - cathode sandwich and electrolyte, is identical to the core of the isoperibolic cell experimented with in Phase I. The new calorimeter incorporates the following features intended to improve upon the current isoperibolic design as discussed above:

- A fully metal-sealed and helium leak tight system so that all potential products (specifically helium and tritium) will be retained and presented for gas and liquid phase analyses. We intend to measure both ³He and ⁴He, and have developed the expertise to do so. The ³He: ⁴He ratio is constant and well measured in ambient air. Any departure from this ratio is a clear indication that one or other of the isotopes was produced selectively in the experiment and that the measured value did not result from sequestration or ambient in-leakage of helium.
- A first-principles mass flow calorimeter of known and tested ⁷⁷ design. Unlike the isoperibolic instrument, a calorimeter that measures as output the temperature difference of a moving mass of water (for example) does not require the calibration of an internal unknown constant (which may change). Temperature sensors can be directly calibrated against a standard, the heat capacity of (say) air saturated water is known accurately from independent experiments, and the mass flow rate can readily be measured using a balance that again can be calibrated independently of the calorimeter. All that requires calibration is the extent to which heat leaves the calorimetric boundary by means other than convection of the calorimetric fluid (*i.e.*, by conduction and radiation). This loss term can be made as small as needed by suitable design and control of the mass flow rate. For example, the SRI labyrinth mass flow calorimeter had a thermal efficiency of 99.3%. Thus only 0.7% needed to be calibrated (or measured) in the experiment. The overall accuracy of this device was better than 0.4%.
- A fully integrated, internal recombiner that will allow us to avoid completely questions of differential separation of hydrogen isotopes in the electrolyzing body and recombination chamber. By including everything inside the same metal-sealed container, thereby avoiding the need for and eliminating the ambiguity of D₂O makeup, we can ensure that the final condition in the calorimeter differs from the initial only in the amount of heat produced and in the quantities of products created. Comparison of these quantities is a powerful test of the reality (or not) of a nuclear source, and will provide needed solid information to theorists (if real).

_

74

⁷⁷ References 1 and 25

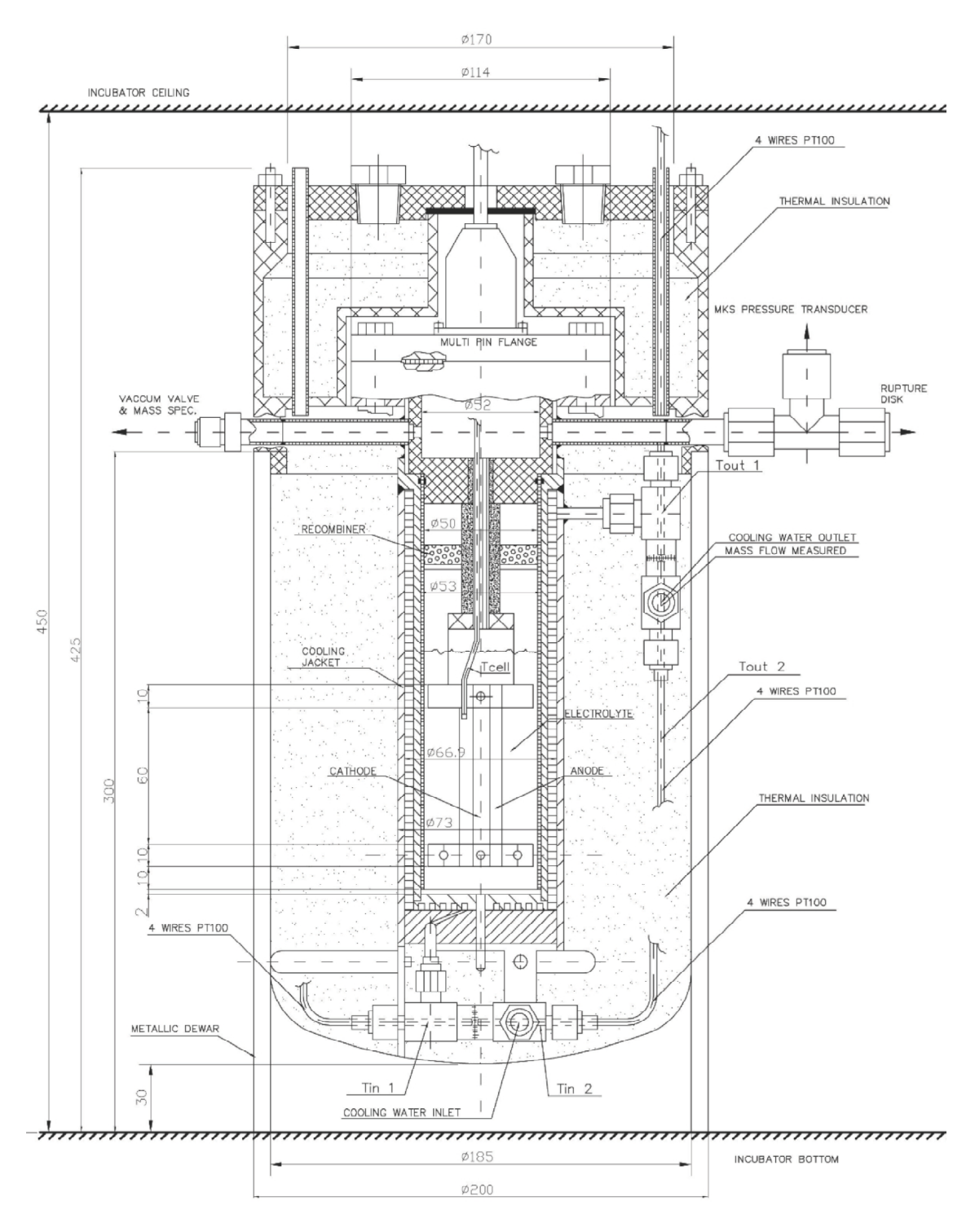


Figure 41 Improved calorimeter design.

POST-PROCESS ANALYSIS SUMMARY

The Naval Research Laboratory provided post-process analysis of selected electrochemical solutions, cathodes, and anodes. A more detailed report of the results will be provided under separate cover. The analytical effort included qualitative broad-mass-range inductively coupled

plasma mass spectrometry (ICPMS) of electrochemical solutions, optical microscopy (OM) and scanning electron microscopy (SEM) of cathodes and anodes, including spot x-ray-fluorescence analyses (EDAX), x-ray diffraction (XRD) of cathodes, and cold-neutron depth profiling (CNDP) for Li concentration in select cathodes. Further composition analysis of cathodes and anodes is envisioned, but not yet completed, as these would be relatively destructive. Some notable observations are described below.

Qualitative yet exhaustive ICPMS was performed on five process solutions, an unused 0.1M LiOD sample, and stock LiOD. Some slight levels of impurities were found, but no dramatic deviations from natural isotopic abundances were observed. The stock LiOD solution contained part per billion (ppb) levels of B, Sn, Pb, and Ba, with trace amounts (part per trillion – ppt) of Hf and U. Some process solutions also contained Fe, Cr, and Ni (consistent with stainless steel), and additional Pb and Sn (consistent with solder). Careful qualitative analysis examined the Li and B isotope ratios. Among all the process solutions, the variation of Li and B isotope ratios (~1%) was within the precision of the measurement. Thus no measurable isotope enrichment of B or Li was observed.

Analyses using OM, SEM, and EDAX revealed a number of interesting features on the samples. Grain boundary grooving was common, but it was much larger (~2-5 µm wide) and more visible in OM on two of the non-heat-producing samples, ETI 035-9 and ETI 043-9. Dark patches a few microns in diameter were seen on many samples, and appear to be from the formation of various oxides. As evidenced by EDAX, these oxides may contain Pt, Ca, Al, Si, or a combination of these. One plate-like precipitate (~2 µm diameter) containing Si, Al, Ca, Mg, and O was seen on the virgin sample ETI 067-1. Hillocks (raised regions, or bumps) of Pd, 10-50 µm in diameter, were seen on numerous samples, apparently associated with stress from the D loading/unloading of Pd. Frequently, steps or terraces were seen within the hillock, and the dark patches mentioned above were seen associated with some hillocks. Small nodules (~100 nm diameter) were also seen on two of the heat producing samples, ETI 056-7 and ETI 035-8. Grain boundary extrusions and faceting of the surface were seen on some samples. A most unusual porous surface was found on sample ETI 057-8, associated with the SWCNT structure used in its construction. Finally, EDAX revealed that Pt impurities were present on some samples (ETI 067-1 and ETI 035-9), and that the Pt wire bonding site of ETI 056-9 besides Pt also contained Cu.

XRD was performed on three cathodes (ETI 056-7, ETI 067-1 "virgin Pd", and ETI 057-8) to assess long-term retention of D following loading. All indicated a modest level of D or H, commensurate with the alpha phase of PdD or PdH. Unexpectedly, the virgin Pd sample had a larger lattice parameter (higher D or H content?) than the loaded sample ETI 056-7. The reason at the moment is unclear, but is under investigation. Perhaps substitutional solid solution additions to the Pd have altered its base lattice parameter.

CNDP was employed to ascertain how much Li was introduced into Pd during the D loading process. The technique uses cold neutron induced nuclear reactions to measure the depth profile of certain light isotopes. In our case, 6 Li was measured within the top 5 μ m of the surface for the three samples examined by XRD. A natural isotope abundance was assumed to compute the total Li concentration. The virgin Pd sample contained about 350 ppb Li in the top 5 μ m. Sample ETI 056-7 contained a total Li content in the top 5 μ m (1.8 x 10¹⁵ Li/cm²), about 150 times larger, with most of the Li at the surface. The exotic SWCNT sample (ETI 057-8) had about three times more Li yet, again with most near the surface. If one presumes the Li present is

largely a residue from the LiOD solution exposure, and corresponds to the amount of surface area available, then the SWCNT structure used must provide about three times more surface area than the conventional samples. It is not clear how adherent the measured Li is to the surface, but it would be interesting to ascertain.

CONCLUSIONS

The results of our experimental program successfully replicate those obtained previously by Energetics (Omer) and simultaneously but independently by ENEA (Frascati). Excess power in the form of heat is produced in unmistakable quantities when specially prepared palladium foil is used as an electrolysis cathode in heavy water, employing complex fractally nested current excitation (superwaves). The measured excess energies of experiments typically lasting 500-1000 h were 100 - 500 kJ, the largest being 553 ± 25 kJ. In some but not all experiments, tritium was produced, but in an amount far less than can account for the excess energy, but nevertheless as a clear signature of nuclear reaction. The quantitative mismatch between the rates of heat and tritium production is not surprising as 4 He is the expected nuclear product associated with the excess heat production. The present experimental setup was not designed to enable measuring helium.

Fifteen experiments were run with SRI hardware, software and staffing, using the Energetics cells and cathodes prepared at ENEA, Energetics. and one other. Of these, ten produced clear evidence of excess heat ranging to over 2 W or 25-75 W per cm³ of cathode. A remarkable feature of this set of experiments was the consistency of loading and of excess heat. The loadings obtained were impressive. Only two had maximum loading D/Pd less than 0.9 (0.88 and 0.89). One cathode exhibited atomic loading ratios apparently greater than unity suggesting the possibility tetrahedral as well as octahedral site occupation. Such high loading values have not previously been reported for foils, and such consistency is unprecedented with any type of electrode in heavy-water electrolysis.

The extreme level of loading and high consistency of good loading are attributable to two features of this set of experiments:

- i. A high degree of microstructural metallurgical control allows electrodes to accept loading without damaging deformation. This treatment process has been developed largely at ENEA and involves not only control of the bulk crystallinity but extends to control of the surface roughness.
- ii. The superwave excitation function produces current driven fields which interact with the deuterium atom—ion dynamics in a number of ways. Regions of interest are: the mass transport controlled boundary layer in the electrolyte, the charged electrochemical double layer and the associated electrochemical kinetic process at the electrode/electrolyte interface, the dynamic diffusion region of absorbing D atoms just below the cathode surface. The role or roles of superwaves in affecting these processes justifies further study both to understand excess heat results and as a potential new and better means to load hydrogen into metals.

Although not extensively tested in the present study, it is apparent that superwave stimulus plays a vital second role in our excess heat results. The superwave modulated currents result in a

very large loading dynamic (interfacial deuterium atom flux) that is not present with dc or sinusoidal ac stimulation. Using superwaves, we have been able to achieve fluxes of up of 6 $\times 10^{16}$ particles per cm² per second through the interface, or 40 transitions per second for every atom site on the cathode surface. We speculate that this huge flux provides a stimulus for the excess heat effect, but further work is needed to understand the detailed causes of this high flux and its nuclear consequences.

Observations were made of sustained excess power at very low input power levels. With the reduced denominator measurements were made of $P_{xs}/P_{In} = 50\%$, 80%, 200% and over 300%. At very low input powers sustained observations were made of $P_{xs}/P_{In} = 28\pm1$ (*i.e.* 2800%) for 40 h or more. In one case with a composite Pd–C cathode, clear heat excess was measured after cessation of all input where the ratio P_{xs}/P_{In} is undefined. Again, further work is needed to understand the causes and consequences of the observation of excess power at low or zero power input.

As a final exercise the results obtained in this phase of experimentation were compared with those obtained during the previous 17 years of Pd/D₂O calorimetry at SRI. Figure 42 plots the maximum loading obtained by a palladium cathode at its measured minimum resistance ratio value (on the right side of the resistance maximum) from a data base of 67 experiments⁷⁹. Data are plotted for six series of experiments. Data from the Energetics data acquisition phase (Step 1, Table 1) of the present program are plotted as diamonds while those measured during the SRI data acquisition phase (Step 2, Table 2) are plotted as squares

Other points plotted in Figure 42 for comparison are from four previous SRI experimental sets performed in the interval 1989 - 1994. The experiments selected are all that were performed in Pd/D₂O electrolysis at SRI with accurate calorimetry and loading measurements lasting 300 hours or more. Series P, C and L were mass flow calorimeters and series AS was a Seebeck calorimeter. In the four SRI experimental series all cathodes were 3 mm or 1 mm diameter palladium wire with the exception of experiment C2 in which a foil cathode was employed having somewhat larger area than those used in the present study.

⁷⁸ With simple ac or pulsed modulation such a dynamic cannot be sustained even in the presence of a dc bias. ⁷⁹ The average experiment duration is approximately 1000 hours so Figure 42 represents more than 7 years of continuous calorimetry.

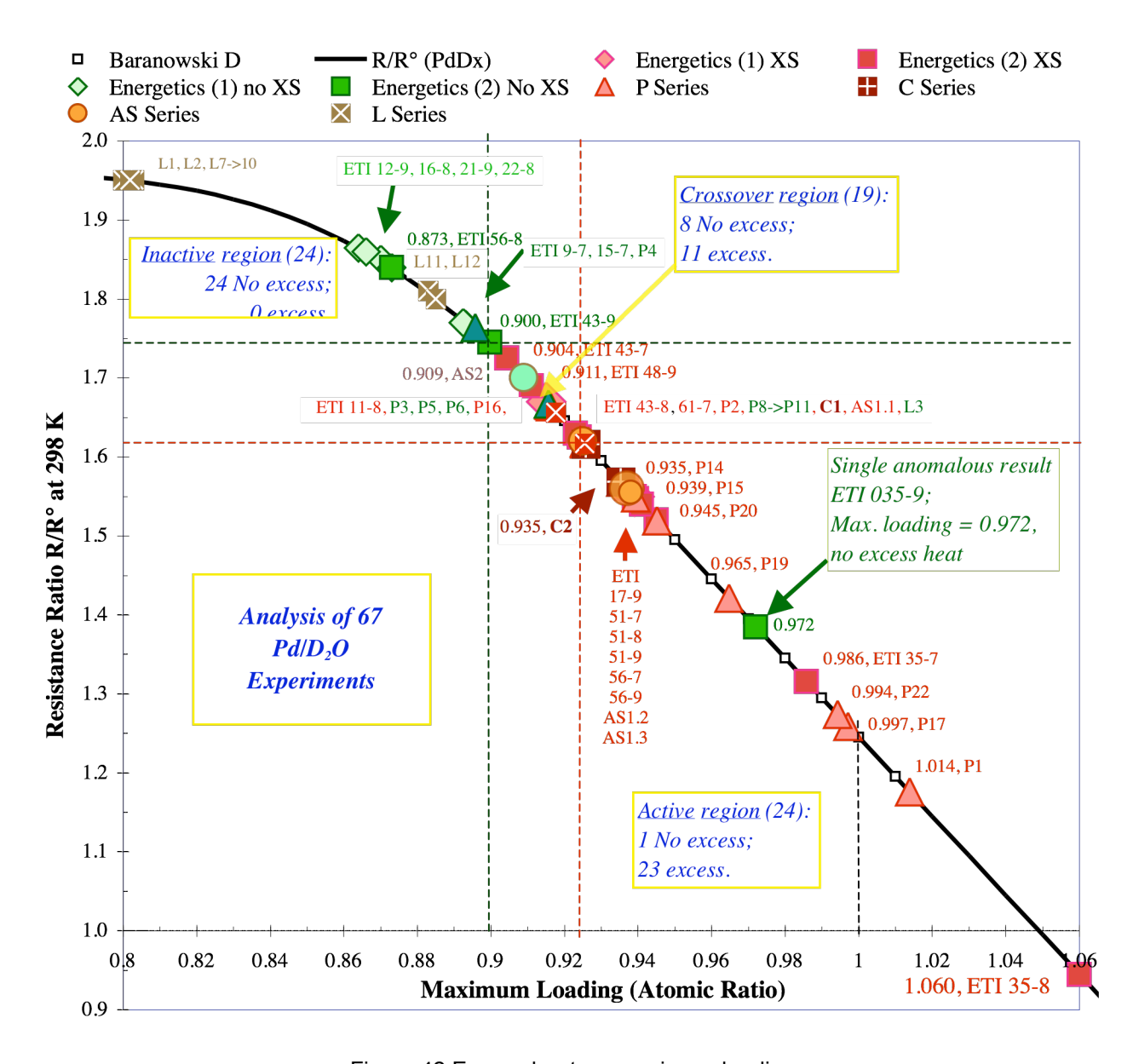


Figure 42 Excess heat vs. maximum loading.

Points are placed in Figure 42 at the position of maximum loading observed during the course of the experiment, and are color coded green-blue if no excess power was observed, and orange-red if significant (more than 3 sigma) excess heat was measured. A clear trend can be observed. Cathodes capable of achieving high average loading are also those capable of producing excess heat. In the inactive region in the top left 24 experiments failing to reach a loading D/Pd_{Max.}= 0.900 all had unmeasurably small excess heat. Of 24 cathodes reaching a maximum loading of D/Pd_{Max.}= 0.925 or more in the active region, 23 exhibited unmistakable excess heat levels. Of the 19 points in the crossover region $0.900 < D/Pd_{Max.} < 0.925$, 11 showed excess heat and 8 did not. Despite the differences in cathodes and calorimetric methods, the 22 new points from the present study are almost completely consistent with the old data base.

This new experimental information allows us to further refine our knowledge of the heat/no-heat boundaries although it should be noted that the maximum loading criterion tells us something about whether (or not) a PdD_x cathode is going to produce excess. In some experiments the maximum heat was produces at times other than maximum loading, the statistically important feature appears to be capacity to obtain high loading. To get more information about when and how much heat is produced⁸⁰ we need to have more information about conditions of surface stimulation (current, laser *etc.*) and surface dynamics (deuterium flux).

One data point in Figure 42 remains anomalous. The inability of cathode ETI 035-9 to evince excess heat cannot be accounted for in terms of the maximum loading criterion or by other obvious factors. At this time the only clue to this failure can be seen in Figure 15 as the tendency of the electrode to lose the average loading gained following each current step. It is important to understand this case as it may provide insight into other successful and unsuccessful experiments and therefore into the apparent irreproducibility of the effect.

The analysis of cathodes, anodes, and solutions has found some common features among them, as well as some associated preferentially with either heat-producing or non-heat-producing cathodes. Whether these features are relevant to the performance of the cathodes is uncertain, but they are worthy of further investigation. Some interesting correlations to consider include: large grain boundary grooving observed only on some non-heat-producing cathodes, and small (~100 nm) nodules only on some heat-producing cathodes. There does not appear to be any critical correlation between an impurity or isotope enrichment and the production of excess heat. However, the precision and sensitivity applied thus far may not be sufficient to observe such a correlation. It is interesting to note that there are measurable amounts of Li, B, and U in the materials analyzed, that have been previously suggested as important contributors to the mysteries of condensed matter nuclear science.

In view of the much larger number of experiments and magnitude of excess heat effects observed in Omer, a major accomplishment of the present work is the experimental validation of Energetics calorimetric method. The two-temperature, isoperibolic calorimeter developed and deployed by Energetics proved to be a very serviceable instrument, capable of stable operation over long periods with limits of accuracy 2-5%. This observation allows us to place a high degree of confidence on the very large absolute and ratio values of excess power and energy reported by Energetics in October 2004 and which formed the impetus for the present study.

As a result of the present study and ongoing work at Energetics and ENEA, suggestions have been made and a development is under way of an improved calorimetric cell. The new design builds from the successful features of the cell experimented with in this phase and incorporates a first principles mass flow calorimeter and all metal sealing to allow more accurate quantification of heat and nuclear product release. We anticipate that temporal and quantitative correlation of these products, together with multiple laboratory replication, will provide a basis for general scientific understanding and acceptance of the phenomenon under study.

_

⁸⁰ More accurately, heat rate or power.

ACKNOWLEDGMENTS

The authors owe a profound debt of gratitude to Mr. Sidney Kimmel; this project and team could not have advanced to the present point of interest without his vision and tenacious support of the work of Energetics. If the second phase of this project is accomplished successfully, it is possible that the entire scientific community, and perhaps the whole world, will also owe Mr. Kimmel this debt.

REFERENCES

- Dardik, I., Branover, H., El-Boher, A., Gazit, D., Golbreich, E., Greenspan, E., Kapusta, A., Khachatorov, B., Krakov, V., Lesin, S., Michailovitch, B., Shani, G., and Zilov, T., Intensification of low energy nuclear reactions using superwave excitation, in *Tenth International Conference on Cold Fusion*, Chubb, P. I. H. a. S. R. World Scientific Publishing Co., Cambridge, MA, 2003, pp. 61.
- 2. Dardik, I., Zilov, T., Branover, H., El-Boher, A., Greenspan, E., Khachatorov, B., Krakov, V., Lesin, S., and Tsirlin, M., Excess heat in electrolysis experiments at Energetics Technologies, in *11th International Conference on Cold Fusion*, Biberian, J.-P. World Scientific Co., Marseilles, France, 2004, pp. 84.
- 3. Dardik, I., Zilov, T., Branover, H., El-Boher, A., Greenspan, E., Khachaturov, B., Krakov, V., S., L., and Tsirlin, M., Progress in electrolysis experiments at Energetics Technologies, in *12th International Conference on Condensed Matter Nuclear Science*, Yokohama, Japan, 2005.
- 4. McKubre, M.C.H. and Tanzella, F., Using resistivity to measure H/Pd and D/Pd loading: method and significance, in *12th International Conference on Condensed Matter Nuclear Science*, Yokohama, Japan, 2005, p392.
- 5. Violante, V., Tripodi, P., Di Gioacchino, D., Borelli, R., Pizzuto, A., McKubre, M. C. H., Tanzella, F., Adrover, A., Giona, M., and Capobianco, L., Metallurgical effects on the dynamic of hydrogen loading in Pd, in *The 9th International Conference on Cold Fusion, Condensed Matter Nuclear Science*, Li, X. Z. Tsinghua Univ. Press, Tsinghua Univ., Beijing, China, 2002, pp. 383.
- 6. Barrowes, S. C. and Bergeson, H. E., Linear, high precision, redundant calorimeter, in *Fourth International Conference on Cold Fusion* Electric Power Research Institute 3412 Hillview Ave., Palo Alto, CA 94304, Lahaina, Maui, 1994, pp. 21.
- 7. Närger, U., Hayden, M. E., Booth, J. L., Hardy, W. N., Whitehead, L. A., Carolan, J. F., Balzarini, D. A., Wishnow, E. H., and Blake, C. C., High precision calorimetric apparatus for studying electrolysis reactions, *Rev. Sci. Instr.* 61 (5), 1504, 1990.
- 8. Ferrari, C., Papucci, F., Salvetti, G., Tognoni, E., and Tombari, E., A calorimeter for the electrolytic cell and other open systems, *Nuovo Cimento Soc. Ital. Fis. D* 18 (11), 1333, 1996.
- 9. Pons, S. and Fleischmann, M., The calorimetry of electrode reactions and measurements of excess enthalpy generation in the electrolysis of D₂O using Pd-based cathodes, in *Second Annual Conference on Cold Fusion*, "*The Science of Cold Fusion*", Bressani, T., Del Giudice, E., andPreparata, G. Societa Italiana di Fisica, Bologna, Italy, Como, Italy, 1991, pp. 349.
- 10. Fleischmann, M., Pons, S., Le Roux, M., and Roulette, J., Calorimetry of the Pd-D₂O system: The search for simplicity and accuracy, *Trans. Fusion Technol.* 26 (4T), 323, 1994.
- 11. Miles, M. H., Imam, M. A., and Fleischmann, M., "Case studies" of two experiments carried out with the ICARUS systems, in *8th International Conference on Cold Fusion*, Scaramuzzi, F. Italian Physical Society, Bologna, Italy, Lerici (La Spezia), Italy, 2000, pp. 105.
- 12. Bush, R. T. and Eagleton, R. D., Evidence for electrolytically induced transmutation and radioactivity correlated with excess heat in electrolytic cells with light water rubidium salt electrolytes, *Trans. Fusion Technol.* 26 (4T), 344, 1994.

- 13. Hansen, W. N., Report to the Utah State Fusion/Energy Council on the analysis of selected Pons Fleischmann calorimetric data, in *Second Annual Conference on Cold Fusion*, "*The Science of Cold Fusion*", Bressani, T., Del Giudice, E., and Preparata, G. Societa Italiana di Fisica, Bologna, Italy, Como, Italy, 1991, pp. 491.
- 14. Koschmieder, E. L., Bénard Cells and Taylor Vortices, <u>Cambridge Monographs on Mechanics</u>, 1993.
- 15. McKubre, M. C. H., Rocha-Filho, R. C., Smedley, S., Tanzella, F. L., Chao, J., Chexal, B., Passell, T. O., and Santucci, J., Calorimetry and electrochemistry in the D/Pd system, in *The First Annual Conference on Cold Fusion*, Will, F. National Cold Fusion Institute, University of Utah Research Park, Salt Lake City, Utah, 1990, pp. 20.
- 16. McKubre, M. C. H., Rocha-Filho, R. C., Smedley, S. I., Tanzella, F. L., Crouch-Baker, S., Passell, T. O., and Santucci, J., Isothermal flow calorimetric investigations of the D/Pd system, in *Second Annual Conference on Cold Fusion*, "*The Science of Cold Fusion*", Bressani, T., Giudice, E. D., and Preparata, G. Societa Italiana di Fisica, Bologna, Italy, Como, Italy, 1991, pp. 419.
- 17. McKubre, M. C. H., Crouch-Baker, S., Riley, A. M., Smedley, S. I., and Tanzella, F. L., Excess power observations in electrochemical studies of the D/Pd system; the influence of loading, in *Third International Conference on Cold Fusion*, "Frontiers of Cold Fusion", Ikegami, H. Universal Academy Press, Inc., Tokyo, Japan, Nagoya Japan, 1992, pp. 5.
- 18. McKubre, M. C. H., Bush, B. F., Crouch-Baker, S., Hauser, A., Jevtic, N., Smedley, S., Srinivasan, M., Tanzella, F. L., Williams, M., and Wing, S., Loading, calorimetric and nuclear investigation of the D/Pd system, in *Fourth International Conference on Cold Fusion* Electric Power Research Institute 3412 Hillview Ave., Palo Alto, CA 94304, Lahaina, Maui, 1993, pp. 5.
- McKubre, M. C. H., Crouch-Baker, S., Hauser, A. K., Smedley, S. I., Tanzella, F. L., Williams, M. S., and Wing, S. S., Concerning reproducibility of excess power production, in 5th International Conference on Cold Fusion, Pons, S. IMRA Europe, Sophia Antipolis Cedex, France, Monte-Carlo, Monaco, 1995, pp. 17.
- 20. McKubre, M. C. H., Crouch-Baker, S., Tanzella, F. L., Williams, M., and Wing, S., New hydrogen energy research at SRI, in *Sixth International Conference on Cold Fusion, Progress in New Hydrogen Energy*, Okamoto, M. New Energy and Industrial Technology Development Organization, Tokyo Institute of Technology, Tokyo, Japan, Lake Toya, Hokkaido, Japan, 1996, pp. 75.
- 21. McKubre, M. C. H. and Tanzella, F. L., Materials issues of loading deuterium into palladium and the association with excess heat production, in *The Seventh International Conference on Cold Fusion*, Jaeger, F. ENECO, Inc., Salt Lake City, UT, Vancouver, Canada, 1998, pp. 230.
- 22. McKubre, M. C. H., Tanzella, F. L., Tripodi, P., and Hagelstein, P. L., The emergence of a coherent explanation for anomalies observed in D/Pd and H/Pd system: evidence for ⁴He and ³He production, in *8th International Conference on Cold Fusion*, Scaramuzzi, F. Italian Physical Society, Bologna, Italy, Lerici (La Spezia), Italy, 2000, pp. 3.
- 23. McKubre, M. C. H., Tanzella, F., Tripodi, P., and Violante, V., Progress towards replication, in *The 9th International Conference on Cold Fusion, Condensed Matter Nuclear Science*, Li, X. Z. Tsinghua Univ. Press, Tsinghua Univ., Beijing, China, 2002, pp. 241.

- 24. McKubre, M. C. H., Crouch-Baker, S., Smedley, S. I., Tanzella, F. L., Williams, M., Wing, S., Maly-Schreiber, M., Rocha-Fiho, R. C., Searson, P. C., Pronko, J. G., and Kohler, D. A., <u>Development of Energy Production Systems from Heat Produced in Deuterated Metals</u>, Final Report No. EPRI TR-104195, 1994.
- 25. McKubre, M. C. H., Crouch-Baker, S., Hauser, A., Jevtic, N., Tanzella, F. L., Smedley, S. I., Williams, M., and Wing., <u>Energy Production Processes in Deuterated Metals</u>, Final Report No. EPRI TR-107843-V1, 1998.
- 26. Dardik, I., Zilov, T., Branover, H., El-Boher, A., Greenspan, E., Khachaturov, B., Krakov, V., Lesin, S., and Tsirlin, M., Excess heat in electrolysis experiments at Energetics Technologies, in 6th International Workship on Anomalies in Hydrogen/Deuterium Loaded Metals, Siena, Italy, 2005.
- 27. Kaushik, T. C., Shyam, A., Srinivasa, M., Rour, R. K., Kulkarni, L. V., Krishnan, M. S., Malhotra, S. K. and Naguenkar, V. B., Preliminary report of direct measurement of tritium in liquid nitrogen treated TID_x chips, Indian Journal of Technology, 667, 1990.
- 28. Srinivasan, M., Nuclear fusion in an atomic lattice, Current Science, 60 #7, 417, 1991.
- 29. Cravens, D. J., Trading views on what works (sometimes), Fusion Facts, 3 #6, 12, 1991.
- 30. Szpak, S., Mosier-Boss, P. A., Dea, J., and Gordon, F., Polarized D+/Pd-D₂O system: hot spots and "mini-explosions", in *Tenth International Conference on Cold Fusion*, Hagelstein, P. I. andChubb, S. R. World Scientific Publishing Co., Cambridge, MA, 2003, pp. 13.
- 31. Bernardini, M., Manduchi, C., Mengoli, G., and Zannoni, G., Anomalous effects induced by D₂O electrolysis at titanium, in 8th International Conference on Cold Fusion, Scaramuzzi, F. Italian Physical Society, Bologna, Italy, Lerici (La Spezia), Italy, 2000, pp. 39.
- 32. Mengoli, G., Bernardini, M., Manducchi, C., and Zannoni, G., Anomalous heat effects correlated with electrochemical hydriding of nickel, *Nuovo Cimento Soc. Ital. Fis. D* 20 (3), 331, 1998.
- 33. Mengoli, G., Bernardini, M., Manduchi, C., and Zannoni, G., Calorimetry close to the boiling temperature of the D₂O/Pd electrolytic system, *J. Electroanal. Chem.* 444, 155, 1998.
- 34. Liaw, B. Y., Tao, P.-L., Turner, P., and Liebert, B. E., Elevated-temperature excess heat production in a Pd + D system, *J. Electroanal. Chem.* 319, 161, 1991.
- 35. Liaw, B. Y., Tao, P.-L., Turner, P., and Liebert, B. E., Elevated temperature excess heat production using molten-salt electrochemical techniques, in *8th World Hydrogen Energy Conf* Hawaii Natural Energy Institute, 2540 Dole St., Holmes Hall 246, Honolulu, HI 96822, Honolulu, HI, 1990, pp. 49.
- 36. Lipson, A., Lyakhov B. F., Zilov, T. and Greenspan, E., System and Methods for Hydrogen Loading and Generation of Thermal Response, PCT Patent Application, 2006.
- 37. Grabowski, K. S. and Hubler, G. K, Post Process Analysis of Materials from "New Physical Effects in Metal Deuterides", Naval Research Laboratory, Washington DC, 2007.
- 38. Morrey, J. R., Caffee, M. W., Farrar IV, H., Hoffman, N. J., Hudson, G. B., Jones, R. H., Kurz, M. D., Lupton, J., Oliver, B. M., Ruiz, B. V., Wacker, J. F., and van Veen, A., Measurements of Helium in Electrolyzed Palladium, *Fusion Technol*. 18, 659, 1990.

- 39. Bush, B. F., Lagowski, J. J., Miles, M. H., and Ostrom, G. S., Helium production during the electrolysis of D₂O in cold fusion experiments, *J. Electroanal. Chem.* 304, 271, 1991.
- 40. Miles, M., Bush, B. F., Ostrom, G. S., and Lagowski, J. J., Heat and helium production in cold fusion experiments, in *Second Annual Conference on Cold Fusion*, "*The Science of Cold Fusion*", Bressani, T., Giudice, E. D., and Preparata, G. Societa Italiana di Fisica, Bologna, Italy, Como, Italy, 1991, pp. 363.
- 41. Chien, C.-C., Hodko, D., Minevski, Z., and Bockris, J. O. M., On an electrode producing massive quantities of tritium and helium, *J. Electroanal. Chem.* 338, 189, 1992.
- 42. Bockris, J., Chien, C., Hodko, D., and Minevski, Z., Tritium and Helium Production in Palladium Electrodes and the Fugacity of Deuterium Therein, in *Third International Conference on Cold Fusion*, "Frontiers of Cold Fusion", Ikegami, H. Universal Academy Press, Inc., Tokyo, Japan, Nagoya Japan, 1992, pp. 231.
- 43. Zhang, Q. F., Gou, Q. Q., Zhu, Z. H., Xio, B. L., Lou, J. M., Liu, F. S., S., J. X., Ning, Y. G., Xie, H., and Wang, Z. G., The detection of 4-He in Ti-cathode on cold fusion, in *Third International Conference on Cold Fusion*, "Frontiers of Cold Fusion", Ikegami, H. Universal Academy Press, Inc., Tokyo, Japan, Nagoya Japan, 1992, pp. 531.
- 44. Miles, M. H., Hollins, R. A., Bush, B. F., Lagowski, J. J., and Miles, R. E., Correlation of excess power and helium production during D₂O and H₂O electrolysis using palladium cathodes, *J. Electroanal. Chem.* 346, 99, 1993.
- 45. Miles, M. H. and Bush, B. F., Heat and helium measurements in deuterated palladium, in *Fourth International Conference on Cold Fusion* Electric Power Research Institute 3412 Hillview Ave., Palo Alto, CA 94304, Lahaina, Maui, 1993, pp. 6.
- 46. Yamaguchi, E. and Nishioka, T., Helium-4 production and its correlation with heat evolution, *Oyo Butsuri* 62 (7), 712 (in Japanese), 1993.
- 47. Gozzi, D., Caputo, R., Cignini, P. L., Tomellini, M., Gigli, G., Balducci, G., Cisbani, E., Frullani, S., Garibaldi, F., Jodice, M., and Urciuoli, G. M., Helium-4 quantitative measurements in the gas phase of cold fusion electrochemical cells, in *Fourth International Conference on Cold Fusion* Electric Power Research Institute 3412 Hillview Ave., Palo Alto, CA 94304, Lahaina, Maui, 1993, pp. 6.
- 48. Aoki, T., Kurata, Y., and Ebihara, H., Study of concentrations of helium and tritium in electrolytic cells with excess heat generation, in *Fourth International Conference on Cold Fusion* Electric Power Research Institute 3412 Hillview Ave., Palo Alto, CA 94304, Lahaina, Maui, 1993, pp. 23.
- 49. Liaw, B. Y., Tao, P.-L., and Liebert, B. E., Helium analysis of palladium electrodes after molten salt electrolysis, *Fusion Technol.* 23, 92, 1993.
- 50. Miles, M., Bush, B. F., and Lagowski, J. J., Anomalous effects involving excess power, radiation, and helium production during D₂O electrolysis using palladium cathodes, *Fusion Technol*. 25, 478, 1994.
- 51. Miles, M. H. and Bush, B. F., Heat and helium measurements in deuterated palladium, *Trans. Fusion Technol.* 26 (#4T), 156, 1994.

- 52. Gozzi, D., Caputo, R., Cignini, P. L., Tomellini, M., Gigli, G., Balducci, G., Cisbani, E., Frullani, S., Garibaldi, F., Jodice, M., and Urciuoli, G. M., Quantitative measurements of helium-4 in the gas phase of Pd + D2O electrolysis, *J. Electroanal. Chem.* 380, 109, 1995.
- 53. Isagawa, S. and Kanda, Y., Mass spectroscopic search for helium in effluent gas and palladium cathodes of D₂O electrolysis cells involving excess power, in *Sixth International Conference on Cold Fusion, Progress in New Hydrogen Energy*, Okamoto, M. New Energy and Industrial Technology Development Organization, Tokyo Institute of Technology, Tokyo, Japan, Lake Toya, Hokkaido, Japan, 1996, pp. 12.
- 54. Arata, Y. and Zhang, Y. C., Helium (⁴He, ³He) within deuterated Pd-black, *Proc. Jpn. Acad., Ser. B* 73, 1, 1997.
- 55. Gozzi, D., Cellucci, F., Cignini, P. L., Gigli, G., Tomellini, M., Cisbani, E., Frullani, S., and Urciuoli, G. M., Erratum to "X-ray, heat excess and ⁴He in the D/Pd system", *J. Electroanal. Chem.* 452, 251, 1998.
- 56. Case, L. C., Catalytic fusion of deuterium into helium-4, in *The Seventh International Conference on Cold Fusion*, Jaeger, F. ENECO, Inc., Salt Lake City, UT, Vancouver, Canada, 1998, pp. 48.
- 57. Ueda, S., Yasuda, K., and Takahashi, A., Study of excess heat and nuclear products with closed electrolysis system and quadrupole mass spectrometer, in *The Seventh International Conference on Cold Fusion*, Jaeger, F. ENECO, Inc., Salt Lake City, UT, Vancouver, Canada, 1998, pp. 398.
- 58. Bush, B. F. and Lagowski, J. J., Methods of generating excess heat with the Pons and Fleischmann effect: rigorous and cost effective calorimetry, nuclear products analysis of the cathode and helium analysis, in *The Seventh International Conference on Cold Fusion*, Jaeger, F. ENECO, Inc., Salt Lake City, UT., Vancouver, Canada, 1998, pp. 38.
- 59. Arata, Y. and Zhang, Y. C., Observation of anomalous heat release and helium-4 production from highly deuterated fine particles, *Jpn. J. Appl. Phys. Part* 2 38 (7A), L774, 1999.
- 60. Miles, M., Imam, M. A., and Fleischmann, M., Excess heat and helium production in the palladium-boron system, *Trans. Am. Nucl. Soc.* 83, 371, 2000.
- 61. Matsunaka, M., Isobe, Y., Ueda, S., Yabuta, K., Ohishi, T., Mori, H., and Takahashi, A., Studies of coherent deuteron fusion and related nuclear reactions in solid., in *The 9th International Conference on Cold Fusion, Condensed Matter Nuclear Science*, Li, X. Z. Tsinghua Univ., Beijing, China, Tsinghua Univ., Beijing, China, 2002, pp. 237.
- 62. Miles, M., Correlation of excess enthalpy and helium-4 production: a review, in *Tenth International Conference on Cold Fusion*, Hagelstein, P. I. and Chubb, S. R. World Scientific Publishing Co., Cambridge, MA, 2003, pp. 123.
- 63. Hagelstein, P. L., McKubre, M. C., Nagel, D. J., Chubb, T., and Hekman, R., New physical effects in metal deuterides, in *11th International Conference on Cold Fusion*, Biberian, J.-P. World Scientific Co., Marseilles, France, 2004, pp. 23.
- 64. Corrigan, D. A. and Schneider, E. W., Tritium separation effects during heavy water electrolysis: implications for reported observations of cold fusion, *J. Electroanal. Chem.* 281, 305, 1990.

- 65. Santandrea, R. P. and Behrens, R. G., A review of the thermodynamics and phase relationships in the palladium- hydrogen, palladium-deuterium and palladium-tritium systems., *High Temperature Materials and Processes* 7, 149, 1986.
- 66. Storms, E. and Talcott, C. L., Electrolytic tritium production, Fusion Technol. 17, 680, 1990.
- 67. Storms, E. and Talcott, C. L., A study of electrolytic tritium production, in *The First Annual Conference on Cold Fusion*, Will, F. National Cold Fusion Institute, University of Utah Research Park, Salt Lake City, Utah, 1990, pp. 149.
- 68. Chêne, J. and Brass, A. M., Tritium production during the cathodic discharge of deuterium on palladium, *J. Electroanal. Chem.* 280, 199, 1990.
- 69. Lin, G. H., Kainthla, R. C., Packham, N. J. C., Velev, O. A., and Bockris, J., On electrochemical tritium production, *Int. J. Hydrogen Energy* 15 (8), 537, 1990.
- 70. Cedzynska, K., Barrowes, S. C., Bergeson, H. E., Knight, L. C., and Will, F. G., Tritium analysis in palladium with an open system analytical procedure, *Fusion Technol.* 20, 108, 1991.
- 71. Mengoli, G., Fabrizio, M., Manduchi, C., Zannoni, G., Riccardi, L., Veronesi, F., and Buffa, A., The observation of tritium in the electrolysis of D₂O at palladium sheet electrodes, *J. Electroanal. Chem.* 304, 279, 1991.
- 72. Lanza, F., Bertolini, G., Vocino, V., Parnisari, E., and Ronsecco, C., Tritium Production Resulting From Deuteration of Different Metals and Alloys, in *Second Annual Conference on Cold Fusion*, "*The Science of Cold Fusion*", Bressani, T., Giudice, E. D., and Preparata, G. Societa Italiana di Fisica, Bologna, Italy, Como, Italy, 1991, pp. 151.
- 73. Srinivasan, M., Shyam, A., Sankaranarayanan, T. K., Bajpai, M. B., Ramamurthy, H., Mukherjee, U. K., Krishnan, M. S., Nayar, M. G., and Naik, Y. P., Tritium and Excess Heat Generation During Electrolysis of Aqueous Solutions of Alkali Salts With Nickel Cathode, in *Third International Conference on Cold Fusion*, "Frontiers of Cold Fusion", Ikegami, H. Universal Academy Press, Inc., Tokyo, Japan, Nagoya Japan, 1992, pp. 123.
- 74. Will, F. G., Cedzynska, K., and Linton, D. C., Reproducible tritium generation in electrochemical cells employing palladium cathodes with high deuterium loading, *J. Electroanal. Chem.* 360, 161, 1993.
- 75. Szpak, S., Mosier-Boss, P. A., and Boss, R. D., Comments on the analysis of tritium content in electrochemical cells, *J. Electroanal. Chem.* 373, 1, 1994.
- 76. Dandapani, B. and Fleischmann, M., Electrolytic Separation Factors on Palladium, *J. Electroanal. Chem.* 39, 323, 1972.
- 77. Iyengar, P. K. and Srinivasan, M., Report No. B.A.R.C.1500, 1989.
- 78. Iyengar, P. K. and Srinivasan, M., Overview of BARC Studies in Cold Fusion, in *The First Annual Conference on Cold Fusion*, Will, F. National Cold Fusion Institute, University of Utah Research Park, Salt Lake City, Utah, 1990, pp. 62.
- 79. Bockris, J. O'M. and Minevski, Z., The mechanism of the evolution of hydrogen on palladium and associated internal damage phenomena, *Int. J. of Hydrogen Energy*, 25, 747, 2000.

- 80. Fleischmann, M., Pons, S., and Hawkins, M., Electrochemically Induced Nuclear Fusion of Deuterium, *J. Electroanal. Chem.* 261, 301 and errata in Vol. 263, 1989.
- 81. Storms, E., <u>The science of low energy nuclear reactions</u>, World Scientific, 2007.
- 82. De Ninno, A., Frattolillo, A., Rizzo, A., and Del Giudice, E., ⁴He detection In a cold fusion experiment, in *Tenth International Conference on Cold Fusion*, Chubb, P. I. H. a. S. R. World Scientific Publishing Co., Cambridge, MA, 2003, pp. 133.
- 83. Violante, V., Moretti, S., Bertolotti, M., Castagna, E., Sibilia, C., Sarto, F., McKubre, M., Tanzella, F., Dardik, I., Lesin, S and Zilov, T., Progress in excess of power experiments with electrochemical loading of deuterium in palladium, in *12th International Conference on Condensed Matter Nuclear Science*, Yokohama, Japan, p 55, 2005.
- 84. Apicella, M., Castagna, E., Capabianco, L., D'Aulerio, L., Mazzitelli, Sarto, F., Rosada, A., Santoro, E., Violante, V., McKubre, M., Tanzella, F., and Sibilia, C., Some recent results at ENEA, in *12th International Conference on Condensed Matter Nuclear Science*, Yokohama, Japan, p 55, 2005.
- 85. Pons, S., and Fleischmann, M., Heat after death, Trans. Fusion Technology, 4, 87, 1994.
- 86. Fleischmann, M. and Pons, S., Calorimetry of the Pd-D₂O system: from simplicity via complications to simplicity, *Phys. Lett. A* 176, 118, 1993, and in *Third International Conference on Cold Fusion*, "Frontiers of Cold Fusion", Ikegami, H. Universal Academy Press, Inc., Tokyo, Japan, Nagoya Japan, 1992, pp. 47.
- 87. Swartz, M. R., Consistency of the biphasic nature of excess enthalpy in solid-state anomalous phenomena with the quasi-one-dimensional model of isotope loading into a material, *Fusion Technol.* 31, 63, 1997.
- 88. Rothwell, J., *introduction to*, Mizuno, T., *Nuclear transmutation: The reality of cold fusion* Infinite Energy Press, Concord, NH, 1998.
- 89. Mengoli, G., Bernardini, M., Manduchi, C., and Zannoni, G., Calorimetry close to the boiling temperature of the D₂O/Pd electrolytic system, *J. Electroanal. Chem.* 444, 155, 1998.
- 90. Miles, M. H., Fleischmann, M., and Imam, M. A., Report No. NRL/MR/6320--01-8526, 2001.
- 91. Miles, M. H., Imam, M. A., and Fleischmann, M., Calorimetric analysis of a heavy water electrolysis experiment using a Pd-B alloy cathode, *Proc. Electrochem. Soc.* 2001 (23), 194, 2001.
- 92. Tian, J., Li, X. Z., Yu, W. Z., Mei, M. Y., Cao, D. X., Li, A. L., Li, J., Zhao, Y. G., and Zhang, C., "Excess heat" and "heat after death" in a gas loading hydrogen/palladium system, in *The 9th International Conference on Cold Fusion, Condensed Matter Nuclear Science*, Li, X. Z. Tsinghua Univ. Press, Tsinghua Univ., Beijing, China, 2002, pp. 360.
- 93. Swartz, M. R. and Verner, G., Excess heat from low-electrical conducting heavy water spiral-wound Pd/D₂O/Pt and Pd/D₂O-PdCl₂/Pt devices, in *Tenth International Conference on Cold Fusion*, Hagelstein, P. L. and Chubb, S. R. World Scientific Publishing Co., Cambridge, MA, 2003, pp. 29.